Cellular Mechanisms for Olfactory Information Processing in the Mushroom Bodies

Inaugural-Dissertation

zur

Erlangung des Doktorgrades

der Mathematisch-Naturwissenschaftlichen Fakultät

der Universität zu Köln

vorgelegt von

Heike Demmer

aus Köln

Köln 2009

Contents

Abbreviations

AL	antennal lobe(s)
BA	benzaldehyde
CA	+/- citral
CO	citronellal
EU	eugenol
GABA	γ-amino-butyric acid
GE	geraniol
HX	1-hexanol
I_A	A-current
I_{Ca}	calcium current
$I_{K,ST}$	slow transient potssium current
$I_{K(V)}$	delayed rectifier current
I_{Na}	sodium current
$I_{O,Ca}$	Ca^{2+}-dependent outward current
IO	α-ionone
KC(s)	Kenyon cell(s)
LLP	lateral lobe of the protocerebrum
LN	local interneuron
MB	mushroom body
ME	methylsalicylate
MGPN	macroglomerular projection neuron
OGB-1	Oregon-Green BAPTA 1
OM	odor mixture
PN	projection neuron
PTX	picrotoxin

Zusammenfassung

Das olfaktorische System von Insekten diente schon oft als Modell für generelle sensorische Informationsverarbeitung. Information, die von olfaktorischen Rezeptorzellen detektiert wird, wird in mehreren Schritten weiterverarbeitet. Innerhalb der Antennalloben wird die olfaktorische Information von lokalen Interneuronen prozessiert und via Projektionsneuronen in höhere Gehirn Regionen geleitet. Die höheren Zentren sind bei Insekten die Pilzkörper und die lateralen Loben des Protocerebrums. Die Pilzkörper der Insekten sind Zentren für multimodale Informationsverarbeitung und essentiell für olfaktorisches Lernen. Elektrophysiologische Ableitungen der Hauptzellen des Pilzkörpers, der Kenyon Zellen, zeigten eine 'spärliche' Wiedergabe der olfaktorischen Signale im Pilzkörper ('sparse coding'). Es wurde vermutet, dass intrinsische gemeinsam mit synaptischen Eigenschaften des Kenyon Zellen-Netzwerks die reduzierte Anzahl an Aktionspotenzialen bewirken und so ein kurzes Intergrationsfenster für synaptische Eingänge bilden. Somit würden die Kenyon Zellen als Koinzidenzdetektoren fungieren. Um eine Reihe von spannungs- und Kalzium abhängigen Einwärts- (I_{Ca}, I_{Na}) und Auswärtsströmen (I_A, $I_{K(V)}$, $I_{K,ST}$, $I_{O(Ca)}$) zu analysieren und damit die genannten speziellen Feuereigenschaften der Kenyon Zellen besser zu verstehen, wurden jene Zellen in einem adulten, intakten Hirnpräparat der Schabe *Periplaneta americana* mit Hilfe der 'whole-cell patch-clamp' Technik untersucht. Grundsätzlich zeigte sich, dass die Parameter der Ströme ähnlich denen in anderen Insekten waren. Bestimmte funktionelle Parameter des I_{Ca} und des $I_{O(Ca)}$ hingegen zeichneten sich als besonders aus und könnten so das 'sparse coding' unterstützen. I_{Ca} hatte im Vergleich zu I_{Ca} in anderen Insekten eine sehr niedrige Aktivierungsschwelle und eine sehr hohe Stromdichte. Zusammen könnten diese Eigenschaften des I_{Ca} die verstärkten und geschärften

EPSPs, wie sie in vorangegangenen Studien beschrieben wurden, zur Folge haben. $I_{O(Ca)}$ wies ebenfalls eine sehr hohe Stromdichte auf und eine sehr hohe Aktivierungsschwelle. In Kombination könnten der große I_{Ca} und $I_{O(Ca)}$ die starke Spike-Frequenz Adaptation vermitteln.

Immunohistochemische Studien haben gezeigt, dass die Pilzkörper von GABAergen Neuronen massiv innerviert werden. Diese GABAergen Neurone verschalten auf Kenyon Zellen und Projektionsneurone. Die intrinsischen Eigenschaften der Kenyon Zellen werden vermutlich auch von tonischem, inhibierenden synaptischen Eingang unterstützt. Dies konnte ich mit spezifischen GABA-Rezeptor Blockern zeigen. Zusätzlich habe ich den Eingang auf die Kenyon Zellen, der hauptsächlich von den olfaktorischen Projektionsneuronen stammt, untersucht. Ich konnte zeigen, dass unterschiedliche, räumlich abgesetzte Eingänge möglicherweise präsynaptisch durch GABA moduliert werden.

Abstract

The insect olfactory system has already served as a model system to analyze general sensory information processing. Olfactory information, which is perceived by olfactory receptor neurons is processed in multiple steps. Within in the first olfactory relay, the antennal lobes (AL), olfactory information is processed by local interneurons and relayed by projection neurons (PNs) to higher order brain centers, which are the mushroom bodies and the lateral lobes of the protocerebrum. The insect mushroom bodies (MBs) are multimodal signal processing centers and essential for olfactory learning. Electrophysiological recordings from the MB principle component neurons, the Kenyon cells (KCs), showed a sparse representation of olfactory signals in the MBs or rather the KCs. It has been proposed that the intrinsic and synaptic properties of the KCs circuitry combine to reduce the firing of action potentials and to generate relatively brief windows for synaptic integration in the KCs, thus causing them to operate as coincidence detectors. I used whole-cell patch-clamp recordings from KCs in the adult, intact brain of the cockroach *Periplaneta americana* to analyze a set of voltage- or Ca^{2+} dependent inward (I_{Ca}, I_{Na}) and outward currents (I_A, $I_{K(V)}$, $I_{K,ST}$, $I_{O(Ca)}$) to better understand the ionic mechanisms that mediate their special firing properties. In general the currents had properties similar to currents in other insect neurons. Certain functional parameters of I_{Ca} and $I_{O(Ca)}$, however, have extreme values suiting them to assist sparse coding. I_{Ca} has a very low activation threshold and a very high current density compared to I_{Ca} in other insect neurons. Together these parameters make I_{Ca} suitable for boosting and sharpening the EPSPs as reported in previous studies. $I_{O(Ca)}$ also has a large current density and a high activation threshold. In combination the large I_{Ca} and $I_{O(Ca)}$ are likely to mediate a strong spike frequency adaptation.

Immunohistochemical studies have shown that the mushroom bodies are contacted by GABAergic neurons, which synapse onto KCs and the input neurons the PNS. The intrinsic properties of the KCs are likely to be shaped in part by their tonic, inhibitory synaptic input, which was revealed by specific GABA receptor blockers. In addition I analyzed the input to the KCs, which is mainly provided by olfactory projection neurons. Here I was able to show, that spatially distinct input is possibly modulated by presynaptic GABAergic inhibition.

1 Introduction

Olfactory discrimination and recognition is a vital task for all living animals. The olfactory system of insects and vertebrates share many features that are remarkably similar across the phyla (for review see Eisthen, 2002; Hildebrand & Sheperd, 1997). Therefore the insect olfactory system has been studied in great detail as a model system for general information processing (Laurent & Davidowitz, 1994; Wang *et al.*, 2004; Galizia *et al.*, 1999; Hansson, 2002; de Bruyne & Baker, 2008). In general an odorant is bound by odorant binding proteins (OBP), which are located in the membrane of olfactory receptor neurons. These cells are housed in olfactory sensilla, which are located on the insect antennae. The olfactory receptor neurons (ORNs) send their excitatory axons to primary olfactory centers, that are in insects the antennal lobes. Here the axons segregate into discrete spherical structures called glomeruli. In insects, all ORNs expressing a particular OBP converge in one distinct glomerulus (Fishilevich & Vosshall, 2005; Couto *et al.*, 2005). The numbers of glomeruli range from 50-160 (*Drosophila*: Laissue *et al.*, 1999, *Manducca*: Rospars & Hildebrand, 1992, *Periplaneta*: Boeckh *et al.*, 1987, *Apis*: Flanagan & Mercer, 1989; Galizia *et al.*, 1999). Within the glomeruli the ORNs provide cholinergic input to either projection neurons (PNs), and local interneurons (LNs). Most PNs innervate a single glomerulus and convey the information from that glomerulus to higher order brain centers, but some PNs innervate multiple glomeruli (Strausfeld *et al.*, 1998; Boeckh & Tolbert, 1993). The functional role of these cells remains unclear. The second class of cells in the antennal lobe are local interneurons, which inter-connect the glomeruli. The first class of LNs are local inhibitory spiking neurons which contain GABA and the second class are non spiking interneurons which do not contain GABA (Husch *et al.*, 2009).

1.1 Olfactory information processing in the AL

One consequence of interglomerular connectivity is that the olfactory information is distributed over greater ensembles of PNs. Studies in insects have shown that PNs respond in a broader range of odors than the matching presynaptic ORNs (Wilson *et al.*, 2004). This broadening of the tuning curves is achieved by local inhibitory and excitatory circuits provided by the local interneurons (Olsen *et al.*, 2007; Olsen & Wilson, 2008). Nevertheless the spatial distribution of olfactory information is not uniform between different component odors. Imaging studies have shown that the odor-evoked responses lead to spatial maps, where different odors activate different glomeruli in a fragmented way with overlapping areas (Galizia *et al.*, 1999; Silbering *et al.*, 2008; Sachse & Galizia, 2002). These areas increase with increasing odor concentrations. In addition to the spatial patterning, electrophysiological studies showed with higher temporal resolution that there is also a temporal patterning in the principal neurons. For example one odor might elicit a temporally complex pattern with phases of strong excitation and inhibition, whereas another odor might elicit a phasic excitation with no inhibition (Laurent *et al.*, 1996; Ito *et al.*, 2008). Different principal neurons, which are simultaneously activated by the same odor, can respond with different temporal patterns (Wehr & Laurent, 1996; Ito *et al.*, 2008). These temporal patterns seem to arise mainly from the local circuitry in the antennal lobe (Bazhenov *et al.*, 2005; Wilson & Laurent, 2005). Studies in honey bees suggested that in addition the output of the PNs is modulated by the GABAergic neurons (Szyszka *et al.*, 2005). This possible modulation could have different consequences on the temporal patterning, the spatial patterning and the absolute strength of responses to different odors.

1.2 Mushroom body

Biochemical, genetic, physiological and behavioral studies have identified the mushroom bodies (MB) as multimodal information processing centers that also play a crucial role during learning and memory formation (for reviewes see Davis, 2004; Dubnau *et al.*, 2003, Heisenberg, 2003). Anatomically first described by Du-
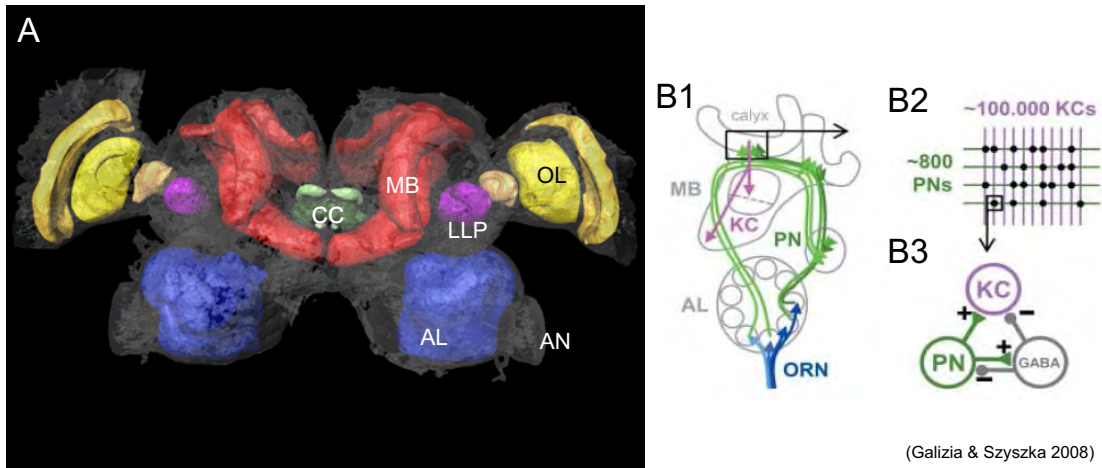
Figure 1.1: Schematic overview of the olfactory pathways in insects. (A) Reconstruction of the neuropils of P. americana. AL: antennal lobe; AN: antennal nerve; CC: central complex; LLP: lateral lobe of the protocerebrum; MB: mushroom body; OL: optical lobe (kindly provided by S. Schleicher). (B1) Schematic overview of honey bee olfactory system (adapted from Galizia & Szyszka, 2008). ORN: olfactory receptor neurons; AL: antennal lobe; PN: projection neurons; MB: mushroom body; KC: Kenyon cell. (B2) Schematic view of the neural network in the MB calyx (black box in B1). In P. americana 260 PNs synapse onto ∼200 000 KCs (Boeckh et al., 1984). (B3) Schematic view of microcircuits within the MB calyx (black box in B2). PNs synapse onto KCs and GABAergic neurons, which, in turn, make synapse with KCs and PNs.

jardin (1850) they are prominent lobed bilateral structures in the protocerebra of nearly all insects. Most of their structure is formed by a large number of intrinsic principal neurons, called Kenyon cells (KCs). Their small cell bodies are located in and around the cup-like structures of the calyces. The calyces contain the main dendritic input region of the KCs. From here they send their axons along the pedunculus towards the two lobes where they bifurcate and make output synapses on efferent neurons. The KCs receive mostly olfactory information but visual input has also been described for some species (for reviews see Fahrbach, 2006; Heisenberg 1998, Strausfeld *et al.*, 1998). Within the calyces of the mushroom bodies, the KCs are contacted by several centrifugal neurons that contain multiple kinds of neurotransmitters and neurohormons. Immunohistochemical studies have shown that both octopamine and dopamine are highly expressed in the mushroom bodies. Blocking these neuromodulators led to drastic impairment of memory tasks.

Behavioral experiments combined with ablation, lesioning, cooling, stimulation or genetic intervention have led to the conclusion that the MBs are in-

volved in sensory information processing, control of motor behavior, and learning and memory (for reviewes see Davis, 2004; Dubnau *et al.*, 2003, Heisenberg, 2003). Concepts how sensory information is integrated and represented in the MBs emerged from electrophysiological studies of olfactory signal processing (MacLeod & Laurent, 1996; Perez-Orive *et al.*, 2002; Perez-Orive *et al.*, 2004). In the MBs, olfactory signals are sparsely represented, which is in strong contrast to the antennal lobes, the first synaptic relay in the insect olfactory system. Sparse coding, which is defined as representation of information by a relatively small number of simultaneously active neurons out of a large population, can be achieved by either the appropriate connectivity in the circuit or the intrinsic firing properties of the network's component neurons (Olshausen & Field, 2004), in this case the KCs. There is evidence for both of these mechanisms in the MBs: immuno-histochemical, electrophysiological and imaging studies suggest that pre- (of the projection neurons) and postsynaptic inhibition (of the KCs) might contribute to sparse coding in the MB (Bazenov *et al.*, 2001; Leitch & Laurent, 1996; Perez-Orive *et al.*, 2002; Perez-Orive *et al.*, 2004; Szyszka *et al.*, 2005; Wang *et al.*, 2004; Yasuyama *et al.*, 2002; Murthy *et al.*, 2008). Second there is evidence from electrophysiological recordings and modeling studies that intrinsic firing properties of KCs support a sparse coding scheme (for review see Laurent, 2002; Wilson & Mainen, 2006; Kay & Stopfer, 2006). It has been proposed that the intrinsic and synaptic properties combine to generate relatively brief integration windows in the KCs, thus causing them to operate as coincidence detectors for synaptic input from projection neurons (Perez-Orive *et al.*, 2002; Perez-Orive *et al.*, 2002). These studies make some assumptions and predictions about the underlying ionic conductances. However, except for in vitro studies of pupal honey bee KCs (Schäfer *et al.*, 1994; Grünewald, 2003; Wüstenberg *et al.*, 2004; Pelz *et al.*, 1999) there are not many quantitative data about the ionic currents that ultimately determine the KCs' intrinsic firing properties. Recent studies of adult cricket KCs showed modulatory effects of monamines on Ca^{2+} currents and Na^+-activated K^+ currents pointing towards a possible cellular mechanism of learning KCs (Aoki *et al.*, 2008; Kosakai *et al.*, 2008).

1.3 Objectives of this Thesis

The aim of this study was to identify different mechanisms, which contribute to olfactory coding in the mushroom bodies of *P. americana*.

- First, I analyzed the intrinsic membrane properties of the Kenyon cells, which are the principal neurons of the mushroom bodies. This part combined odor evoked responses of Kenyon cells and a detailed analysis of voltage- and Ca^{2+}-dependent currents.

- Second I investigated the effect of GABAergic postsynaptic inhibition on the Kenyon cells in consideration of appropriate circuit connectivity.

- Last I examined the GABAergic modulation of spatial and temporal aspects of the synaptic output boutons of projection neurons KCs.

The combination of the different parameters leads to a better understanding of mechanisms which mediate olfactory coding in insect mushroom bodies.

2 Material

2.1 Animals and materials

P. americana were reared in crowded colonies at $\sim 27°$C under a 13:11 h light/dark photoperiod regimen and reared on a diet of dry rodent food, oatmeal and water. The experiments were performed with adult males. All chemicals, unless stated otherwise, were obtained from Applichem (Darmstadt, Germany) or Sigma-Aldrich (Taufkirchen, Germany) in a 'pro analysis' purity grade.

2.2 Intact brain preparation

The intact brain preparation was based on an approach described previously (Kloppenburg *et al.*, 1999a; Kloppenburg *et al.*, 1999b), in which the entire olfactory network is left intact. The animals were anaesthetized by CO_2, placed in a custom build holder and the head with antennae was immobilized with tape (Tesa ExtraPower Gewebeband, Tesa, Hamburg, Germany). The head capsule was opened by cutting a window between the two compound eyes and the bases of the antennae. The brain with antennal nerves and antennae attached was dissected from the head capsule in 'normal saline' (see below) and pinned in a Sylgard-coated (Dow Corning Corp., Midland, Michigan, USA) recording chamber. To gain access to the recording site and facilitate the penetration of pharmacological agents into the tissue, I desheathed parts of the MBs using fine forceps. Some preparations were also enzyme treated with a combination of papain (0.3 mg ml^{-1}, P4762, Sigma) and L-cysteine (1 mg ml^{-1}, 30090, Fluka/Sigma,) dissolved in 'normal' saline ($\sim$ 3 min, RT). The KCs were visualized with a fixed stage upright microscope (BX51WI, Olympus, Hamburg, Germany) using a 20x

water-immersion objective (XLUMPLFL, 20x, 0.95 NA, 2 mm WD, Olympus) with a 4x magnification changer (U-TAVAC, Olympus) and IR-DIC optics (Dodt & Zieglgänsberger, 1994).

2.3 Whole-cell recordings

Whole-cell recordings were performed at 24°C following the methods described by Hamill *et al.* (1981). Electrodes with tip resistances between 4-5 MΩ were fashioned from borosilicate glass (0.86 mm ID, 1.5 mm OD, GB150-8P, Science Products, Hofheim, Germany) with a temperature controlled pipette puller (PIP5, HEKA-Elektronik, Lambrecht, Germany). For current clamp recordings the pipettes were filled with 'normal' intracellular saline solution containing (in mM): 190 K-aspartate, 10 NaCl, 1 $CaCl_2$, 2 $MgCl_2$, 10 HEPES and 10 EGTA adjusted to pH 7.2 (with KOH), resulting in an osmolarity of $\sim$ 415 mOsm. During the experiments, if not stated otherwise, the cells were superfused constantly with 'normal' extracellular saline solution containing (in mM): 185 NaCl, 4 KCl, 6 $CaCl_2$, 2 $MgCl_2$, 10 HEPES, 35 D-glucose. The solution was adjusted to pH 7.2 (with NaOH) and to 430 mOsm (with glucose). Whole-cell voltage- and current-clamp recordings were made with an EPC9 patch-clamp amplifier (HEKA-Elektronik) that was controlled by the program Pulse (version 8.63, HEKA-Elektronik) running under Windows. The electrophysiological data were sampled at intervals of 100 μs (10 kHz), except the tail current and sodium current measurements were sampled at 20 kHz. The recordings were low pass filtered at 2 kHz with a 4-pole Bessel-filter. The offset potential and capacitive currents were compensated using the 'automatic mode' of the EPC9 amplifier. Whole-cell capacitance was determined by using the capacitance compensation (C-slow) of the EPC9. Cell input resistances were calculated from voltage responses to hyperpolarizing current steps. The calculated liquid junction potential between intracellular and extracellular solution of 15.4 mV for 'normal' and of 4.8 mV for 'calcium' and 'sodium' extra-/intracellular saline was also compensated (calculated with Patcher's-Power-Tools plug-in from http://www.mpibpc.gwdg.de/abteilungen/140/software/index.html

for Igor Pro [Wavemetrics, Portland, Oregon]). To remove uncompensated leakage and capacitive currents, a p/6 protocol was used (see Armstrong & Bezanilla, 1974). Voltage errors due to series resistance (R_S) were minimized using the RS-compensation of the EPC9. R_S was compensated between 30% and 70% with a time constant (τ) of 200 ms.

2.4 Current isolation

Membrane currents were isolated using a combination of ion substitution, pharmacological blockers, voltage inactivation and digital current subtraction protocols, based on protocols that have been effective in insect preparations (Heidel & Pflüger, 2006; Husch *et al.*, 2009; Kloppenburg & Hörner, 1998; Kloppenburg *et al.*, 1999b; Mercer *et al.*, 1995; Mercer *et al.*, 1996; Schäfer *et al.*, 1994). Sodium currents were blocked by tetrodotoxin (10^{-7} M, TTX, T-550, Alomone, Jerusalem, Israel). Calcium currents were blocked by $CdCl_2$ (5 x 10^{-4} M). Tetraethyl-ammonium (2 x 10^{-2} M, TEA, T2265, Sigma-Aldrich) was used to block sustained K^+ currents ($I_{K(V)}$) and also a Ca^{2+} activated outward current ($I_{O(Ca)}$). $I_{O(Ca)}$ was also indirectly eliminated when the Ca^{2+} currents were blocked by $CdCl_2$. The transient K^+ current (I_A) was blocked with 4-aminopyridine (4 x 10^{-3} M, 4-AP, A78403, Sigma-Aldrich), or was eliminated by depolarized holding potentials, at which I_A is significantly inactivated. To compensate for changes in osmolarity, the glucose concentration was appropriately reduced. Details of recording solutions and voltage protocols for each set of experiments are provided in the Results.

To measure steady state activation, incrementing voltage steps were applied from a constant holding potential (see in Results and figure legends). The voltage dependencies of voltage dependent K^+ currents were determined by converting the peak currents to peak conductance, G, which were scaled as a fraction of the calculated maximal conductance. The voltage dependence of activation of I_{Ca} and I_{Na} was determined from tail currents. The resulting conductance/voltage (G/V) or current/voltage (I/V) curves were fit to a 1st order Boltzmann equation of the form

$$\frac{A}{A_{max}} = \frac{1}{(1 + e^{\frac{-(V-V_{0.5})}{s}})}$$

where *A* is the amplitude of the conductance (or tail current) and *s* is a slope factor. $V_{0.5}$ is the voltage of half-maximal activation ($V_{0.5_{act}}$). Equilibrium potentials (for 24°C) was calculated using the Nernst equation, assuming the intracellular ion concentration equals the concentration in the pipette solution.

Steady state inactivation of voltage dependent currents was measured from a constant holding potential and incrementing pre-steps were followed by a constant voltage step, for which the peak currents were measured. The data, scaled as a fraction of the calculated maximal conductance (K^+ currents) or maximal current ($I_{Ca_{max}}$, $I_{Na_{max}}$), were fitted to a 1st order Boltzmann equation, where $V_{0.5}$ is the voltage for half maximal inactivation ($V_{0.5_{inact}}$).

2.5 Data analysis

We used the software Pulse (version 8.63, HEKA-Electronics), Igor Pro 6 (Wavemetrics, including the Patcher's PowerTools plug-in), Sigma Stat, and Sigma Plot (Systat Software GmbH, San Jose, California) for analysis of electrophysiological data. All calculated values are expressed as mean $\pm$ standard deviation. Significance of differences between mean values was evaluated with paired and unpaired t-tests. A significance level of 0.05 was accepted for all tests.

2.6 Odor stimulation

We delivered odors using a continuous air flow system. Carbon-filtered, humidified air flowed continuously across the antennae at a rate of 2 l min^{-1} ('main airstream') through a glass tube (10 mm ID) placed perpendicular to and within 20-30 mm of the antennae. Odors were quickly removed with a vacuum funnel (3.5 cm ID) placed 5 cm behind the antennae. 5 ml of the liquid odorants (pure or diluted in mineral oil [M8410, Sigma]) were filled in 100 ml glass vessels. During a 500 ms odor stimulus, 22.5 ml of the headspace was injected into the airstream. To ensure a continuous air flow across the preparation, the air delivering the odor was redirected from the 'main airstream' by a solenoid valve system. The solenoids were controlled by the D/A-interface of the EPC9 patch-clamp am-

plifier and the Pulse software. The odorants were adjusted with mineral oil to a final volume of 5 ml. The concentration was adjusted to the odorant with the lowest vapor pressure (eugenol). Stripes of filter paper were used to facilitate evaporation. Final concentrations were as follows: eugenol 100 % (E51791, Aldrich), a-ionone 72.4 % (I12409, Aldrich), methyl salicylate 14.9 % (M6752,Aldrich), +/- citral 14.6 % (C83007, Aldrich), citronellal 4.9 % (W230715, Sigma), 1-Hexanol 1.1 %(52830, Fluka), benzaldehyde 1.1 % (418099, Aldrich), pyrrolidine 0.02 % (83241, Fluka). In addition an odor mixture was used, where the same amounts of all single component odors were combined. The headspace of pure mineral oil was used as control stimulus ('blank'). Odor stimuli arrived at least 60 s apart except for the imaging experiments where all odors were applied as fast as possible to reduce recording time.

2.7 Single cell labeling

To label single cells, 1% biocytin (B4261, Sigma) was added to the pipette solution. After the recordings, the brains were fixed in Roti-Histofix (P0873, Carl Roth, Karlsruhe, Germany) overnight at 4 °C and rinsed in 0.1 M Tris-HCl buffered solution (3 x 10 min, pH 7.2, TBS). To facilitate the streptavidin penetration, the brains were treated with a commercially available collagenase/dispase mixture (1 mg ml-1, 269638, Roche Diagnostics, Mannheim, Germany) and hyaluronidase (1 mg ml-1, H3506, Sigma-Aldrich) in TBS (20 min, 37 °C), rinsed in TBS (3 x 10 min, 4 °C) and incubated in TBS containing 1% Triton X-100 (30 min, RT, Serva, Heidelberg, Germany). Afterwards, the brains were incubated in Alexa Fluor 633 (Alexa 633) conjugated streptavidin (1:600, 1-2 days, 4 °C, S21375, Molecular Probes, Eugene, OR) that was dissolved in TBS containing 10% Normal Goat Serum (S-1000, Vector Labs, Burlingame, CA). Brains were rinsed in TBS (3 x 10 min, 4°C), dehydrated, and cleared and mounted in methyl salicylate (M6752, Sigma-Aldrich).

After taking images of the whole mount preparations, the brains were rinsed in 100% ethanol for 10 min to remove the methylsalicylate, rehydrated, and rinsed in TBS (3 x 10 min, RT). The brains were embedded in agarose (4% in TBS, 11380,

Serva, Heidelberg, Germany) and 100 mm frontohorizontal sections were cut in
TBS with a vibratome (Leica VT1000 S, Heidelberg, Germany). The slices were
rinsed in H_2O, dried on coated slides (0.05 % chrome-alum [60151, Fluka/Sigma]
and 0.5% gelatin [4078, Merck, Darmstadt, Germany]), treated with xylene for
10 min and mounted in Permount (SP15B, Fisher Scientific, Fair Lawn, NJ). The
fluorescence images were captured with a confocal microscope (LSM 510, Carl
Zeiss, Göttingen, Germany) equipped with Plan-Neofluar 10x (0.3 NA), Plan-
Apochromat 20x (0.75 NA), and Plan-Apochromat 63x (1.4 NA Oil) objectives.
Streptavidin-Alexa 633 was excited with a He-Ne Laser at 633 nm. Emission of
Alexa 633 was collected through a 650 nm LP filter. Scaling, contrast enhance-
ment and z-projections were performed with ImageJ v1.35d and the WCIF plu-
gin bundle (www.uhnresearch.ca/facilities/wcif/). Single labeled neurons were
reconstructed with a custom module (Evers *et al.*, 2004) implemented in Amira
4.1 (Mercury Computer Systems, San Diego,CA). The final figures were prepared
with Photoshop and Illustrator CS2 (Adobe Systems Incorporated, San Jose, CA).

2.8 Calcium imaging

The imaging setup for fluorimetric measurements consisted of an Imago/Sensi-
Cam CCD camera with a 640 x 480 chip (Till Photonics, Planegg, Germany) and
a polychromator IV (Till Photonics) that was coupled via an optical fibre into an
BXWI fixed stage upright microscope (Olympus, for details see above). The cam-
era and the polychromator were controlled by the software Vision (version 4.0,
Till Photonics) run on a Windows PC. For the analysis of odor-evoked calcium
signals in the boutons of the PNs the boutons were visualized with Alexa Fluor
568 (0.2% in the patch pipette). The boutons were illuminated with 570nm light
from the polychromator, that was reflected onto the cells with a tripleband mir-
ror (62002BS, Chroma). The emitted fluorescence was detected through a triple
band filter (61002m, Chroma). The odor evoked calcium signals were measured
using the Ca^{2+} indicator Oregon-Green-BAPTA-1 (OGB-1). This indicator is a sin-
gle wavelength, high affinity indicator suitable to measure fast Ca^{2+} signals. All
neurons were filled with OGB-1 (800μM) via the patch pipette and illuminated

with 490 nm light from the polychromator. The light was reflected onto the cells with a 505nm mirror (Q5051p, chroma) and the emitted fluorescence was detected through a 515-555 nm band-pass filter (HQ535/40, chroma). Data were acquired as 80 x 60 frames using 8x8 on-chip binning with 28 - 65 ms exposure time. Images were sampled in analog to digital units (adu) and stored and analyzed as 12 bit grayscale images. The signals were analyzed off-line using Igor 6.

After establishing the whole-cell configuration the mode was changed to current clamp. To estimate the input resistance hyperpolarizing and depolarizing current injections were applied. Afterwards the neurons were held for about 1.5 h at $\sim$ -100 mV ($\sim$ -300 pA) to enhance dye loading. When the boutons became visible, up to 11 component odors were puffed for 500 ms onto the ipsilateral antenna. The elicited calcium transients were monitored by images acquired at 490 nm at least 10 Hz for typically 4s. The signals were all analyzed off-line with a dynamic background removal procedure, which has already successfully been used on local interneurons (Pippow, 2008). Ca^{2+} signals were obtained from regions of interest (ROI), which were defined on the images obtained from the Alexa 568 fluorescence. To remove background from the calcium signals, first the time course of the signal was fit with a biexponential function omitting the period of Ca^{2+} influx, which started 1 second after signal onset and decayed back to resting level 2 seconds after signal onset. Second the whole kinetic was divided by the fit, resulting in a relative signal normalized to 1 ($\Delta F/F$ + 1) with dynamically removed background.

3 Results

The aim of this study was to identify different kinds of cellular mechanisms, which mediate olfactory coding. This goal was approached in two parts. First I investigated the mechanisms that determine the special firing properties of KCs. Therefore I established an intact brain preparation of *P. americana*, which allowed long lasting experiments. Voltage and current-clamp recordings were used to characterize ionic conductances in KCs, their odor specific response profiles, the effect of GABAergic postsynaptic inhibition on the general electrophysiological properties and KC morphology. Secondly, I investigated the main input sites of the KCs, the PN boutons. Odor evoked Ca^{2+} signals were qualitatively and quantitatively compared between individual boutons of single PNs. The response profiles before and after blocking of GABAergic inputs were compared.

3.1 Kenyon cell morphology

Current- and voltage-clamp recordings were used to analyze physiological parameters of Kenyon cells ($n = 100$) in an intact brain preparation of *P. americana*. The goal was to characterize and better understand the electrophysiological properties that mediate the special firing properties observed in these neurons. The Kenyon cells were identified by the size and position of their somata in the calyces of the MB. For all neurons ($n = 16$) that were labeled by dye injection via the recording pipette the identity was confirmed by the characteristic anatomy (Fig. 3.1). All stained neurons had a similar axonal branching pattern in the MB neuropil. The axon ran along the pedunculus towards the lobes, where it bifurcated into the vertical and medial lobe. In the calyces, however, their dendritic branching patterns varied substantially as demonstrated in Figure 3.1A-D. Nev-

ertheless, the data of the ionic currents was pooled from all recorded KCs, because there were no significant differences in the cellular properties between KCs and different types of KCs could not be classified at this point of my analysis.

3.2 Current-clamp

In this part of the study I characterized the current-clamp properties of KCs (n = 25). The resting potential, measured directly after breaking into the cells, was -53 mV $\pm$ 9 mV and -55 $\pm$ 10 mV 5 min after break in. The input resistance of the KCs was 2.5 $\pm$ 1 GΩ and they had a whole-cell capacitance of 2.7 $\pm$ 0.8 pF. The neurons showed very little or no spontaneous activity (mean firing rate < 0.1 Hz), but action potentials could be elicited in all recorded neurons by injecting depolarizing current (Fig. 3.2A). The spike threshold was -47 $\pm$ 6 mV. The APs could be abolished by TTX (data not shown), and accordingly, a TTX-sensitive, fast inward current was detected in the voltage-clamp recordings (Fig. 3.1B). During sustained depolarizing current injection I observed a strong spike frequency adaptation (Fig. 3.2A and H; τ = 1.8 $\pm$ 0.3 s). The Kenyon cells received abundant excitatory and inhibitory synaptic input. In a given neuron, often either excitatory or inhibitory input appeared to predominate (Fig. 3.2C and D). In 10 of 25 neurons, odor application induced sub threshold graded depolarization, up to 10 mV amplitude, which were time locked to the stimulus (Fig. 3.2E and F). In three of the odor sensitive KCs the odor-induced depolarization gave rise to action potentials (Fig. 3.2F and G). All odor responsive neurons reacted to more than one out of the five presented odors (Fig. 3.2G). They did not respond to the blank stimulus.
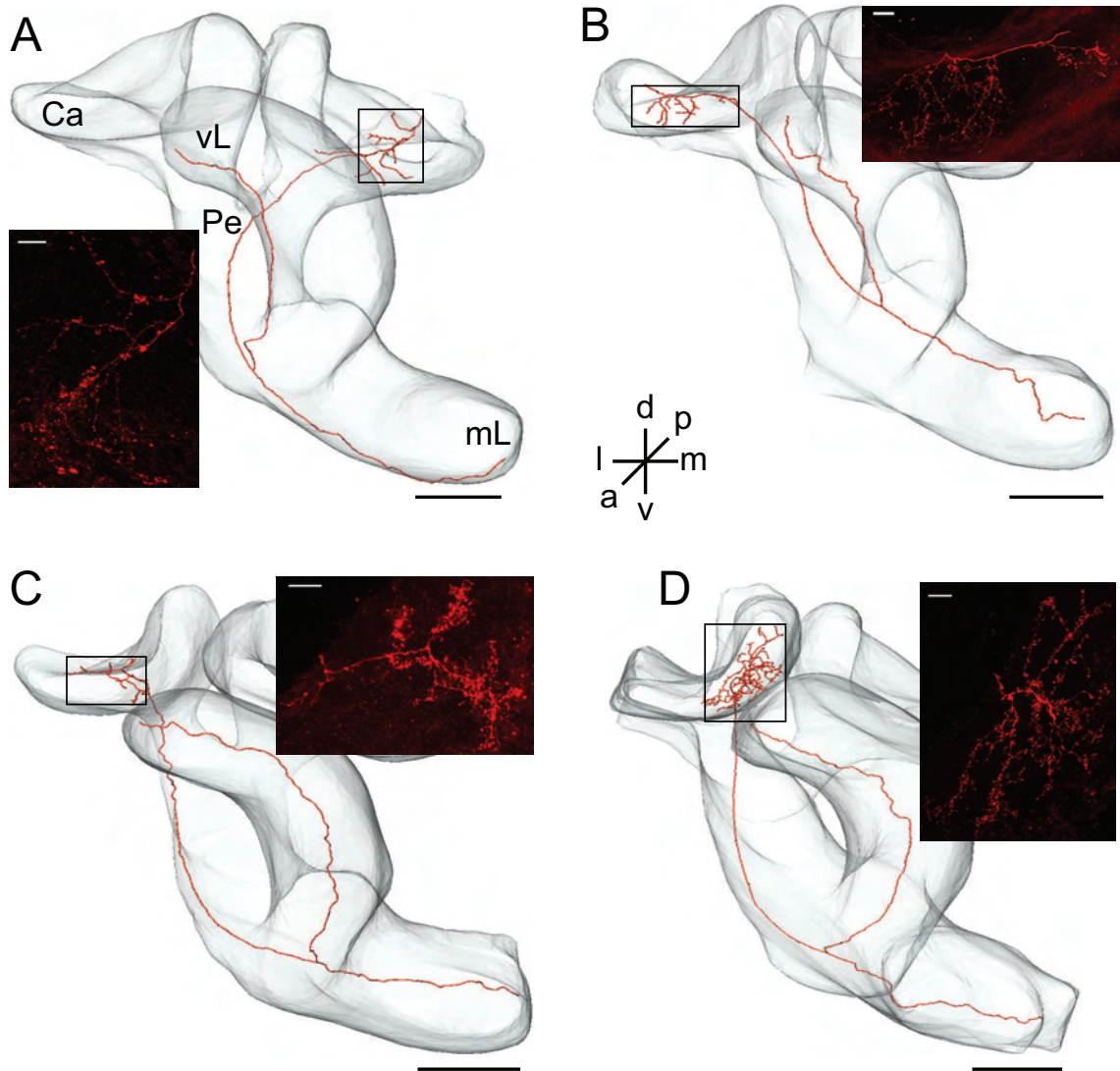
Figure 3.1: Kenyon cells' morphology. *(A-D) Schematic reconstructions of four recorded KCs that were stained with biocytin via the patch pipette. All somata were located at the frontal rim of the calyces but were lost during histological processing. The axons of all stained neurons ran along the pedunculus (Pe) towards the lobes, where they bifurcate into the medial (mL) and vertical (vL) lobes. In the calyces (Ca) their dendritic branching patterns varied between neurons (for detail see insets). Insets are maximum intensity projections of confocal images from the framed areas in the reconstructions. Scale: 100 µm; inset: 10 µm.*
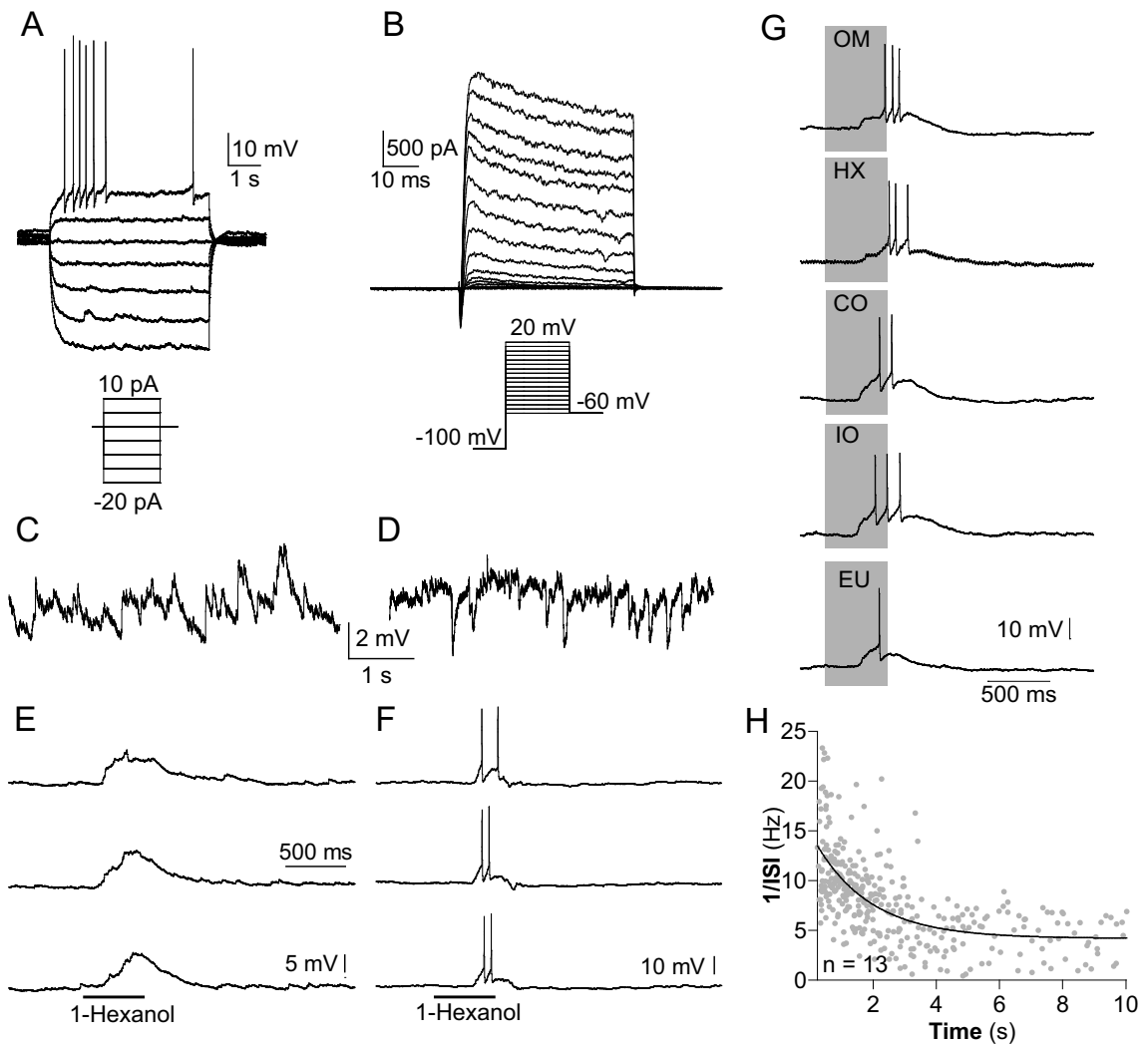
Figure 3.2: Current- and voltage-clamp recordings of Kenyon cells without channel blockers applied. (A) Injection of depolarizing current induced action potentials that showed a strong spike frequency adaptation. Current was injected for 5 s from -20 to 10 pA in 5 pA increments. (B) Whole-cell recordings of (mainly) voltage-activated currents in 'normal' saline. Depolarizing voltage steps from a holding potential of -100 mV elicited a fast transient inward current followed by transient and more sustained outward currents. (C,D) Most KCs received abundant, spontaneous synaptic input. In a given neuron either excitatory (C) or inhibitory (D) input was more obvious. (E,F) Recordings of odor responsive KCs during repetitive stimulation with 1-Hexanol. (E) Odor induced sub threshold, graded depolarizations (as in ∼ 30 % of the recorded KCs), which were time locked to the stimulus. (F) Odor induced depolarizations gave rise to action potentials (as in ∼ 25 % of the odor responsive KCs). (G) Odor induced depolarizations gave rise to action potentials. This particular neuron responded to all presented odors. (H) Instantaneous spike frequency. Every gray dot represents a single interspike interval. All cells showed a strong spike frequency adaptation of $\tau = 1.8 \pm 0.3$ sec.

3.3 Voltage-clamp

To investigate the cellular basis for the sparse KC responses to odors the ionic currents that shape their intrinsic firing properties were studied. To minimize synaptic input the brains were deantennated for voltage-clamp recordings. De-

polarizing voltage steps from a holding potential of -60 mV elicited a transient inward current that was followed by transient and sustained outward currents (Fig. 3.2B). Both the inward and outward currents represented a combination of several ionic currents, some of which I isolated and describe here. Individual currents were isolated using a combination of pharmacological blockade, ion substitution, appropriate holding potential, and current subtraction protocols. Current profiles that were clearly dominated by a certain current as a result of using these current isolation protocols, may still have included small residuals of other currents. Since I recorded from the soma, which has a long thin neurite connecting it to the rest of the cell, it seems likely that the currents I have measured originate primarily from the cell body. Ionic currents generated by channels selectively located in very distal regions of the neuron may not be detectable by voltage-clamp of the soma.

3.3.1 Outward currents

To measure voltage and Ca^{2+} dependent outward currents, the transient inward sodium currents (I_{Na}) were blocked by TTX (10^{-7} M). To record purely voltage dependent outward currents, I used Cd^{2+} (5×10^{-4} M) to abolish Ca^{2+} currents. At least 4 outward currents were apparent in all KCs: 1) a 4 AP- sensitive, transient, fast activating/inactivating K^+ current (I_A), 2) a 4-AP insensitive more slowly inactivating component ($I_{K,ST}$, see Wüstenberg et al., 2004), 3) a sustained, virtually non inactivating K^+ current ($I_{K(V)}$), and 4) a Ca^{2+} dependent outward current ($I_{O(Ca)}$). The four currents had differential, concentration-dependent sensitivity to standard pharmacological tools such as 4-AP and TEA, and had differences in their activation and inactivation properties.

Transient K^+ current (I_A)   To isolate the A-type K^+ current the cells were bathed with saline containing (in M) 10^{-7} TTX, 2×10^{-2} TEA and 5×10^{-4} CdCl$_2$ to greatly reduce non-I_A currents. 4-AP has been shown (Wüstenberg *et al.*, 2004) to be an effective blocker for the fast transient potassium current in insect neurons (Fig. 3.3). The neurons were held at -60 mV. Two series of 10 mV steps between -60 and 40 mV were delivered. The first series had a 500 ms pre-step to
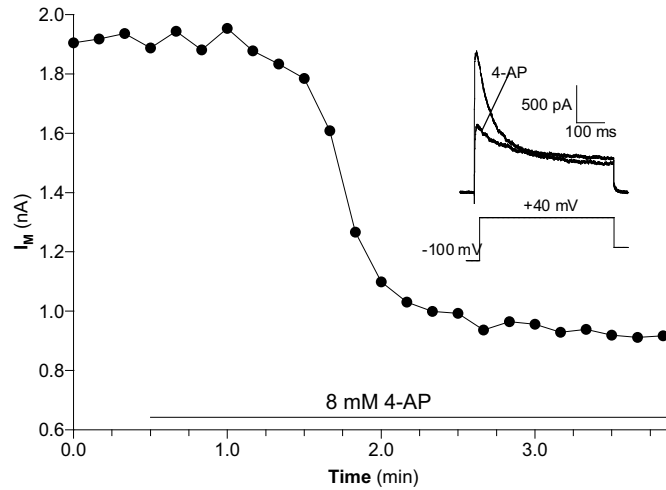
Figure 3.3: Separation of 4-AP sensitive and insensitive current. Bath application of 8 x $10^{-3}M$ 4-AP halved after 2 minutes the maximum current. The 4-AP insensitive portion of the current shows still some inactivation and was dubbed as $I_{K,ST}$.

-100 mV to maximally deinactivate I_A (3.4A). The second series had a pre-step to -30 mV, where I_A is almost entirely inactivated, and evoked residual non-I_A-currents were evoked (Fig. 3.4B).These were digitally subtracted from the first series, resulting in 'pure' I_A (Fig. 3.4C). I_A started to activate at voltages above -40 mV. This current was transient and decayed with a single time constant (at 0 mV: $\tau = 42 \pm 5$ ms; $n = 11$) during a maintained depolarization. Once inactivated, the inactivation had to be removed by hyperpolarization prior to new activation. The peak currents evoked by each voltage pulse (Fig. 3.4E and F) were used to construct the conductance/voltage (G/V) relation (assuming $E_K =$ -98.5 mV). These curves showed typical voltage dependence for activation of I_A, and were fit to a first order Boltzmann relation (*Eq. 1*; Fig 3.4G). This fit showed a half-maximal activation of the peak current ($V_{0.5_{act}}$) at -13 $\pm$ 4 mV ($s = 12.1 \pm 1.7$; $n = 11$). The maximal conductance determined from the Boltzmann fits was 8.2 $\pm$ 1.4 nS, which was reached around 30 mV. Given a mean whole-cell capacitance of 3.3 $\pm$ 1 pF ($n = 11$), this corresponds to a mean conductance density of 2.6 $\pm$ 0.6 nS pF^{-1} (26 $\pm$ 6.2 pS mm^{-2}). The mean peak current at 40 mV was 1.1 $\pm$ 0.2 nA ($n = 11$; Fig. 3E), corresponding to a mean current density of 360 $\pm$ 100 pA pF^{-1} (3.6 $\pm$ 1 pA mm^{-2}; Fig. 3.4F). Steady state inactivation of I_A was measured from a holding potential of -60 mV (Fig. 3.4D). The voltage pre-steps were delivered at 10 mV increments from -100 mV to 20 mV, followed by a test pulse to 40 mV.

Steady state inactivation began at pre-pulse potentials around -80 mV and

increased with depolarization of the pre-pulse. The *G/V* relation (Fig. 3.4G) was constructed from the data in Fig 3.4D. This curve was well fit by a first order Boltzmann relation (*Eq. 1*), with a voltage for half maximal inactivation ($V_{0.5_{inact}}$) of -56 $\pm$ 5 mV ($s = 8.6 \pm 0.9$; $n = 11$).
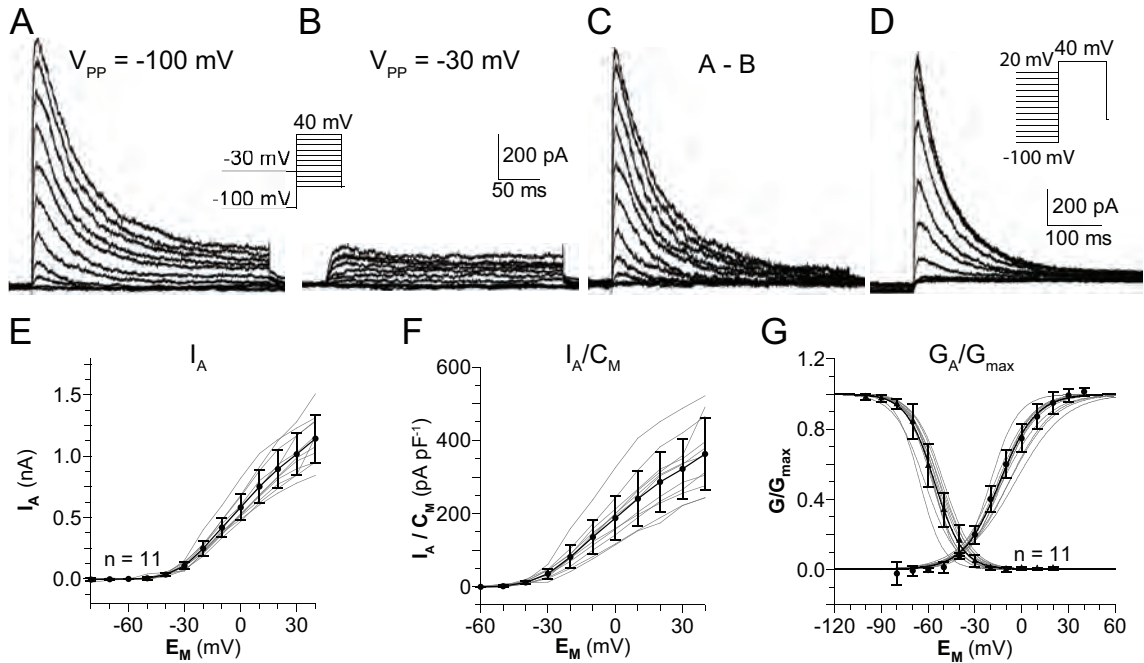
fast transient K$^+$ current (I$_A$)

Figure 3.4: Transient Potassium current (I_A). (A-D) Example current traces for steady state activation and inactivation. The holding potential was -60 mV. (A) Current traces for steady state activation elicited by 300 ms depolarizing steps from -60 mV to 40 mV in 10 mV increments after a 500 ms prepulse to -100 mV. (B) Current traces for steady state activation elicited by the same depolarizing steps as in A, but after a different prestep (-30 mV). (C) Subtraction of the traces in B from those in A yields I_A. (D) Steady state inactivation. Currents elicited by 300 ms test pulses to 40 mV that were preceded by 500 ms pulses between -100 and 20 mV in 10 mV increments. (E) I/V relationship for steady state activation of I_A. (F) Current density for steady state activation of I_A. Current density was calculated from the ratio of I_A and the cells capacitance. (G) G/V curves for steady state activation (circles) and inactivation (triangles). Conductances were calculated assuming a potassium equilibrium potential (E_K) of -98.5 mV. Values are expressed as a fraction of the calculated maximal conductance. The curves are fits to first order Boltzmann relations (Eq. 1) with the following parameters: $G_{Max} = 8.2 \pm 1.4$ nS. Steady state activation: $V_{0.5_{act}} = -13 \pm 4$ mV; $s_{act} = 12.1 \pm 1.7$. Steady state inactivation: $V_{0.5_{inact}} = -56 \pm 5$ mV; $s_{inact} = 8.6 \pm 0.9$; n = 11 (grey: individual cells; black: mean $\pm$ SD).

4-AP insensitive currents

To isolate voltage dependent and 4-AP insensitive outward currents the preparations were bathed with saline containing (in M) 10^{-7} TTX, 4 x 10^{-3} 4-AP and 5 x 10^{-4} CdCl$_2$. The neurons were held at -60 mV and two series of 300 ms volt-

age steps between -60 and 40 mV in 10 mV increments were delivered. The first series was preceded by a 500 ms voltage pulse to -100 mV to maximally deinactivate voltage dependent 4-AP resistant currents (Fig. 3.5A). The second series prepulse potential was -30 mV and evoked a very slowly or non-inactivating outward current, $I_{K(V)}$ (Fig. 3.5B). $I_{K(V)}$ was digitally subtracted from the first series, which additionally possessed an inactivating current. The difference current (Fig. 3.5C and D), which activates faster than $I_{K(V)}$ and inactivates significantly slower than I_A, was named $I_{K,ST}$ (Wüstenberg *et al.*, 2004).

Slow inactivating K$^+$ current ($I_{K,ST}$) $I_{K,ST}$ started to activate at membrane potentials more depolarized than -25 mV (Fig. 3.5C,E and F). The *G/V* relation for activation had a half-maximal voltage ($V_{0.5_{act}}$) of -9.3 $\pm$ 7.8 mV (s = 10.4 $\pm$ 3; n = 11; Fig. 3.5G). The maximal conductance determined by the Boltzmann fits was 5.9 $\pm$ 3.6 nS and was reached around 40 mV. Given a mean whole-cell capacitance of 3.8 $\pm$ 0.7 pF (n = 11), this corresponds to a conductance density of 1.3 $\pm$ 0.3 nS pF^{-1} (13 $\pm$ 3 pS mm^{-2}). The peak current at 40 mV was 760 $\pm$ 410 pA (n = 11; Fig. 3.5E) corresponding to a mean current density of 200 $\pm$ 90 pA pF^{-1} (2 $\pm$ 0.9 pA mm^{-2}; Fig. 3.5F). During a maintained depolarizations $I_{K,ST}$ decayed with a single time constant (at 0 mV: τ = 103 $\pm$ 30 ms; n = 7), which was significantly slower than in I_A (P = 0.001, n = 7, unpaired t-test). This inactivation could be removed by hyperpolarization. Steady state inactivation curves were obtained by measuring the peak current elicited by a voltage pulse to 40 mV, which was preceded by 500 ms pulse incrementing in 10 mV steps from -120 to 0 mV (Fig. 3.5D and G). Steady state inactivation began at pre-pulse potentials around -90 mV. The voltage for half-maximal inactivation ($V_{0.5_{inact}}$) was -50 $\pm$ 5 mV (s = 13.2 $\pm$ 2.3; n = 6; Fig. 3.5G).

Sustained K$^+$ current ($I_{K(V)}$) $I_{K(V)}$ activated with voltage steps above -30 mV (Fig. 3.5B, H and I). The current was sustained and showed little or no decay during a maintained depolarizing voltage step. The *G/V* relation for activation showed a typical voltage dependence for $I_{K(V)}$ with a voltage for half-maximal activation ($V_{0.5_{act}}$) of 0 $\pm$ 4.6 mV (s = 13.2 $\pm$ 1.5; Fig. 3.5J). The maximal conductance of 4.8 $\pm$ 1.3 nS was reached around 50 mV. Given a mean whole-cell
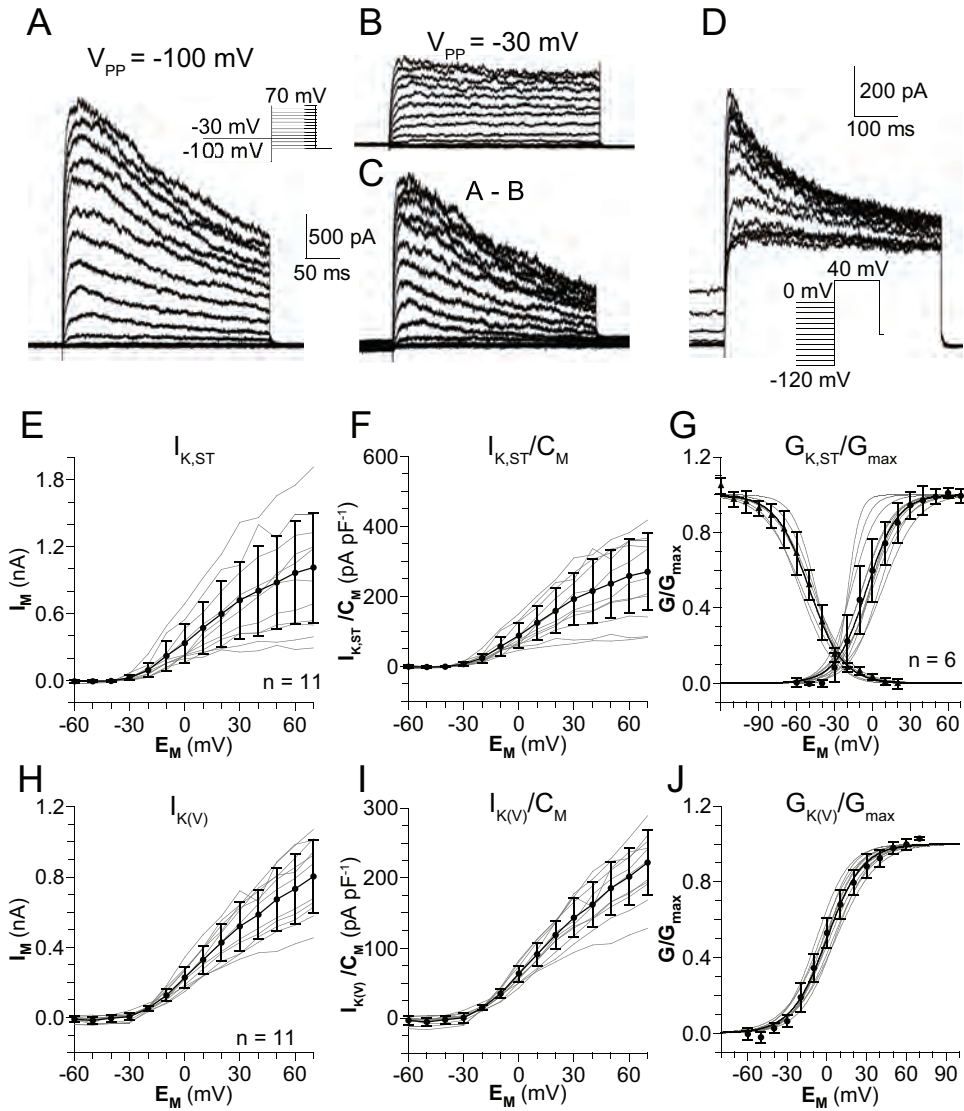
4-AP insensitive K⁺ currents ($I_{K,ST}$ and $I_{K(V)}$)

Figure 3.5: 4-AP insensitive voltage activated potassium currents *($I_{K,ST}$ and $I_{K(V)}$). (A-D) Example current traces for steady state activation and inactivation of $I_{K,ST}$. The holding potential was -60 mV. (A) Activation was elicited by 300 ms depolarizing voltage steps from -60 to 70 mV in 10 mV increments after a 500 ms prepulse to -100 mV. (B) Current traces elicited by the same depolarizing steps as in A, but after a pre-step to -30 mV. (C) Subtraction of the traces in B from those in A yields $I_{K,ST}$. (D) Steady state inactivation. Currents elicited by 300 ms test pulses to 40 mV that were preceded by 500 ms pulses between -120 and 40 mV in 10 mV increments. (E) I/V relation for steady state activation of $I_{K,ST}$. (F) Current density / voltage relationship for steady state activation of I_A. Current density was calculated as in Fig. 3.4.(G) G/V curves for steady state activation and inactivation of $I_{K,ST}$, calculated as in Fig. 3.4. Mean G/V relation for steady state activation (circles) and inactivation (triangles) of $I_{K,ST}$ were fit to a Boltzmann relation (Eq. 1) with the following parameter: $G_{K,ST_{Max}} = 5.9 \pm 3.6$ nS. Steady state activation: $V_{0.5_{act}} = -9.3 \pm 7.8$ mV; $s_{act} = 10.43 \pm 3$; n = 11. Steady state inactivation: $V_{0.5_{inact}} = -50 \pm 5$ mV; $s_{inact} = 13.2 \pm 2.3$; n = 6. (H) I/V relation for steady state activation of $I_{K(V)}$. (I) Current density for steady state activation of $I_{K(V)}$. (J) G/V relation for steady state activation of $I_{K(V)}$ with the following parameters: $G_{K(V)_{Max}} = 4.8 \pm 1.3$ nS. Steady state activation: $V_{0.5_{act}} = 0 \pm 4.6$ mV; $s_{act} = 13.2 \pm 1.5$; n = 11 (grey: individual cells; black: mean $\pm$ SD).*

capacitance of 3.8 ± 0.7 pF ($n = 11$), this corresponds to a mean conductance density of 1.6 ± 0.6 nS pF^{-1} (16 ± 6 pS mm^{-2}). The mean peak current at 50 mV was 670 ± 180 pA ($n = 11$; Fig. 3.5H) corresponding to a current density of 190 ± 40 pA pF^{-1} (1.9 ± 0.4 pA mm^{-2}; Fig. 3.5I). $I_{K(V)}$ showed little or no inactivation even with depolarization lasting 1s or longer and there was no detectable voltage-dependence of steady state inactivation (data not shown).

Calcium dependent outward Current ($I_{O(Ca)}$) To record $I_{O(Ca)}$ the preparation was superfused with saline containing 10^{-7} M TTX and 4×10^{-3} 4-AP. The neurons were held at -60 mV and two series of 200 ms voltage steps were delivered in 10 mV increments between -60 and +90 mV. The second series was recorded with saline that additionally contained 5×10^{-4} M CdCl$_2$ (Fig. 3.6A and B), which completely abolished voltage activated Ca^{2+} currents (Husch *et al.*, 2008). Accordingly, under Cd^{2+} the current was drastically reduced (Fig. 3.6B) and the inverted U-shape in the *I/V* relation was eliminated (*I/V* relation not shown). The difference between the 'untreated'and the 'Cd^{2+} treated' current series was defined as a Ca^{2+}-dependent outward current with a pronounced inverted U-shaped *I/V* relation (Fig. 3.6C and D). $I_{O(Ca)}$ consisted of an inactivating and a non-inactivating component (Fig. 3.6C). $I_{O(Ca)}$ activated with voltage steps more depolarized than -20 mV (Fig. 3.6D). The maximal peak current of 2.4 ± 1 nA is reached at 25 ± 11 mV ($n = 8$; Fig. 5D,E and F) and decreased at higher voltages as the driving force for Ca^{2+} declined. Given a mean whole-cell capacitance of 4.3 ± 1.1 pF ($n = 8$), this corresponds to a mean current density of 600 ± 340 pA pF^{-1} (Fig. 3.6E). Assuming that the main charge carrier is K$^+$ this corresponds to a conductance density of 4.8 ± 2.5 nS pF^{-1} (48 ± 25 pS mm^{-2}).
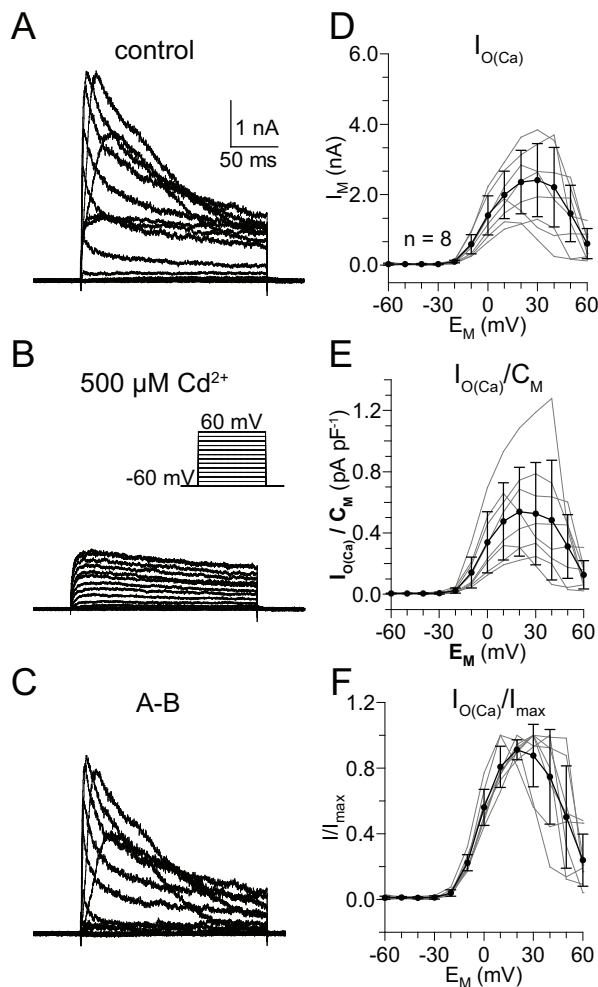
Ca^{2+} dependent outward current (I$_{O(Ca)}$)

Figure 3.6: Calcium dependent outward current (I$_{O(Ca)}$). (A-C) Current traces for steady state activation of I$_{O(Ca)}$. The holding potential was -60 mV. (A) Current traces for steady state activation elicited by 300 ms depolarizing steps from -60 mV to 70 mV in 10 mV increments. (B) Current traces elicited by the same depolarizing steps as in A, but during the application of a 500 µM Cd^{2+}. (C) Subtraction of the B traces and A traces yields I$_{O(Ca)}$. (D and E) Voltage dependence of I$_{O(Ca)}$. (D) I/V relationship of I$_{O(Ca)}$. (E) current density for steady state activation of I$_{O(Ca)}$, calculated as in Fig. 3.4. (F) I/V relation the peak I$_{O(Ca)}$ as fractions of the maximal I$_{O(Ca)}$. The graph demonstrates that I$_{O(Ca)}$ has a similar activation threshold in all recorded neurons (grey: individual cells; black: mean ± SD).

3.3.2 Inward currents

To analyze the inward currents in KCs, the outward currents were blocked by substituting the intracellular K$^+$ with Cs$^+$ and by adding 4 x 10^{-3} M 4-AP and 2 x 10^{-2} M TEA to the extracellular solution. The remaining inward current consisted of a transient, fast activating/inactivating component and a more slowly activating and inactivating component. The fast transient component was a iden-

tified as voltage activated, TTX sensitive Na^+ current, whereas the more slowly inactivating component represented a voltage activated, Cd^{2+} sensitive Ca^{2+} current.

Na^+ currents   To measure I_{Na} (Fig. 3.7) the brains were superfused with saline containing 4×10^{-3} M 4-AP, 2×10^{-2} M TEA and 5×10^{-4} $CdCl_2$ and in the pipette solution K^+ was substituted with Cs^+. T he remaining inward current could be blocked with TTX (10^{-7} M) and was reversibly eliminated, when the extracellular Na^+ was substituted with choline (Fig.3.7G). The neurons were held at -80 mV. The *I/V* relationship of the peak currents was determined by increasing voltage steps between -80 mV and 40 mV in 5 mV increments (Fig. 3.7A). I_{Na} activates and inactivates very rapidly. Once inactivated, inactivation must be removed by hyperpolarization prior to a new activation (Fig. 3.7B). I_{Na} started to activate at potentials more positive than -40 mV. The mean peak currents reached its maximum amplitude ($I_{Na_{max}}$) of -420 $\pm$ 130 pA at -6 $\pm$ 5 mV ($n = 14$; Fig. 3.7C) and decreased during more positive test pulses as Na^+ driving force declined (Fig. 3.7D and E). Given a mean whole-cell capacitance of 3 $\pm$ 0.9 pF ($n = 14$), this corresponded to a mean current density ($I_{Na_{max}} C_M^{-1}$) of -140 $\pm$ 50 pA pF^{-1} (1.4 $\pm$ 0.5 pA mm^{-2}).

Steady state inactivation of I_{Na} was measured from a holding potential of -60 mV. 500 ms voltage pre-pulses were delivered in 10 mV increments from -95 mV to 20 mV, followed by a 50 ms step to -5 mV. Steady state inactivation started at pre-pulse potentials around -70 mV and increased with the amplitude of the depolarization. The voltage for half-maximal inactivation ($V_{0.5_{inact}}$) was -48 $\pm$ 4 mV ($s_{inact} = 5.4 \pm 0.5$; $n = 9$; Fig. 3.7F).
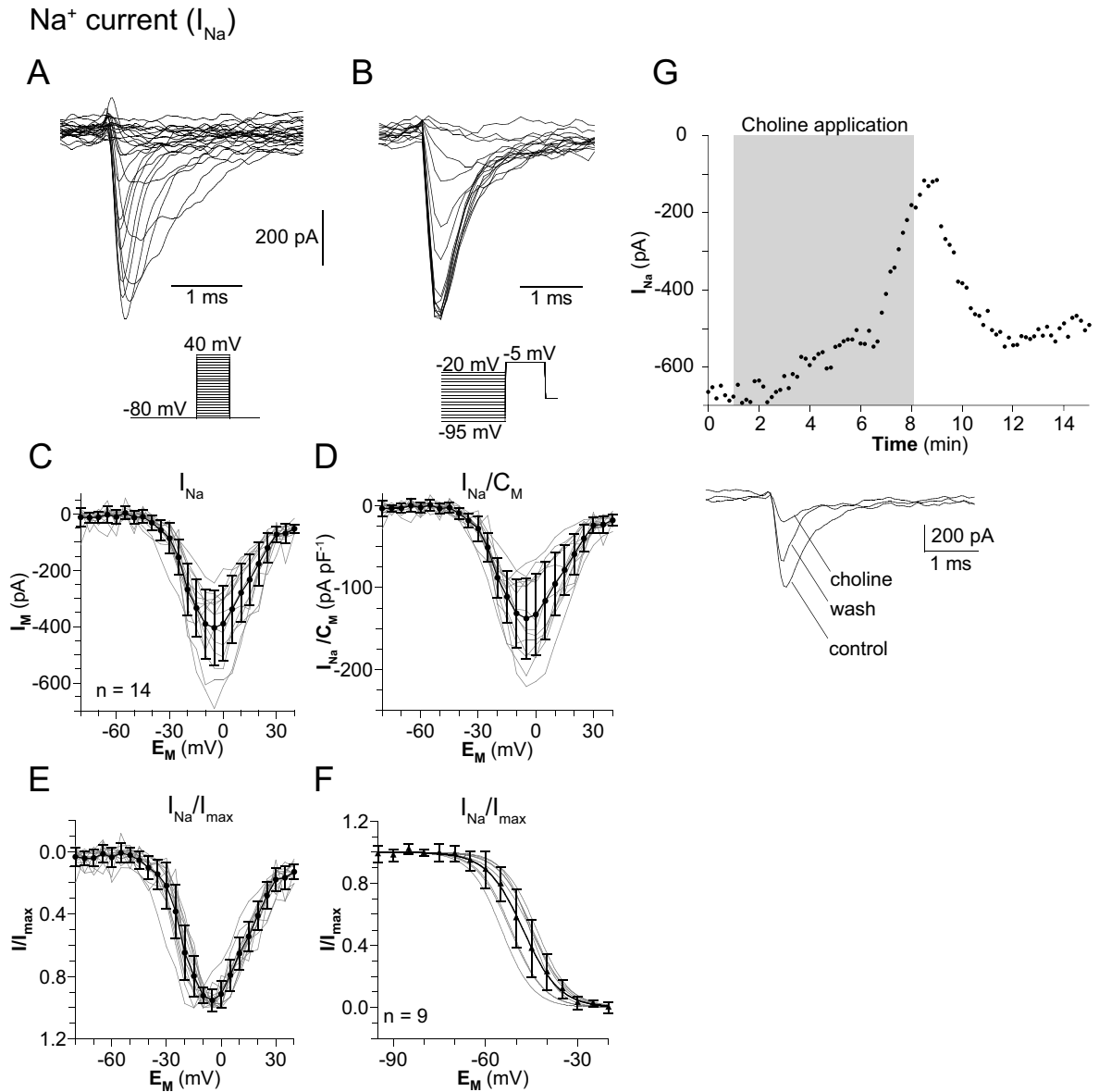
Na$^+$ current (I$_{Na}$)

Figure 3.7: Transient sodium current (I$_{Na}$). *(A and B) Current traces for steady state activation and inactivation. (A) Steady state activation elicited by 5 ms depolarizing voltage pulses from -80 to 40 mV in 5 mV increments. The holding potential was -80 mV. (B) Steady state inactivation. Currents were elicited by 5 ms pulses to -5 mV that were preceded by 500 ms pulses between -95 and -20 mV in 5 mV increments. The holding potential was -60 mV. (C) I/V relation of I$_{Na}$. (D) Current density for steady state activation of I$_{Na}$, calculated as in Fig. 3.4. (E) I/V relation of peak I$_{Na}$ normalized to the maximal current of each cell. (F) I/V relations for steady state inactivation. Curves are fits to a Boltzmann relation (Eq. 1) with the following parameters: V$_{0.5_{inact}}$ = -48 ± 4 mV with s$_{inact}$ = 5.4 ± 0.5; n = 7 (grey: individual cells; black: mean ± SD). (G)Choline substitution. The extracellular Na$^+$ was replaced for 7 min by choline chloride. The current decreased and increased when the choline chloride was washed out.*

Voltage activated Calcium Currents (I$_{Ca}$) To measure I$_{Ca}$ (Fig. 3.8) the neurons were superfused with saline containing 10^{-7} M TTX, 4 x 10^{-3} M 4-AP, and 2 x 10^{-2} M TEA. In the pipette solution K$^+$ was replaced with Cs$^+$. If not stated otherwise, the holding potential was -80 mV. The *I/V* relationship of the peak cur-

rents was determined by increasing 50 ms voltage steps between -80 mV and 30 mV in 5 mV increments (Fig. 3.8A). The voltage dependence for activation of I_{Ca} was determined from tail currents, which are independent of the changing driving force during a series of varying voltage pulses. Tail currents were evoked by 5 ms voltage steps between -80 mV and 50 mV in 10 mV increments (Fig. 3.8B). The *I/V* relation of the tail current peaks was fit to a Boltzmann relation (*Eq. 1*; Fig. 3.8G). To measure steady state inactivation 500 ms pre-pulses were delivered in 5 mV increments from -95 mV to -5 mV, followed by a test-pulse to -5 mV, and the peak currents were determined (Fig. 3.8C). The *I/V* curves were fit to a Boltzmann equation (*Eq. 1*). During depolarizing voltage steps I_{Ca} activated relatively quickly and decayed during a maintained voltage step (Fig. 3.8A and D). The activation and inactivation kinetics during a voltage step are voltage dependent (Fig. 3.8A). I_{Ca} started to activate with voltage steps more depolarized than -55 mV (Fig. 3.8A and E). The peak current reached its maximum amplitude ($I_{Ca_{max}}$) of 350 $\pm$ 80 pA at 0.6 $\pm$ 4.6 mV (*n* = 16; Fig. 3.8E,F and G) and decreased during more positive test pulses as the Ca^{2+} driving force fell (Fig. 3.8E,F and G). The *I/V* relation of the tail currents had a mean voltage for half-maximal activation ($V_{0.5_{act}}$) of -17.4 $\pm$ 3.6 mV (s_{act} = 12.7 $\pm$ 3.0; *n* = 12; Fig. 3.8G). The maximum amplitude of the tail currents ($I_{Ca,tail_{max}}$) determined from Boltzmann fits was 600 $\pm$ 160 pA (*n* = 12), which corresponded to a maximal conductance ($G_{Ca,tail_{max}}$) of 4.6 $\pm$ 1.2 nS. Given a mean whole-cell capacitance (C_M) of 3.3 $\pm$ 0.8 pF (*n* = 16), this corresponded to a mean current density ($I_{Ca,tail_{max}} C_M^{-1}$) of 190 $\pm$ 60 pA pF^{-1} (1.9 $\pm$ 0.6 pA mm^{-2}; Fig. 3.8F). Steady state inactivation started at pre-pulse potentials around -70 mV with a voltage for half-maximal inactivation ($V_{0.5_{inact}}$) of -40 $\pm$ 5 mV (s_{inact} = 10.8 $\pm$ 2.8; *n* = 12; Fig. 3.8G).

3.4 Effects of GABA blocker

To test whether tonic GABAergic input contributes to the KCs resting potential, I measured the effects of two different GABA blockers: Picrotoxin (10^{-4} M, PTX, P1675, Sigma), a $GABA_A$ receptor blocker, and CGP54626 (5 x 10^{-5} M, BN0597, Biotrend, Cologne, Germany) a $GABA_B$ receptor blocker (Fig. 3.9A and
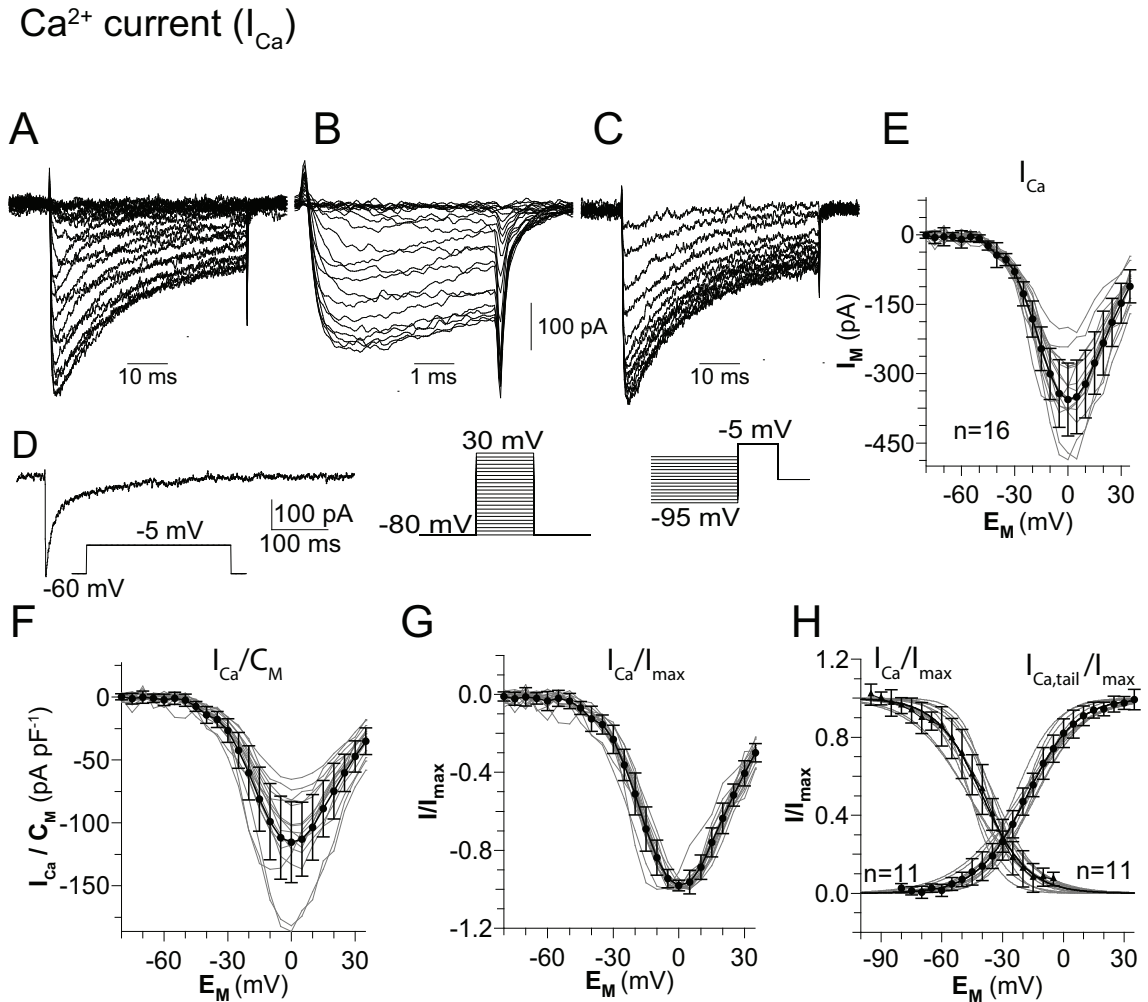
Ca²⁺ current (I$_{Ca}$)

***Figure 3.8: Calcium current** (I$_{Ca}$). (A-C) Current traces for steady state activation, steady state activation of tail currents, and steady state inactivation, respectively. (A) Steady state activation was elicited by 50 ms voltage steps from -80 to 30 mV in 5 mV increments. The holding potential was -80 mV. (B) Tail currents were elicited by 5 ms voltage steps from -80 to 30 mV in 5 mV increments. The holding potential was -80 mV. (C) Steady state inactivation. Currents elicited by 50 ms test pulses to -5 mV that were preceded by 500 ms pulses between -95 mV and -5 mV in 5 mV increments. The holding potential was -60 mV. (D) Longpulse. I$_{Ca}$ inactivated completely during a maintained (500 ms) voltage step. (E) I/V relation I$_{Ca}$. (F) Current density for steady state activation of I$_{Ca}$, calculated as in Fig3.4. (G) I/V relation of peak I$_{Ca}$ normalized to the maximal current of each cell. (H) I/V relations of steady state inactivation of peak I$_{Ca}$ (triangles) and tail current activation (circles). The curves are fits to a first order Boltzmann relation (Eq. 1) with the following mean parameters: Tail current activation: $V_{0.5_{act}}$ = -17.4 ± 3.6 mV; s_{act} = 12.7 ± 3; n = 12. Steady state inactivation: $V_{0.5_{inact}}$ = -40 ± 5 mV; s_{inact} = 10.8 ± 2.8; n = 11 (grey: individual cells; black: mean ± SD).*

B). The blockers were bath applied for at least 5 min at concentrations and have been shown to be effective in other insect olfactory systems (Wilson & Laurent, 2005). All recordings were performed with intact antennae to permit spontaneous synaptic input.

PTX blocked inhibitory synaptic potentials (Fig. 3.9C), increased the input resistance by 75 % from 2.5 ± 1.3 GΩ to 4.2 ± 1.7 GΩ ($P = 0.01$; $n = 5$; Fig. 3.9A), and depolarized the membrane potential from -61.2 ± 6.2 mV to -59.1 ± 5.3 mV ($P = 0.005$; $n = 7$; Fig. 3.9B). CGP54626 increased the input resistance by 51 % from 2.8 ± 1.3 GΩ to 4.1 ± 1.4 GΩ ($P = 0.038$; $n = 5$; Fig. 3.9A) depolarized the membrane potential from -60.7 ± 3.9 mV to -59.6 ± 4.1 mV ($P = 0.021$; $n = 8$; Fig. 3.9B). PTX treatment induced no changes in the KC neuron odor responses (Fig. 3.9D1 and D2) but combined application of both blockers induced strong changes in the odor responses. After a slight depolarization, which was comparable to the odor response during control and PTX, the KCs depolarized above threshold and elicited a burst of APs ($n = 4$; Fig. 3.9D3). The repolarization to resting potential took approximately 1 min. Combined application of both GABA blockers induced in one case spontaneous, longlasting depolarizations in the absence of odor presentations with bursts of APs and the repolarization lasts at least 1 min before the KC depolarized again ($n = 1$; Fig. 3.9E). This spontaneous bursting behavior was never observed during application of either PTX or CGP54626.

3.5 Imaging of odor evoked signals in PN boutons

The main question in this part of the study was, whether PNs act as a simple relay to higher order brain centers such as the mushroom bodies (MBs) or whether the output is modulated in an odor-specific manner. One candidate for such a modulator is GABA because the MB calyces, which are the input zones for olfactory information, are woven with GABAergic arborizations. In order to answer this question, I used patch-clamp recordings with simultaneous Ca^{2+} imaging of odor evoked signals. With patch-clamp recordings I was able to monitor the electrical activity of single PNs and hence know the information which was relayed to the MBs. I expected that the spike trains I observed at the patch pipette were
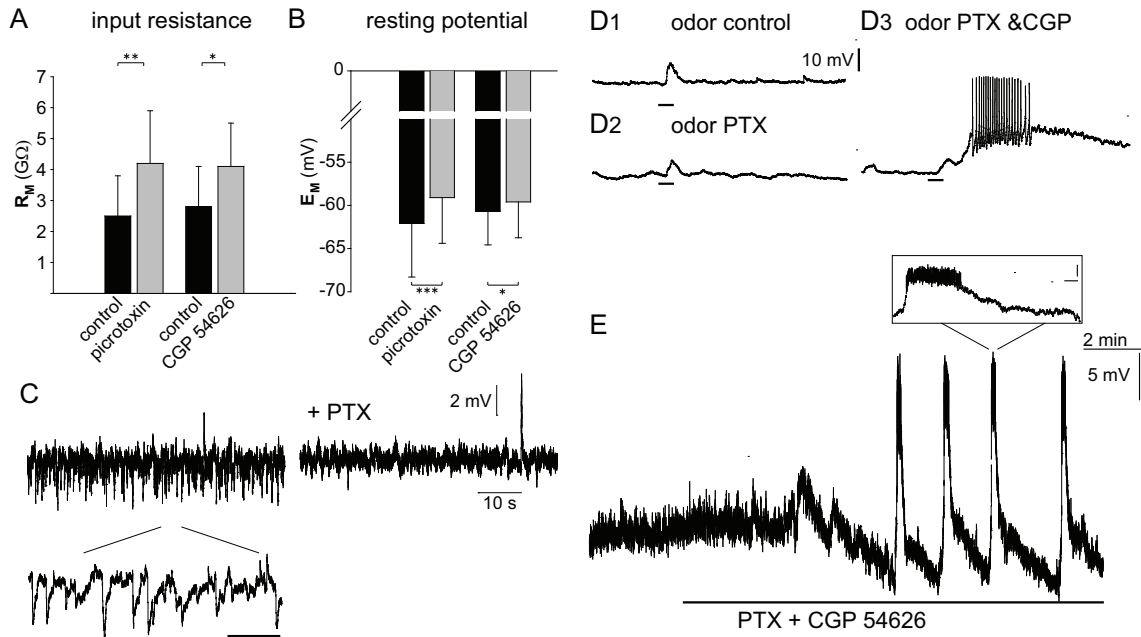
*Figure 3.9: **Effect of two GABA blockers on intrinsic electrophysiological properties.** (A) Input resistance. Bath application of 100 μM PTX increased the input resistance increased by 75 ± 45 % from 2.5 ± 1.3 GΩ to 4.2 ± 1.7 GΩ (P = 0.01; n = 5; paired t-test). 50 μM CGP 54626 increased the input resistance increased by 52 ± 35 % from 2.8 ± 1.3 GΩ to 4.1 ± 1.4 GΩ (n = 5; P = 0.038; paired t-test). (B) Resting potential. 100 μM PTX depolarized the membrane by 3.4 % from -61.2 ± 6.2 mV to -59.1 ± 5.2 significantly (n = 7; P = 0.005; paired t-test). 50 μM CGP 54626 depolarized the membrane potential from -60.7 ± 3.9 mV to -59.6 ± 4.1 mV (n = 8; P = 0.021). The resting potential was measured before and after 5 min of application. (C) Representative examples of effects of PTX. After 5 min application of PTX the IPSPs where dramatically reduced. (D) Effect of GABA blockers on odor responses. (D1) Control. KC responded to the odor mixture with graded depolarization. (D2) PTX treatment. KC responded similar to odor mixture as shown in D1. (D3)Combined application of PTX and CGP 54626. After graded depolarization the KC depolarized further beyond threshold and elicited a burst of APs. Repolarization took approximately 1 min. (E) Spontaneous depolarization with bursts of APs and slow repolarization. Inset: Enlargement of single depolarization. Scale bar vertical: 5 mV; scale bar horizontal: 10 s.*

relayed to the boutons unmodified, which are the output regions of the PNs. If this output was not altered by any modulator, all boutons should have shown the same response for a single odor, and by comparing different odors the ratios of the responses should have been the same. In contrast, if modulation did occur and if it was is driven by GABAergic circuits within the calyces, application of The GABA$_A$ blocker PTX should have abolished the differences between different boutons. In the following I define the different parameters which were used to analyze the odor evoked Ca^{2+} signals in the boutons.

3.5.1 Analysis methods

The study is based on recordings of 46 PNs, of which I show 3 examples. Due to the challenging experimental conditions (recording times > 2h; odor-responsiveness; drug application; photo-damage, etc.) these examples are three of the rare cases in which single PNs were simultaneously recorded and the output at the synapses were monitored.

    All neurons were held at hyperpolarized levels ($\sim$ -100 mV) for 1.5 h to enhance dye loading of Alexa568 and the calcium indicator OGB-1. When the fluorescent dye OGB-1was easily detectable (usually after 1.5 h) up to 11 odors were applied on the ipsilateral antenna for 500 ms each (control measurements). The fluorescence of the boutons was measured with a CCD imaging system. After the control measurement the whole brain was superfused for at least 10 min with saline containing 100 μM PTX. The odor application was repeated while the order of the odors was changed randomly. The fluorescence recordings were analyzed as shown in Fig. 3.10. The Alexa568 fluorescence image was used to identify the boutons with regions of interest (white ovals in Fig. 3.10A). The background fluorescence F$_0$ of the calcium indicator was then taken from 10 frames before the odor onset (Fig. 3.10B). During a 500 ms current injection the fluorescence increased (F$_1$; Fig. 3.10C). The background fluorescence was subtracted from the images taken during the stimulation and divided by the background fluorescence resulting in relative change in fluorescence (ΔF/F$_0$; 3.10D). The response patterns to odors were analyzed in the same way. Additionally the following parameters were extracted from the data:

- **Image sequences**. For every recording of the fluorescence increase in the boutons, the $\Delta F/F_0$ images were calculated over 600 - 850 ms after odor onset (as described above). To reduce noise level 2 - 5 of these single images were averaged resulting in 6 images. Each image now represented an interval of 100 -150 ms. To enhance the contrast the color codes were set to the same level during the control and during PTX, respectively. An example of this data processing is shown in Fig. 3.10E. The image sequences of the three presented PNs are shown in Figs. 3.12, 3.18, 3.24, respectively.

- **Color coded intensities of identified boutons over time.** Ca^{2+}-signals from identified boutons, were obtained from regions of interests (ROIs) defined on the Alexa 568 image. To remove background from these signals, first the decay of the signals were fit with a biexponential function omitting the period of Ca^{2+} influx. Then the whole kinetics were divided by the fit, resulting in a relative signal normalized to 1 ($\Delta F/F+1$). By application of this procedure the decay induced by bleaching effects can be dynamically removed. Therefore the resulting relative fluorescence changes are more precise than those obtained with a static removed background. The intensities of each signal were then color coded (see Fig. 3.10F). In this way a false color coded image was obtained for each odor, where the x-axis represents time, each row along the y-axis represents the a single bouton and the color represents intensity. In addition to the fluorescence changes of the boutons, the associated electrophysiological signal was displayed for each odor.
The color coded intensities of identified boutons over time of the three presented PNs are shown in Figs. 3.13, 3.19, 3.25, respectively.

- **Analog signal of relative fluorescence changes.** The relative fluorescence signals of the color coded intensity plots (see above) were displayed as analog signals. The responses of all boutons to a single odor were superimposed. This figure allowed the direct comparison of the extremes in the odor evoked fluorescence changes (Fig. 3.10G)
The analog signals of relative fluorescence changes of the three presented PNs are shown in Figs. 3.14, 3.20, 3.26, respectively.

- **Time to peak analysis I**. From the analog signals of relative fluorescence changes (see above), the time to peak was calculated for each bouton and each odor (Fig. 3.10H). A time to peak plot was obtained for each odor, where the x-axis represents the time from stimulus onset to the peak of the signal and the y-axis represents the single boutons. This allows the direct comparison of the spatio-temporal pattern evoked by an odor.

  The time to peak analysis I of the three presented PNs are shown in Figs. 3.15, 3.21, 3.27, respectively.

- **Time to peak analysis II.** The times to peak from the time to peak analysis I were plotted for each bouton, where the x-axis represents the different odor qualities and the y-axis represents the time to peak (Fig. 3.10I). The resulting histograms show the different boutons and their individual latencies to different odors. This resulted in temporal tuning curves.

  The time to peak analysis II of the three presented PNs are shown in Figs. 3.16, 3.22, 3.28, respectively.

- **Tuning curves.** To quantify intensity differences of bouton responses, tuning curves for each bouton were obtained (Fig. 3.10J). This was done by measuring the relative fluorescence change from baseline to peak in each bouton for each odor. These were then normalized to the maximum response elicited in that bouton across the number of tested odors. For instance a putative bouton which responded to odor A with a relative fluorescence change ($\Delta F/F$) of 5 %, to odor B with 8 % and to odor C with 10 % would have a tuning curve: C 100 % , B 80 % and A 50 % of max. Tuning curves allowed an easy comparison of intensities between boutons. The resulting histograms mirror a spatial intensity mosaic.To estimate a comparable value for the assumed inhomogeneity between the boutons I calculated the mean standard deviation for each odor across the identified boutons. If odor tuning across the boutons is similar the mean standard deviation should be low and for great differences between the boutons it should be large (Fig. 3.10J).

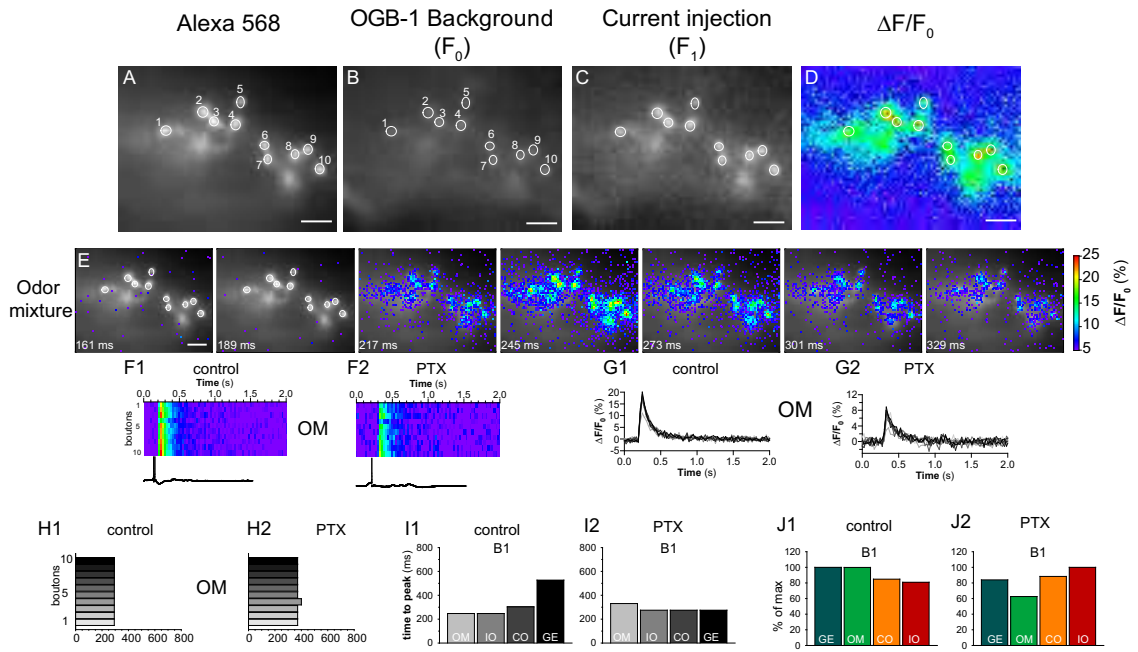 The tuning curves of the three presented PNs are shown in Figs. 3.17, 3.23, 3.29, respectively.

Figure 3.10: Analysis of the odor evoked signals. *(A) Image of the boutons filled with Alexa 568 exited at 570 nm. Picture was collected at the end of the experiments. The white circles depict the selected boutons. (B) OGB-1 background image. Average intensity of 10 frames before stimulation. (C) Fluorescent image during current injection scaled to the same maximum as in B. (D) Color coded image of the relative fluorescence increase. (E)Temporal sequence of odor mixture induced fluorescence changes. Response started 217 ms after the odor onset and decayed over time. (F) Color coded intensities of identified boutons over time. Example for single odor (odor mixture) each row represents a single bouton. (G) Analog signal of relative fluorescence changes. Example for single odor (odor mixture). Each line represents the analog signal of a single bouton. (H) Time to peak analysis I. Example for single Odor (odor mixture). Y axis represents the boutons and the x-axis represents the time to peak. (I) Time to peak analysis II. Example for single bouton showing the time to peak of different odors. The x-axis represents the different odors while the y-axis represents the time to peak. (J)Tuning curves.Example for a single bouton. Scale bar : 10 µm*

3.5.2 PN morphology

All presented PNs are uniglomerular PNs. These neurons received input from a single glomerulus and projected via the iACT to the calyces of the mushroom bodies and the lateral lobe of the protocerebrum (Fig. 3.11). In the mushroom bodies each PN branched and ramified within the upper rim of the calyces. The varicosities at the LLP were never observable during the experiments. Usually, 6-13 boutons in the medial calyx were simultaneously imaged during one experiment. The position of the recording chamber and the focus plane were never changed during the experiments to allow a comparison between control and PTX application.
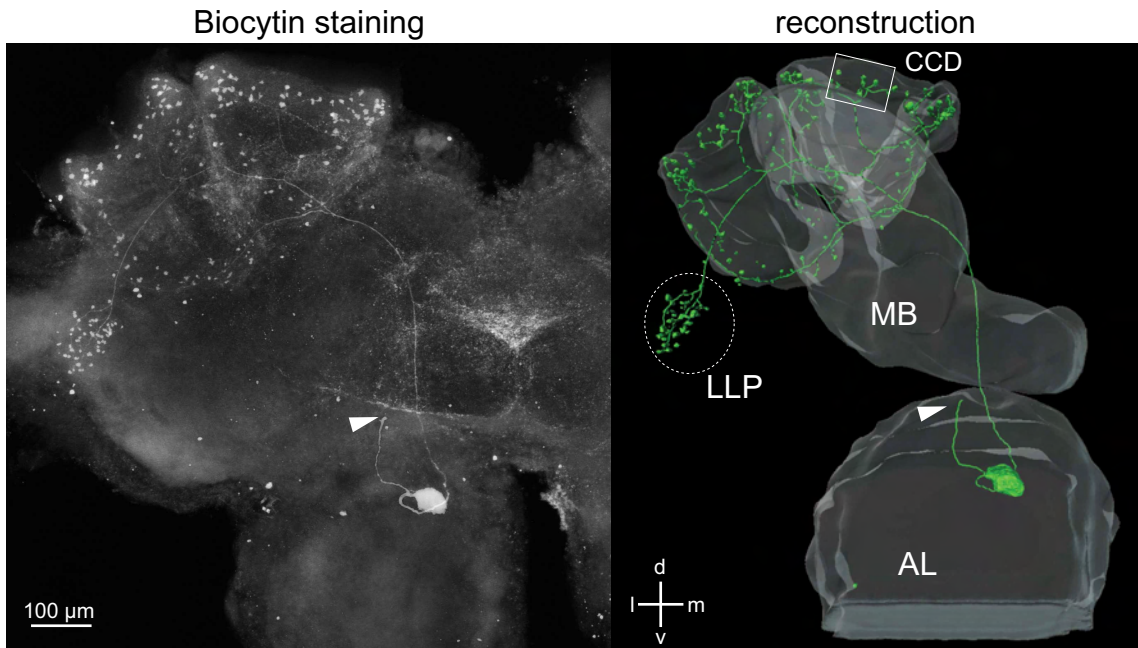
Figure 3.11: PN morphology. *(A) Biocytin staining as standard deviation projection. The PN soma was located at the tip of the arrowhead, but was lost during processing. The PN has its input side in the massively stained glomerulus and projects via the iACT to the calyces of the MB and to the lateral lobe of the protocerebrum. (B) 3D reconstruction of the PN (green) and the different neuropils (light grey).*

3.5.3 Example PN1

Image Sequences (Fig. 3.12)   Each image of the sequence in Fig. 3.12 represents an 130 ms interval. All odors elicited an progressive increase from the second interval. Same onset was observed during PTX application. During control the fluorescence signals developed differentially depending on the applied odor. The sharpest response was seen to the odor mixture (OM) and the most delayed to 1-hexanol (HX). Every other odor evoked an intensity pattern across all boutons which developed uniquely during the control and more uniformly during PTX. Geraniol (GE), 1-hexanol and citronellal (CO) evoked the strongest absolute response during the control regardless of the order of the presentation. During PTX all odor evoked response intensities were very similar but benzaldehyde (BA) induced only a weak response. For the following analysis 13 distinguishable boutons were identified by the Alexa568 image.

Color coded intensities of identified boutons over time (Fig. 3.13)   In general, the temporal patterns of activity in the boutons agree with the spike trains

recorded from the cell body. However, in a few cases this is not so, pointing to-
wards a possible modulation of individual boutons. One characteristic of PNs
is an elaborate odor response pattern with periods of excitation and inhibition,
which can exceed the odor pulse for seconds. For this PN no inhibition was ob-
served, which might be caused by the slightly hyperpolarized membrane poten-
tial. The response period to odor mixture was very short among all boutons and
did not exceed the odor pulse, except for geraniol and 1-hexanol where the re-
sponses were long lasting and exceeded the odor pulse.

Spike timing appears to be essential for the response in the boutons. While
high frequency spikes as apparent at α-ionone (IO) or in the beginning of 1-
hexanol elicited no high calcium fluorescent increases, lower frequencies as cit-
ronellal or in the end of 1-hexanol elicited higher fluorescence transients. This
phenomenon was even more pronounced after the application of PTX. Here high
frequency spike rates elicited nearly no, as at geraniol, or only small changes in
fluorescence as at 1-hexanol. Generally, the spiking patterns and fluorescence
responses were more similar for the different odors after PTX application. Inter-
estingly, although PTX reduced the spikes elicited to benzaldehyde the relative
fluorescence change was not considerably changed. In contrast the spiking pat-
terns to odor mixture and +/- citral (CA) were altered after PTX application, and
accordingly the fluorescence signal was also considerably changed.

Analog signal of relative fluorescence changes (Fig. 3.14) Every single line rep-
resents a single bouton. During control, the response maxima during odor mix-
ture ranged from 6 % in bouton 6 to 2 % in bouton 2. All other boutons' response

---

*Figure 3.12 (following page): Image sequence of PN1. Each image of the sequence represents an 130
ms interval (average of 2 single images). In the upper part of the panel the control recordings are displayed
and in the lower part the recordings after PTX treatment. In general the relative fluorescence increases were
doubled after PTX treatment. The temporal patterns during the control developed over the period shown
here in odor dependent manner. After PTX treatment the temporal patterns across the odors were more
common. From the ALexa5 568 image 13 distinguishable boutons were identified and depicted as ovals in
$\Delta F_1/F$ interval. OM - odor mixture; CA - +/- citral; BA - benzaldehyde; CO - citronellal; IO - α-ionone;
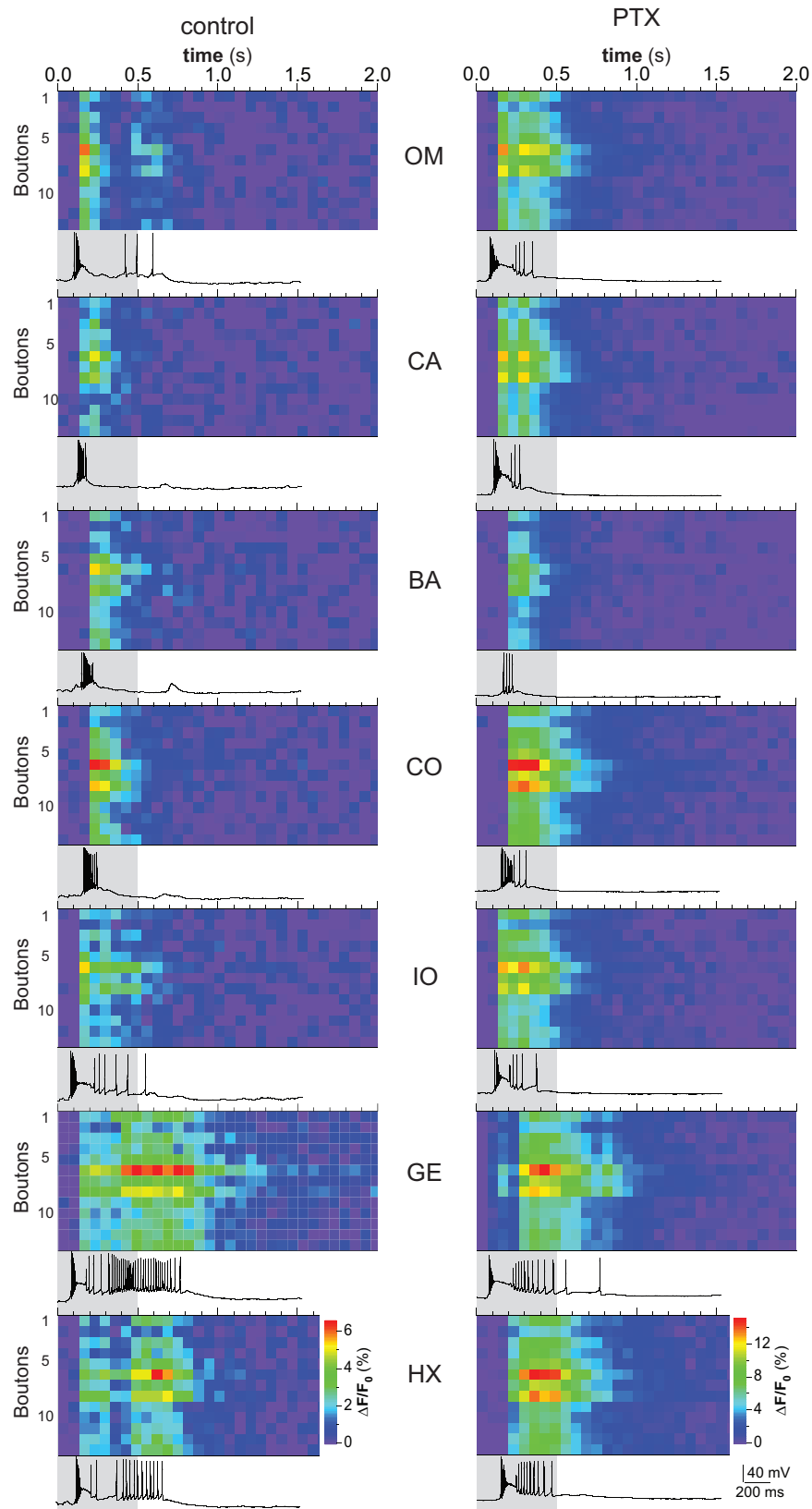GE - geraniol; HX - 1-hexanol. Scale bars 10 μm*
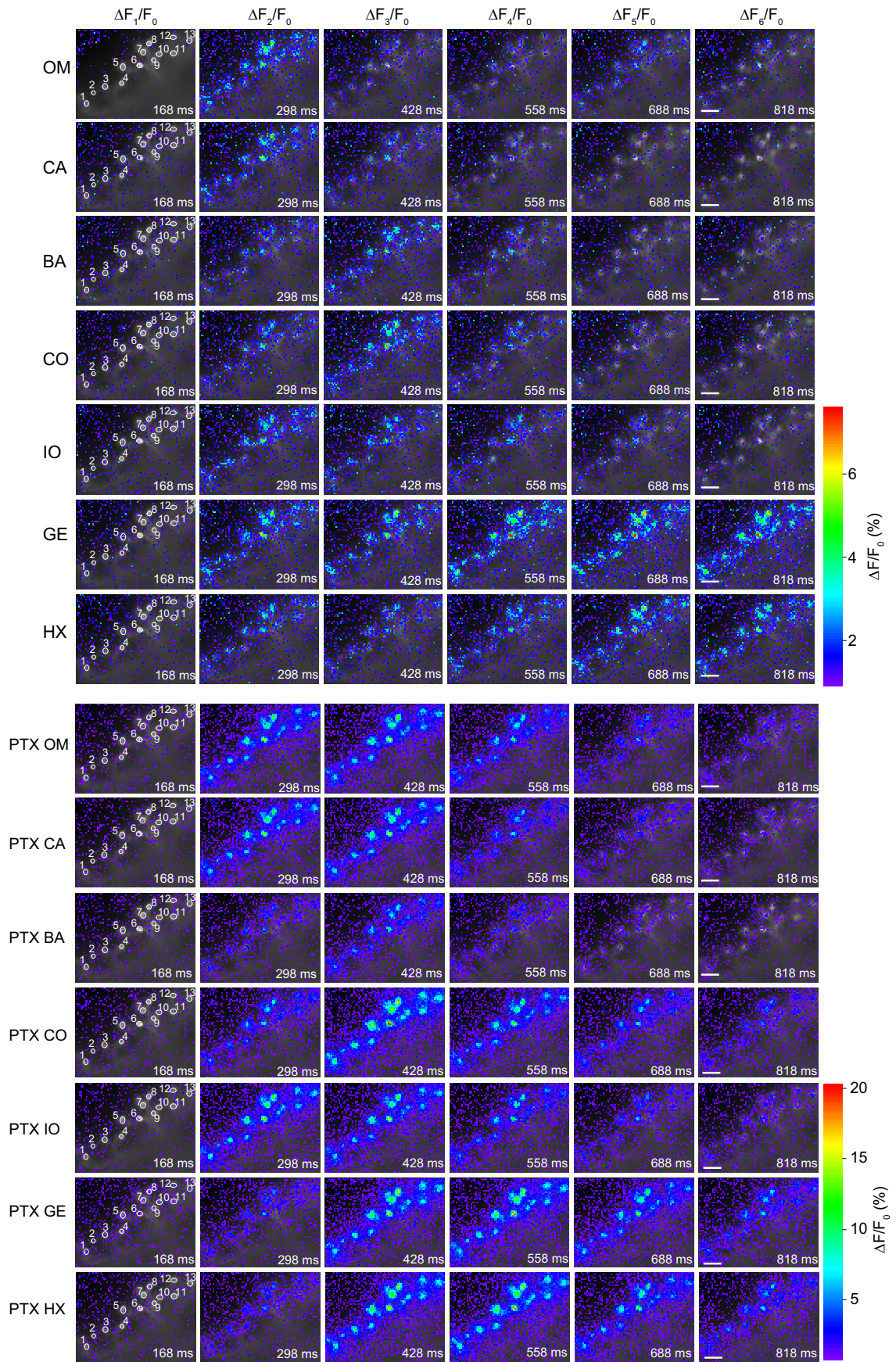
Figure 3.13: Color coded intensities of identified boutons over time of PN1. *Ca^{2+} signals of ROIs with dynamically removed background. On the left side the control recordings are shown and on the right side the according recordings after PTX treatment. In general the temporal patterns of activity agree with the recorded spike trains. During control the response patterns show differences and after application of PTX the responses were more similar. OM - odor mixture; CA - +/- citral; BA - benzaldehyde; CO - citronellal; IO - α-ionone; GE - geraniol; HX - 1-hexanol.*

intensities varied uniformly between those two extremes. The responses to +/- citral of bouton 6 and bouton 8 were considerably larger ($\sim$4.5 %) than all other boutons' response intensities (maximal 3 %) to this odor, indicating that some boutons responded stronger to some odors than other boutons did. During PTX application, all response intensities were approximately doubled. At the same time the boutons response intensities varied uniformly between the extremes. For illustration, the responses to citronellal and 1-hexanol were compared. At citronellal stimulation the most responsive bouton 6 showed a fluorescence increase of $\Delta F/F = 16$ % and the least responsive bouton 2 an increase of $\Delta F/F = 5$ %. All other boutons show increases that varied uniformly between those extremes. For 1-hexanol the distribution of the fluorescence signals was strikingly similar. In the most responsive bouton 6 the fluorescence increased also about $\Delta F/F = 15$ % and the least responsive bouton 2 responded also with approximately $\Delta F/F = 5$ %. The other boutons varied, as shown for citronellal, also uniformly between the two extremes. This uniform distribution of activity after PTX treatment continues across all odors.

Time to peak analysis I (Fig. 3.15)   The boutons were plotted over the time to peak latencies. During odor mixture stimulation, all boutons showed the same time to peak value. Also during +/- citral, benzaldehyde and citronellal the latencies of the boutons were mostly uniform. For geraniol and 1-hexanol the latency between different boutons varied a lot. For geraniol bouton 2 and 3 had the shortest latencies with 343 ms whereas boutons 8, 9 and 13 had their response maximum 400 ms later at approximately 700 ms after odor onset. During the PTX application the individual variations in bouton time to peak latencies for different odors are nearly lost. Thus, all but one bouton had their response maximum 300 ms after odor onset (for GE). It is obvious that the variations of delayed responses to geraniol and 1-hexanol converged. The spike train during the 1-hexanol-response did not change a lot from control to PTX (Fig. 3.13) but the time to peak value were altered a lot. This shows that individual boutons were potentially modulated in their time to peak latency by GABAergic inhibition and that this might be odor specific.
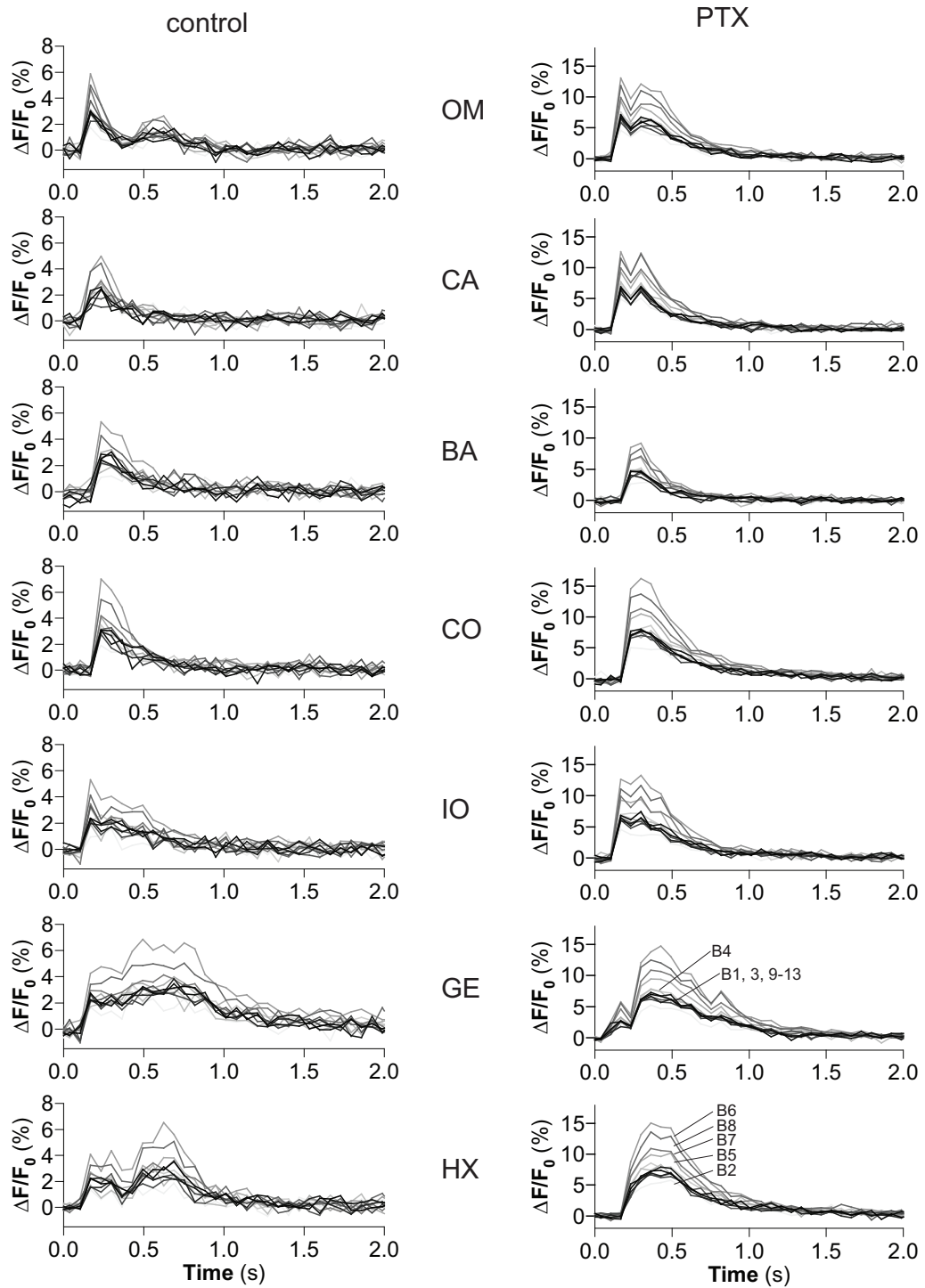
Figure 3.14: Analog signal of relative fluorescence changes of PN1. *The responses of all boutons to a single odor were superimposed. On the left hand side the recordings during control were displayed and on the right hand side the signals after PTX treatment. Each line represents a single bouton. OM - odor mixture; CA - +/- citral; BA - benzaldehyde; CO - citronellal; IO - α-ionone; GE - geraniol; HX - 1-hexanol.*
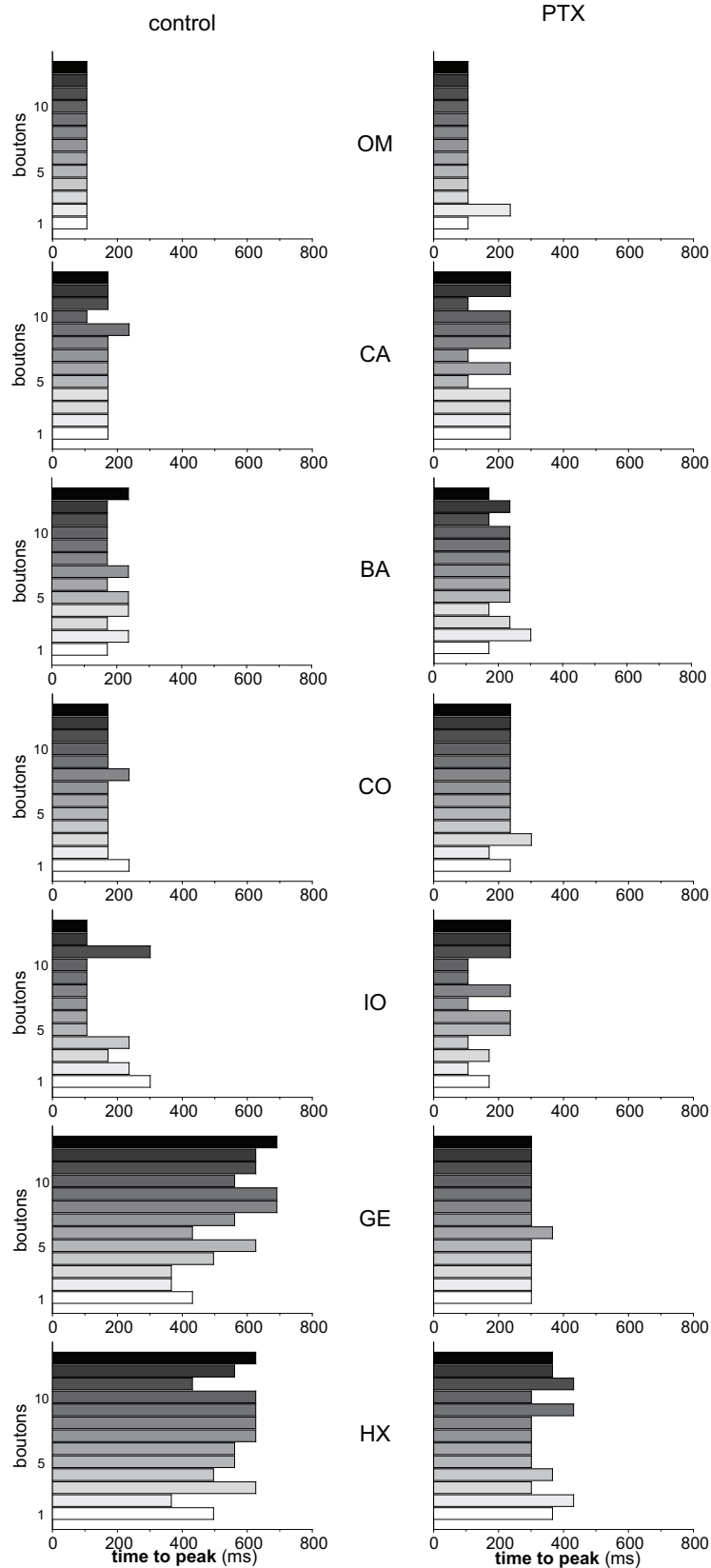
Figure 3.15: Time to peak analysis I of PN1. The time to peak of each bouton after stimulus onset was calculated. The x-axis represents the time to peak and the y-axis represents the single boutons. On the left side the controls were displayed and on the right hand side the time to peak values after PTX treatment were displayed. OM - odor mixture; CA - +/- citral; BA - benzaldehyde; CO - citronellal; IO - α-ionone; GE - geraniol; HX - 1-hexanol.

Time to peak analysis II (Fig. 3.16) The different odors were plotted against the time to peak values for each bouton. This figure illustrates that there were differences between the boutons in the absence of PTX. All boutons were fast responding to odor mixture, +/- citral, benzaldehyde, citronellal, and α-ionone and delayed to geraniol and 1-hexanol. The absolute times to peak were different in most boutons for the different odors. This is most evident for example in bouton 5 and bouton 7. Both boutons responded similar to odor mixture, +/- citral, benzaldehyde, citronellal and α-ionone but bouton 5 responded faster to 1-hexanol than to geraniol and bouton 7 responded faster to geraniol than to 1-hexanol. Only in boutons 5 and 13 did the patterns looked more or less the same. Furthermore, in bouton 1 all odors induced different latencies and in bouton 2 the time to peak was constant between the different odors. During PTX application the temporal tuning curves converged. Only small differences between the histograms of different boutons were still obvious. These results further supports the hypothesis that single boutons were individually modulated by GABA.

Tuning curves (Fig. 3.17) For each bouton, the peaks of the odor responses were expressed as a percentage of the maximum response. For example in bouton 1 geraniol was set to 100 % and in bouton 7 odor mixture was set to 100 % and accordingly all other odors were scaled to these maxima. The resulting tuning curves showed great variations among the different boutons. While citronellal in bouton 1 only led to 60 % increase, citronellal led to the strongest response in other boutons such as B6 or B8. In contrast odor mixture, which induced an 80 % change in boutons 1, 5 and 11, induced the strongest response in bouton7. In B8 only slight differences across the odors were apparent. After application of PTX these differences were nearly lost. The tuning curves of all boutons were of a similar shape and only slight differences were apparent. To illustrate the variance within relative peak responses to the different odors, I plotted the distribution of relative responses of all boutons for each odor (Fig. 3.17 bottom right). For each odor the standard deviation from the mean response intensity across all boutons was calculated. The mean standard deviation before and after application of PTX were than compared and statistically tested. For the control the variability of the
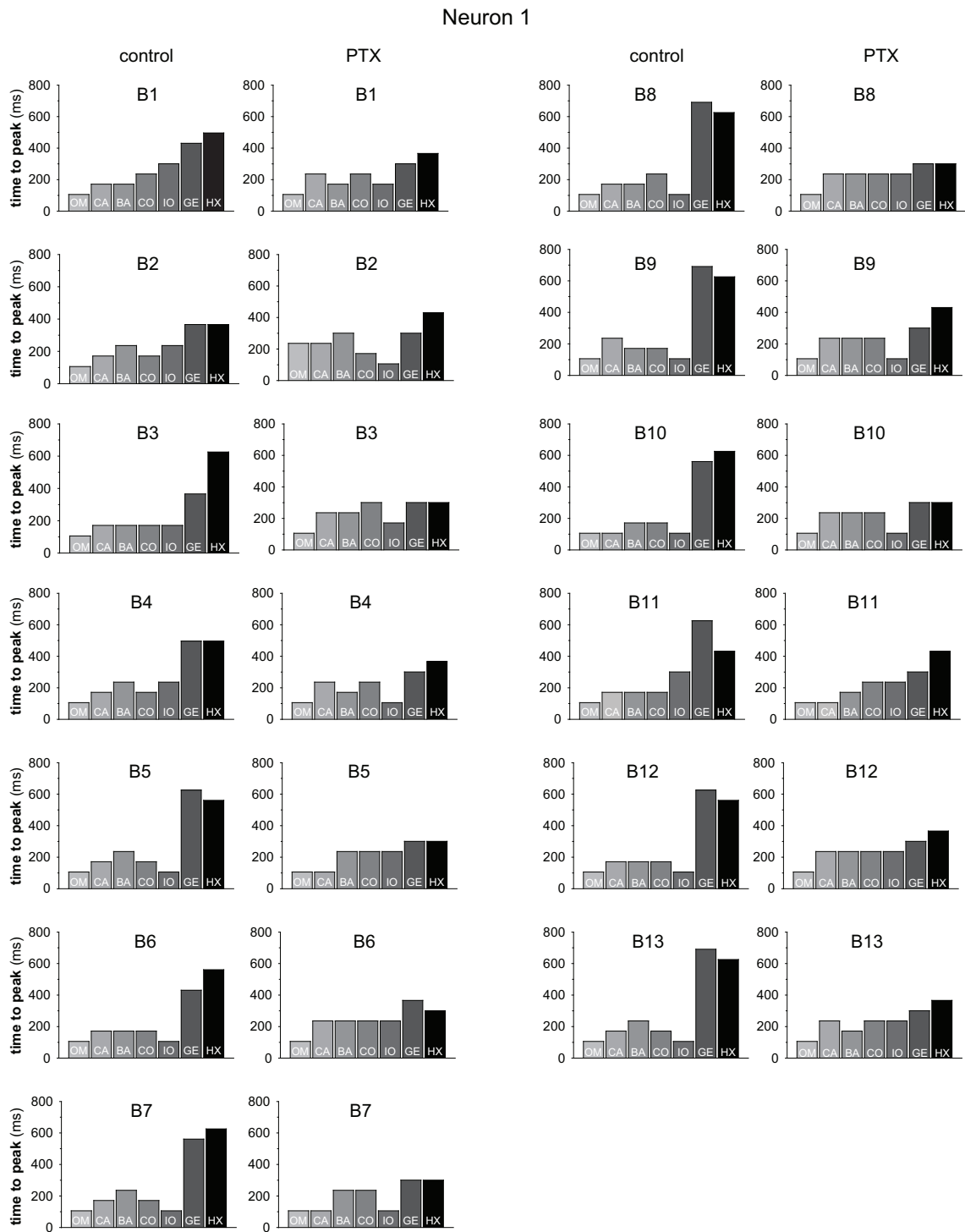
Neuron 1

Figure 3.16: Time to peak analysis II of PN1. *The time to peak value plotted for each bouton. The y-axis represents the time to peak after stimulus onset and the x-axis represents the different odors. On the left hand side the time to peak values for the control were displayed and on the right hand side the time to peak values after PTX treatment. The individual curves during control show more differences than those after PTX treatment. OM - odor mixture; CA - +/- citral; BA - benzaldehyde; CO - citronellal; IO - α-ionone; GE - geraniol; HX - 1-hexanol.*

boutons to the different odors, expressed as mean standard deviation, was quite large (10.9 $\pm$ 3.2 %), but after application of PTX this variance was significantly smaller (4.2 $\pm$ 0.6 %; P=0.002; unpaired t-test).

These results support the idea that boutons of the same neuron were individually modulated to respond individually to different odors. Figs. 3.15 and 3.16 show that the temporal patterns comprise of an odor quality and a bouton specific component. The intensity analysis in Fig.3.17 shows that the bouton specific tuning is apparently mediated by GABAergic synapses. Taken together these results boutons of PN1 form a spatio-temporal intensity mosaic to different odors.

3.5.4 Example PN2

Image sequences (Fig. 3.18) . Each image of the sequence in Fig. 3.18 represents an interval of 100 ms. The onset of the odor evoked responses were different at different stimuli during the control. For geraniol, citronellal, eugenol, benzaldehyde and α-ionone this neuron the onset was in the third interval. The other odors elicited responses starting from the second interval. After application of PTX all odors induced responses staring from the second interval, which corresponds to the latency of 243 ms. The response intensities varied during the control while only minor differences were observable during PTX application. For the following analysis 6 distinguishable boutons were identified by the Alexa 568 image.

Color coded intensities of identified boutons over time (Fig. 3.19) In general, the temporal patterns of activity in the boutons agree with the spike trains recorded from the cell body. However, in a few cases this is not so pointing towards a possible modulation of individual boutons. One characteristic of PNs is an elaborate odor response pattern with periods of excitation and inhibition, which can exceed the odor pulse for seconds. The response periods of the boutons to the odors sometimes exceeded the odorpulse but not for a long period. For example, during the response of bouton 4 to eugenol. The spike train at the cell body persisted for about 200 ms, whereas the response in the bouton lasted for approximately 600 ms. The electrophysiology shows that, a short hyperpolar-
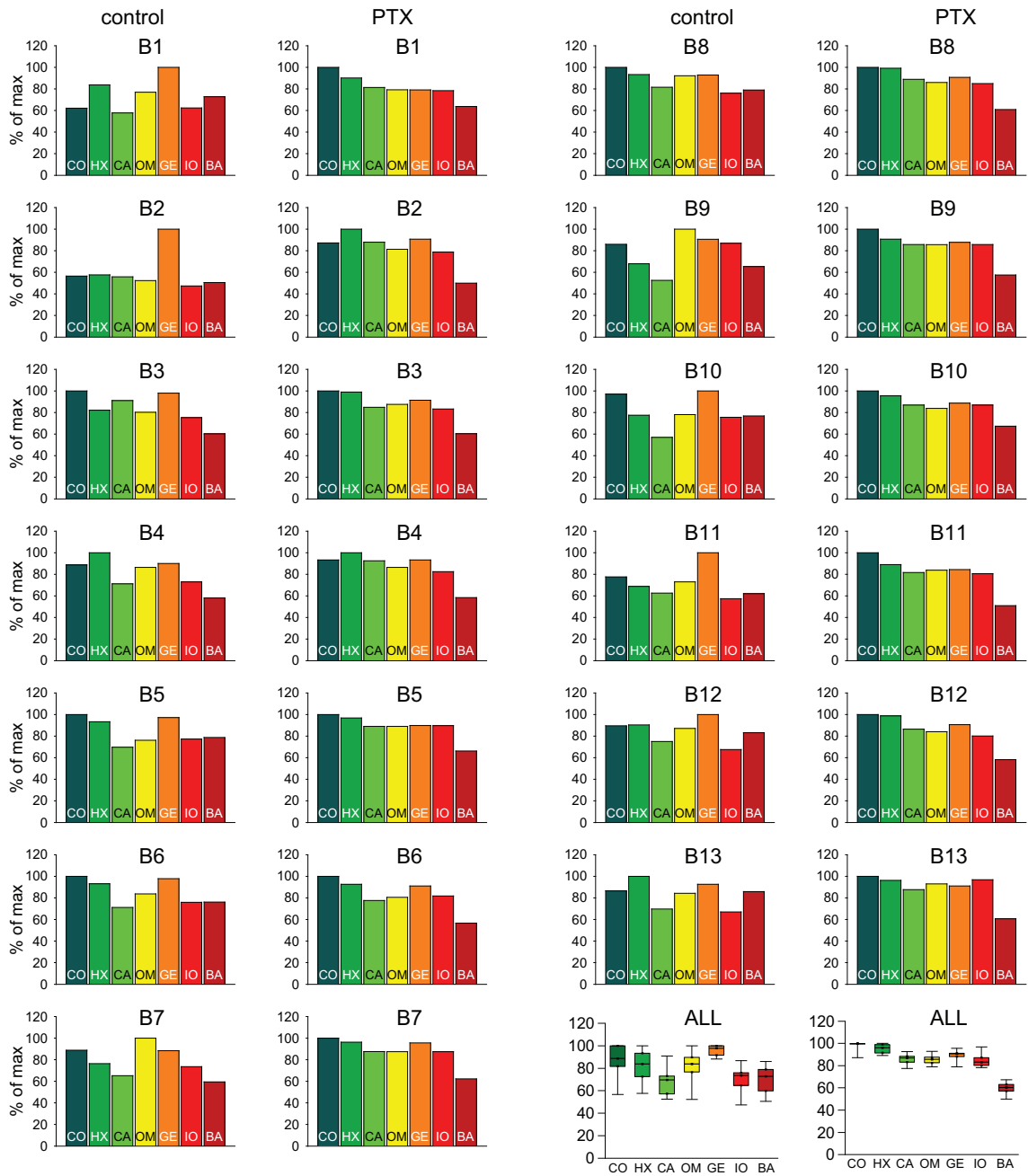
Figure 3.17: Tuning curves of PN1. *For each bouton the peak intensities were expressed as a percentage of the maximum response. To the left the tuning curves during control and to the right the tuning curves after PTX treatment were displayed. The box plot illustrates the difference within one odor. During control the tuning curves were more variable than after PTX application. This was also illustrated by the smaller boxes during PTX application in the box plot. OM - odor mixture; CA - +/- citral; BA - benzaldehyde; CO - citronellal; IO - α-ionone; GE - geraniol; HX - 1-hexanol.*
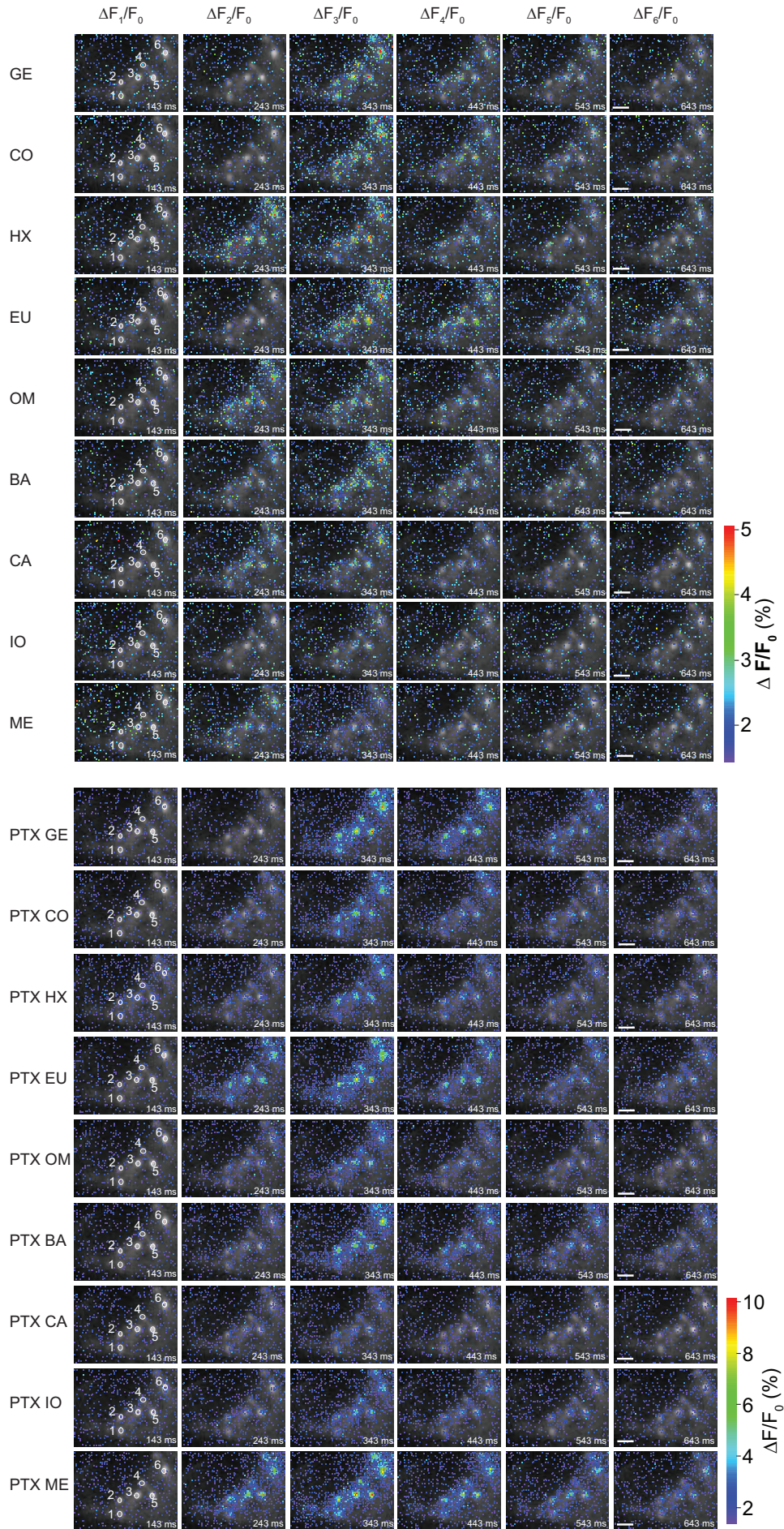
ization after 1.5 seconds was observed in response to methyl salicylate, α-ionone, geraniol, citronellal, +/- citral and 1-hexanol. After PTX treatment all odors induced a pronounced after-hyperpolarization.

Spike timing seems to be crucial for the intensity of the response. While high frequency spikes as apparent for α-ionone or methyl salicylate elicited no high calcium fluorescent increases, lower frequencies as citronellal or geraniol elicited higher fluorescence transients. This phenomenon was also present after the application of PTX. Here high frequency spike rates elicited nearly no, as for α-ionone, or only small changes in fluorescence as for 1-hexanol. After the application of PTX the general spiking changed as observed for+/- citral or methyl salicylate or stayed the same as for α-ionone. Interestingly although the spiking pattern during PTX for methyl salicylate and odor mixture were alike the odor evoked calcium signals were considerably different. Another interesting example is 1-hexanol, where the spiking pattern did not change greatly when PTX was added but the responsiveness was considerably lower during PTX.

Analog signals of relative fluorescence changes (Fig. 3.20) Every single line represents a single bouton. During control the response maxima to geraniol ranged from $\Delta F/F = 3.2$ % in bouton 4 to $\Delta F/F = 2.1$ % in bouton 5. All other boutons' response intensities varied uniformly between those two extremes. In contrast the responses to eugenol of bouton 4 and bouton 6 were considerably larger ($\Delta F/F \sim 3$ %) than the maximal response intensity of boutons 5 ($\Delta F/F \sim 1$%). During PTX application, all response intensities were approximately doubled. Simultaneously 5 of the six identified boutons showed comparable response intensities and only the response intensities of bouton 5 were considerably smaller.

Figure 3.18 (following page): Image sequence of PN2. Each image of the sequence represents an 100 ms interval resulting in an image sequence of 600 ms after stimulus onset. In the upper part of the panel the control recordings were displayed and in the lower part of the panel the recordings after PTX treatment. In general the relative fluorescence increases were doubled after PTX treatment. By means of the Alexa 568 image 6 distinguishable boutons were identified and depicted as ovals in the $\Delta F_1/F$ interval. GE - geraniol; CO - citronellal; HX - 1-hexanol; EU - eugenol; OM - odor mixture; BA - benzaldehyde; CA - +/- citral; IO - α-ionone; ME - methylsalicylate. Scale bars: 10 μm.

	$\Delta F_1/F_0$	$\Delta F_2/F_0$	$\Delta F_3/F_0$	$\Delta F_4/F_0$	$\Delta F_5/F_0$	$\Delta F_6/F_0$

GE, CO, HX, EU, OM, BA, CA, IO, ME

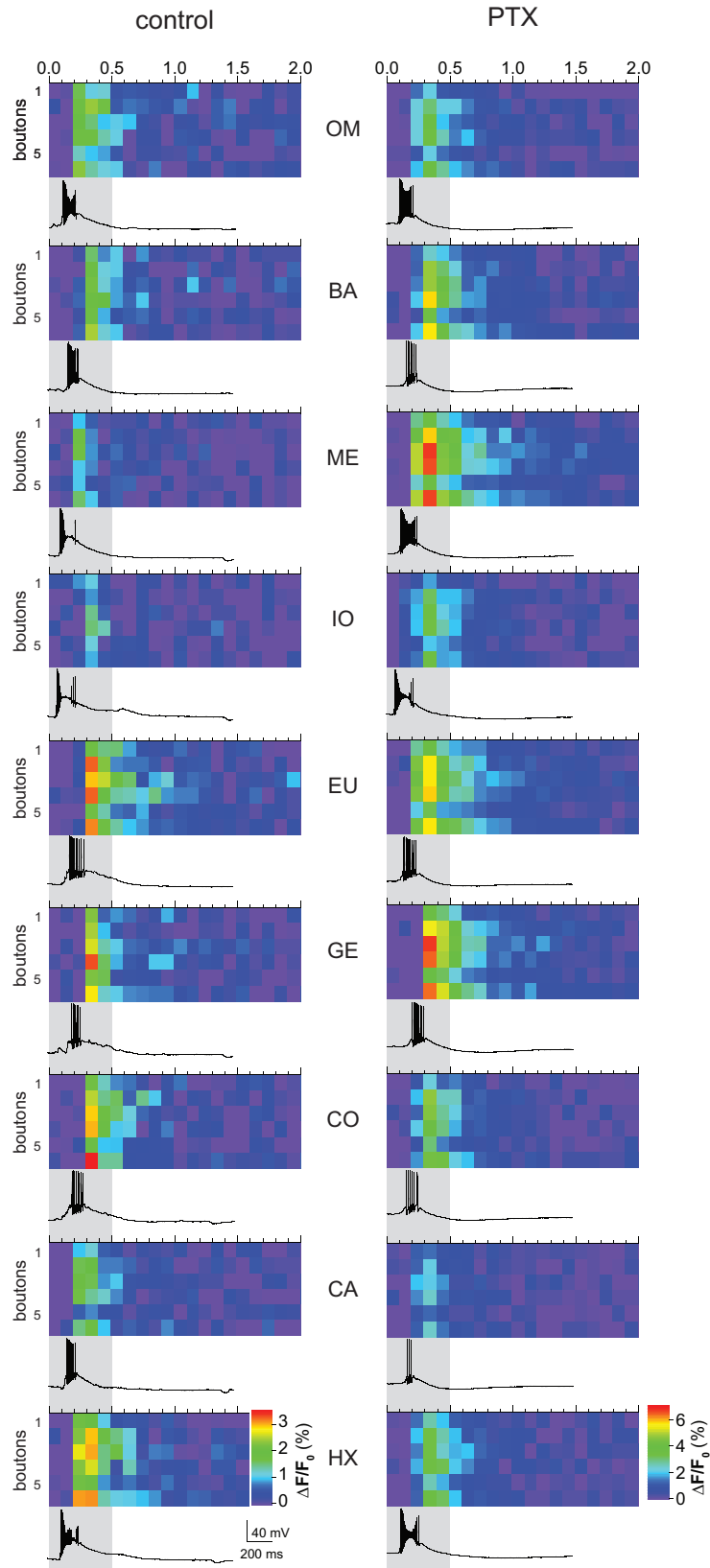PTX GE, PTX CO, PTX HX, PTX EU, PTX OM, PTX BA, PTX CA, PTX IO, PTX ME

Figure 3.19: Color coded intensities of identified boutons over time of PN2. *Ca²⁺ signals of ROIs with dynamically removed background. To the left the recordings during control and to the right the recordings after PTX treatment were displayed. In general the temporal patterns of activity agree with the recorded spike trains. GE - geraniol; CO - citronellal; HX - 1-hexanol; EU - eugenol; OM - odor mixture; BA - benzaldehyde; CA - +/- citral; IO - α-ionone; ME - methylsalicylate.*

56

For instance, during the response to methyl salicylate the most responsive bouton 4 showed a fluorescence increase of $\Delta F/F = 7\,\%$ and the least responsive bouton 5 an increase of $\Delta F/F = 4\,\%$. All other boutons show nearly the same amount of fluorescence increase. For geraniol the distribution of the fluorescence signals was strikingly similar. In the most responsive bouton 6 the fluorescence increased also about $\Delta F/F = 7\,\%$ and the least responsive bouton 5 responded also with approximately $\Delta F/F = 4\,\%$. This distribution of activity after PTX treatment continues across all odors.

Time to peak analysis I (Fig. 3.21). The boutons were plotted over the time to peak latencies. Nearly all odors elicited responses at the same time in the different boutons. Only during stimulation with odor mixture and +/- citral the latency between different boutons were somewhat variable. During the PTX application all boutons responded for either odor with the same time to peak latency. Thus all boutons had their response maximum 300 ms after odor onset.

Time to peak analysis II (Fig. 3.22). I plotted the different odors against the time to peak values for each bouton. The figure illustrates that there were almost no differences between the boutons. Bouton 1, 5 and 6 and bouton 3 and 4 show the same temporal tuning curve. After application of PTX the temporal tuning curves were even more stereotype for all boutons showing no differences.

Tuning curves. For each bouton the peak of the odor responses were expressed as a percentage of the maximum response. The resulting tuning curves showed great variations among the different boutons. While +/- citral in bouton 1 only led to 30 % increase and 40 % increase in bouton 5, +/- citral led to a stronger response in bouton 4 (70 %) and bouton 3 (65 %). In contrast geraniol, which induced an 70 % change in bouton 2 and 3, induced the strongest response in bouton 1 and bouton 5. After application of PTX these differences were nearly lost. The tuning curves of all boutons were of the same shape and only slight differences were apparent. To illustrate the variance within in the relative peak responses to the different odors, I plotted the distribution of relative responses of all boutons for each odor (Fig. 3.23 bottom). For each odor the standard deviation
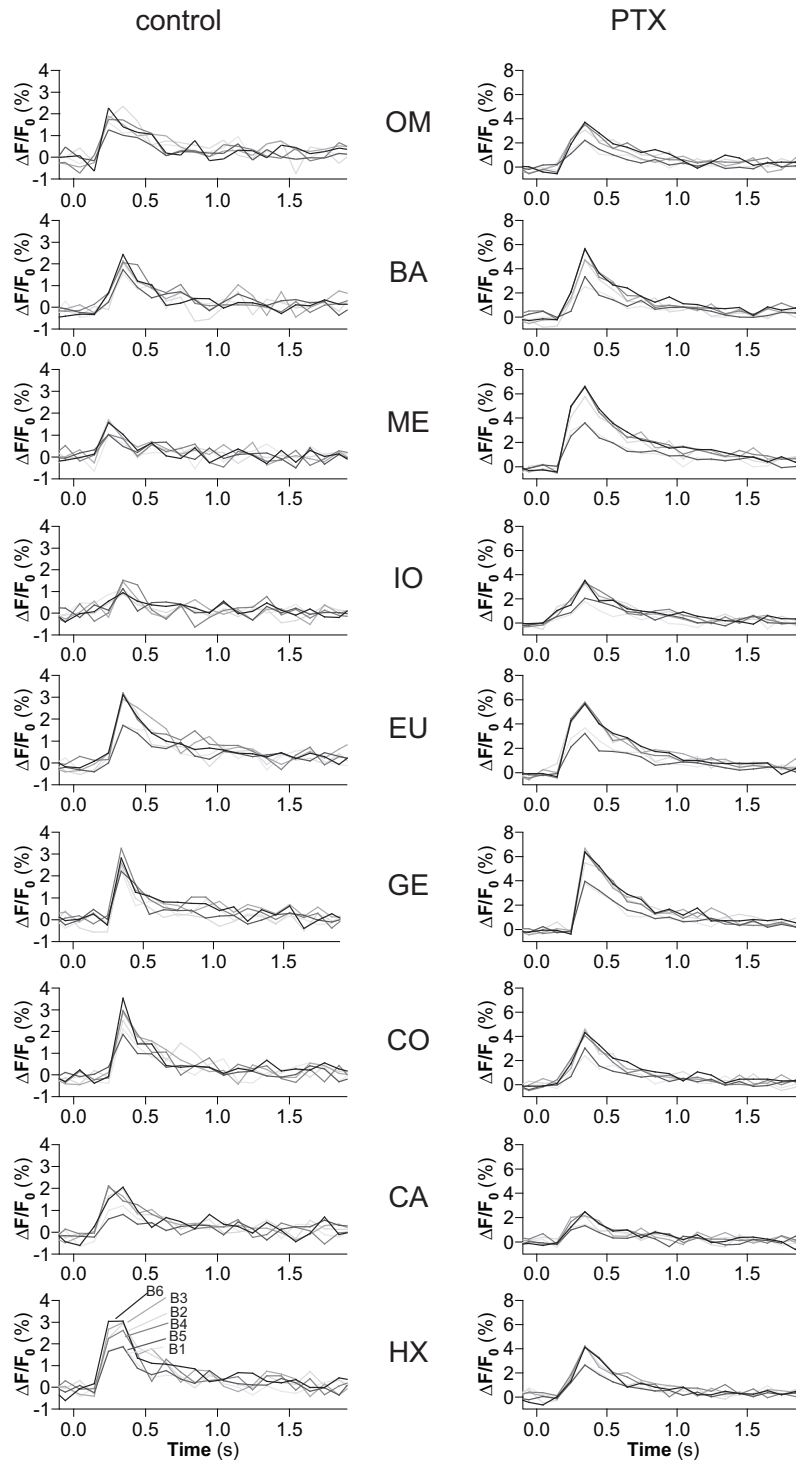
Figure 3.20: Analog signals of relative fluorescence changes of PN2. *The responses of all boutons to a single odor were superimposed. The recordings during control were displayed to the left and the recordings after PTX application were illustrated to the right. GE - geraniol; CO - citronellal; HX - 1-hexanol; EU - eugenol; OM - odor mixture; BA - benzaldehyde; CA - +/- citral; IO - α-ionone; ME - methylsalicylate.*
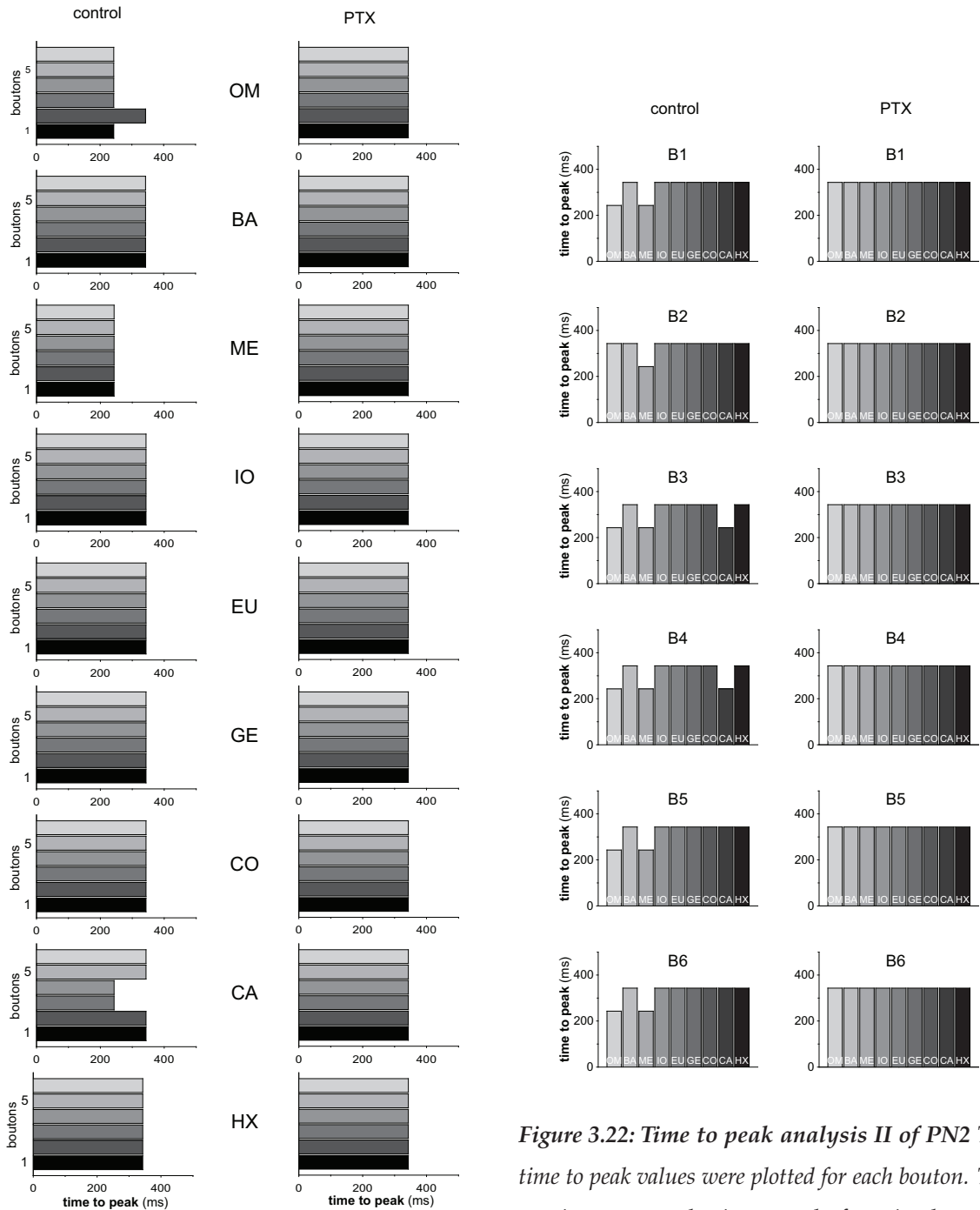
Figure 3.21: Time to peak analysis I of PN2. The time to peak of each bouton after stimulus onset was calculated for each odor. The time to peak after stimulus onset was plotted on the x-axis and the single boutons were plotted on the y-axis. Nearly all odors elicited responses at the same time in the boutons. After PTX application all odors elicited unitary response in the boutons. GE - geraniol; CO - citronellal; HX - 1-hexanol; EU - eugenol; OM - odor mixture; BA - benzaldehyde; CA - +/- citral; IO - α-ionone; ME - methylsalicylate.

Figure 3.22: Time to peak analysis II of PN2 The time to peak values were plotted for each bouton. The y-axis represents the time to peak after stimulus onset and the x-axis represents the different odors. The time to peak values for the control were displayed on the left hand side and the time to peak values after PTX treatment were illustrated on the right hand side of this figure. The individual curves during control show more differences than those after PTX treatment. GE - geraniol; CO - citronellal; HX - 1-hexanol; EU - eugenol; OM - odor mixture; BA - benzaldehyde; CA - +/- citral; IO - α-ionone; ME - methylsalicylate.

from the mean response intensity across all boutons was calculated. The mean standard deviation before and after application of PTX were than compared and statistically tested. For the control the variability of the boutons to the different odors, expressed as mean standard deviation, was quite large (13.7 $\pm$ 2.4 %), but after application of PTX this variance was significantly smaller (5.3 $\pm$ 3 %; P=0.002; unpaired t-test).

These results support the idea, that boutons of the same neuron were differentially modulated to respond individually to different odors. Although the temporal analysis revealed no great differences before and after PTX application the tuning curves give evidence, that GABAergic modulation is also present in the presented PN2. The lack of temporal modulation is discussed in detail below.

3.5.5 Example PN3

Image sequences (Fig. 3.24).   Each image of the sequence represents an 140 ms interval (average of 5 images). In the last PN I present the responses differed considerably to the responses shown above. PN3 only responded to 4 out of 11 different odors. The responses were large, as during control fluorescence increased up to $\Delta F/F$ 25 %. The different odors evoked an intensity pattern across the boutons. During citronellal stimulation the second spike train was not regarded because after repetitive stimulation with citronellal the second spike train was not robust during the entire experiment. After PTX application the fluorescence transients were not as big as in the control. For the following analysis 10 distinguishable boutons were identified by means of the Alexa 568 image.

Color coded intensities of identified boutons over time (Fig. 3.25).   The temporal pattern in this PN is in full agree with the spike trains recorded from the cell body. Both odor mixture and α-ionone stimulation resulted in 2 spikes followed by a hyperpolarization. After geraniol stimulation 1.8 seconds after stimulus onset an inhibition was observed. citronellal evoked no such hyperpolarization. For analysis of the maximum intensity I only chose the first Ca^{2+} influx because the second spike train was not robust throughout the entire experiment. After the PTX application this PN only responded with single spikes, which were highly
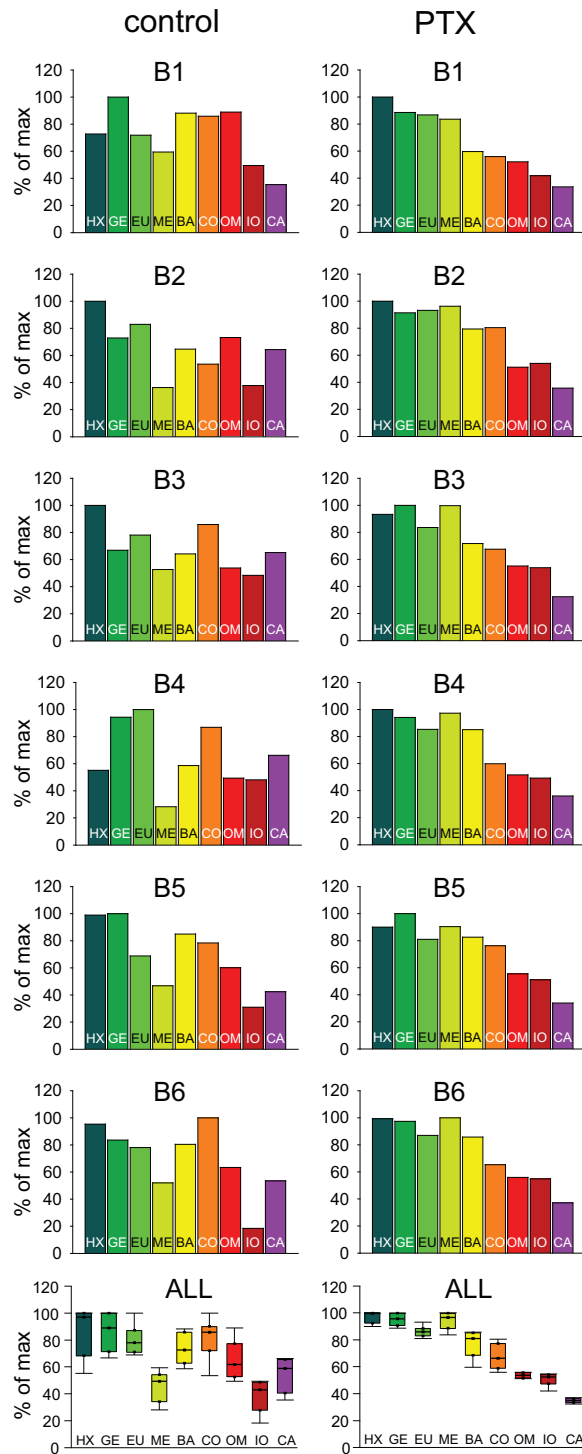
Figure 3.23: *Tuning curves of PN2.* *For each bouton the peak intensities were expressed as a percentage of the maximum response. To the left the tuning curves during control and to the right the tuning curves after PTX treatment were displayed. The box plot illustrates the difference within one odor. During control the tuning curves were more variable than after PTX application. This was also illustrated by the smaller boxes during PTX application in the box plot. GE - geraniol; CO - citronellal; HX - 1-hexanol; EU - eugenol; OM - odor mixture; BA - benzaldehyde; CA - +/- citral; IO - α-ionone; ME - methylsalicylate.*
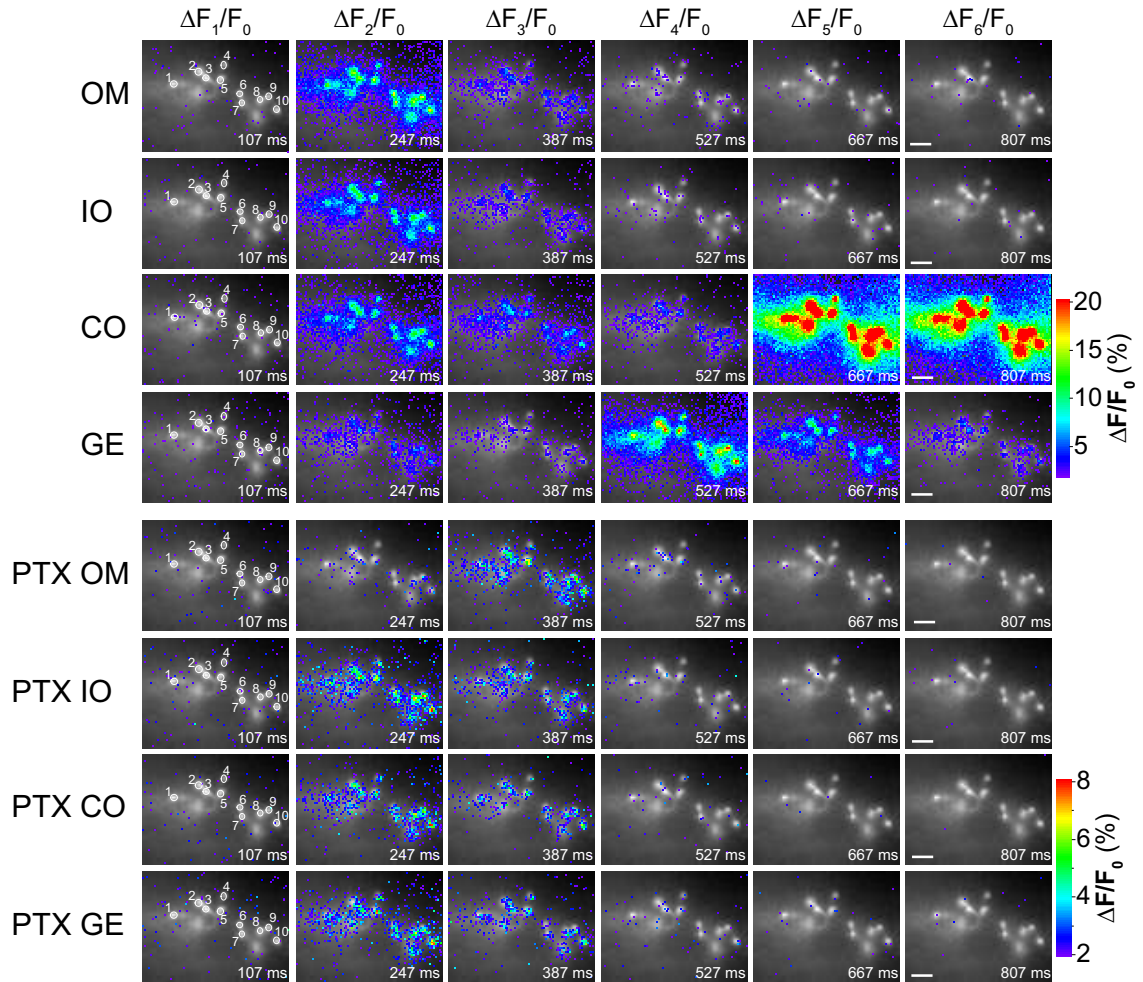
Figure 3.24: Image sequences of PN3 *Each image of the sequence represents an 140 ms interval (average of 5 single images). In the upper part of the panel the control recordings were displayed and in the lower part the recordings after PTX treatment. In general the relative fluorescence increases were halved after PTX treatment. The delayed response to citronellal was not regarded because this second response was not always observable when the PN was repetitively stimulated with citronellal. From the ALexa5 568 image 13 distinguishable boutons were identified and depicted as ovals in $\Delta F_1/F$ interval. GE - geraniol; OM - odor mixture; CO - citronellal; IO - α-ionone. Scale bars: 10 μm*
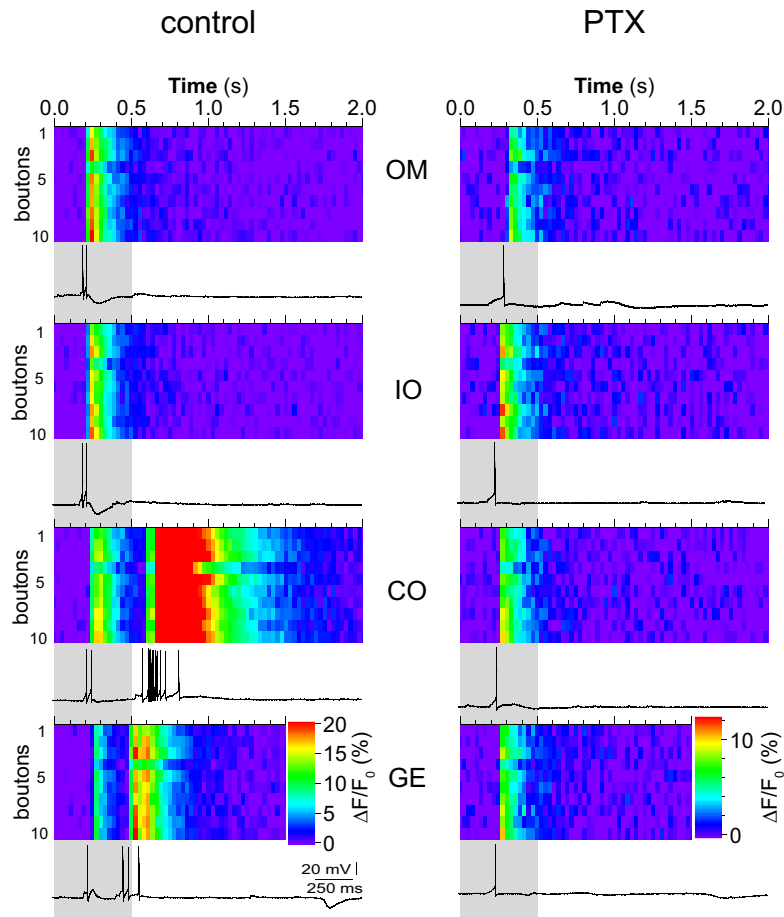
Figure 3.25: Color coded intensities of identified boutons over time of PN3. Ca^{2+} signals of ROIs with dynamically removed background. To the left the recordings during control and to the right the recordings after PTX treatment were displayed. In general the temporal patterns of activity agree with the recorded spike trains. GE - geraniol; OM - odor mixture; CO - citronellal; IO - α-ionone.

reproducible (tested for citronellal over 1h, data not shown). The second spike train during geraniol was completely lost after PTX application.

Analog signals of relative fluorescence changes (Fig. 3.26). In Fig. 3.26 absolute changes in fluorescence were compared for the different odors I applied. Every single line represents a single bouton. Absolute changes of fluorescence were equally distributed among all boutons and during all stimuli over the entire range from 20 % in bouton 10 to 10 % in bouton 4. During PTX application absolute fluorescent changes were still dispersed equally over the entire range of all fluorescent signals. Only at geraniol stimulation the fluorescence signals changed significantly. Additionally Fig. 3.26 shows that the peak fluorescence changes were proximately halved during PTX compared to control. The relative
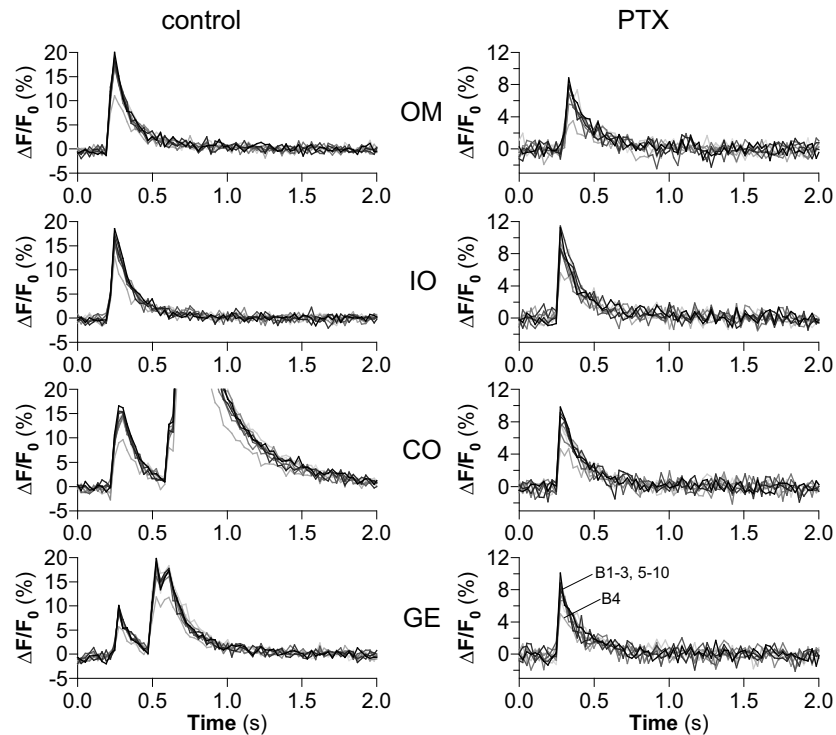
Figure 3.26: Analog signals of relative fluorescence changes of PN3 The responses of all boutons to a single odor were superimposed. The recordings during control were displayed to the left and the recordings after PTX application were illustrated to the right. GE - geraniol; OM - odor mixture; CO - citronellal; IO - α-ionone.

differences within the bouton tuning curves were further emphasized in Fig. 3.29.

Time to peak analysis I (Fig. 3.27). All boutons responded in nearly the same time frame for the different odors. For odor mixture and α-ionone all boutons had their response maximum at 245 ms after odor onset. The time to peak differed among the boutons at maximum 56 ms for citronellal and geraniol. Only for this two odors 3 boutons responded in different time frames. During PTX application this uniform timing was even more pronounced.

Time to peak analysis II (Fig. 3.28). I plotted the time to peak values against the different odors for each bouton. No obvious differences could be observed neither during control nor after PTX applications. During control boutons 1, 3, 4, and 6 had exactly the time to peak latencies and after PTX treatment boutons 1, 2, 3, 5, 8,9, and 10 showed exactly the same time to peak values. These results
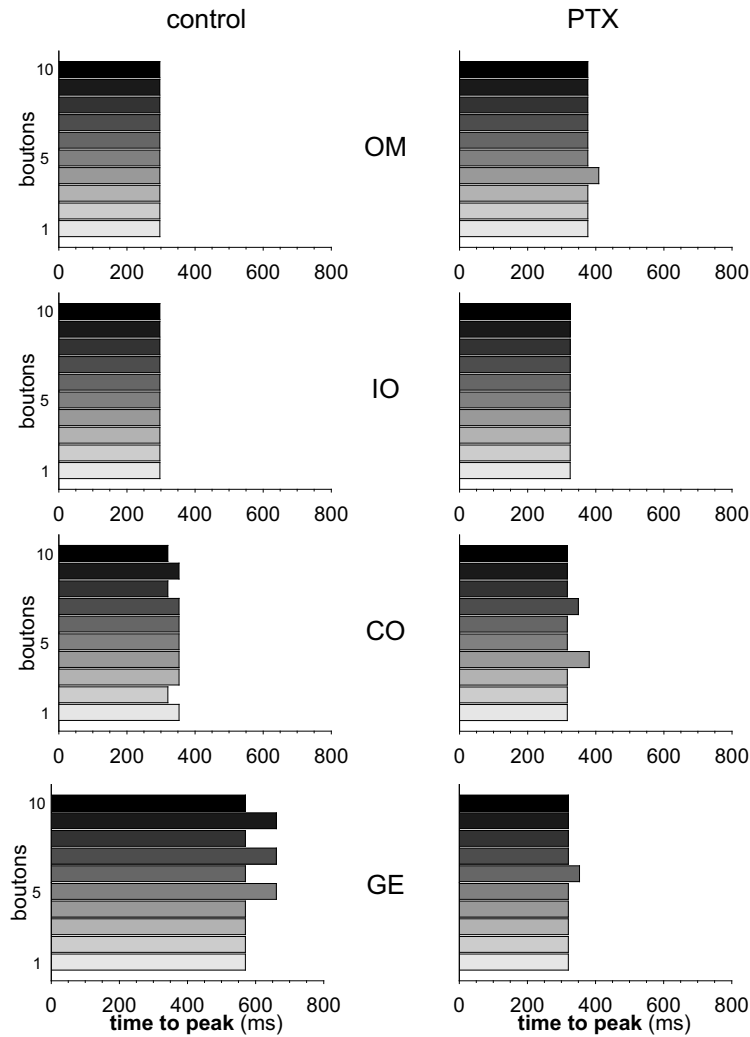
Figure 3.27: Time to peak analysis I of PN3. The time to peak of each bouton after stimulus onset was calculated for each odor. The time to peak after stimulus onset was plotted on the x-axis and the single boutons were plotted on the y-axis. Nearly all odors elicited responses at the same time in the boutons before and after application of PTX. GE - geraniol; OM - odor mixture; CO - citronellal; IO - α-ionone.

suggest that this particular PN is not modulated in terms of temporal patterns.

Tuning curves (Fig. 3.29) For each bouton the peak of the odor responses were expressed as a percentage of the maximum response. The resulting tuning curves showed no great variations among the different boutons. During control all boutons similar tuning curves to the different odors. The maximum deviation from the maximum during the control was obvious in bouton 10, where citronellal elicited only 80 % change. After PTX treatment the tuning curves were altered a bit resulting in reduced responses to odor mixture but this was applied for all boutons. The box plot showed that the odors were nearly equally represented in
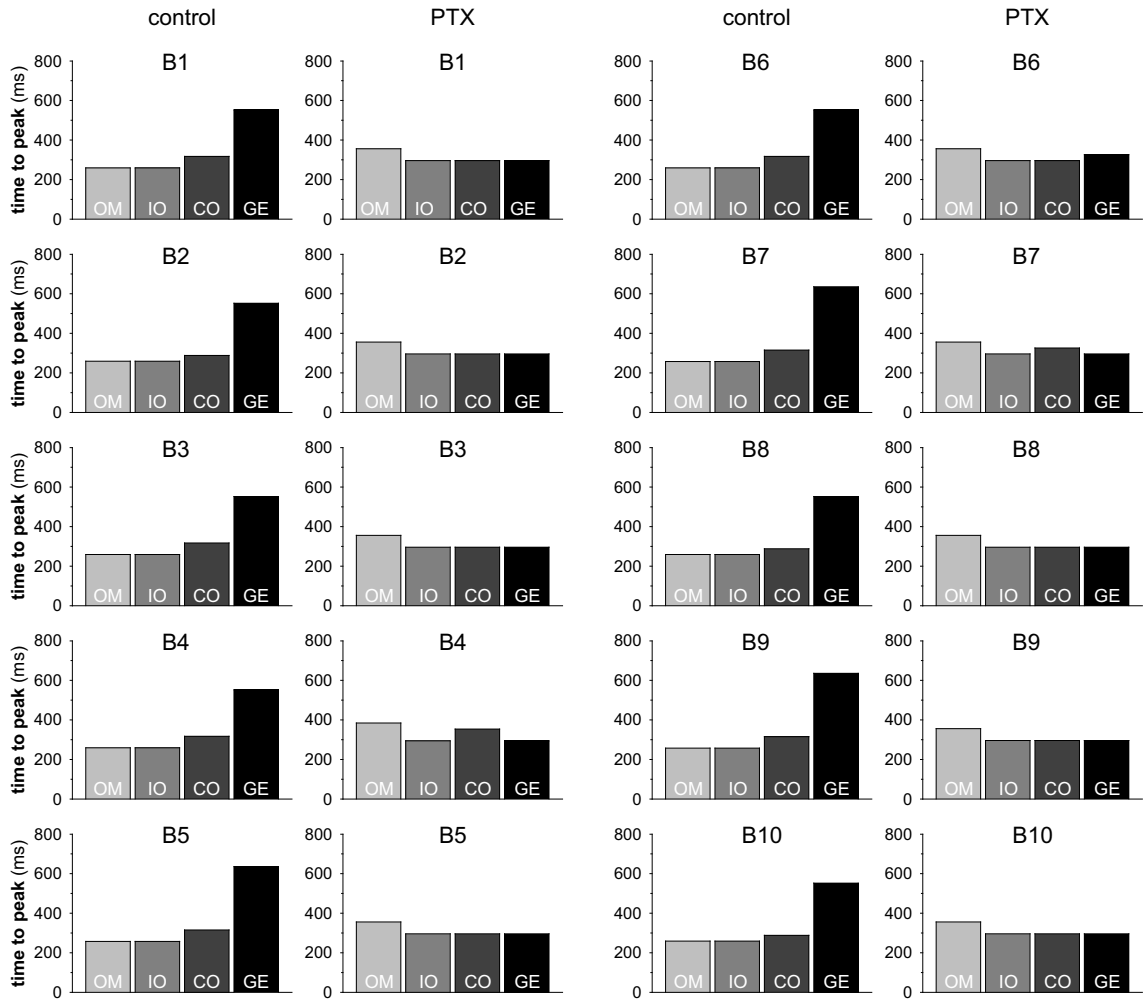
Figure 3.28: Time to peak analysis II of PN3. *The time to peak values were plotted for each bouton. The y-axis represents the time to peak after stimulus onset and the x-axis represents the different odors. The time to peak values for the control were displayed on the left hand side and the time to peak values after PTX treatment were illustrated on the right hand side of this figure. The individual curves during control and after PTX treatment show no great differences. GE - geraniol; OM - odor mixture; CO - citronellal; IO - α-ionone.*

the boutons before as well as after application of PTX. For the control the individual variability was small (4.2 ± 1.9 %) and after application of PTX this variance was not significantly different (6.1 ± 4.2 %; P=0.446; unpaired t-test).

These results suggest that this particular PN is not modulated in terms of intensity patterns. Additionally this PN was also not modulated in the temporal pattern. This result is contradictory to the results from the previously shown PNs and has to be discussed below.
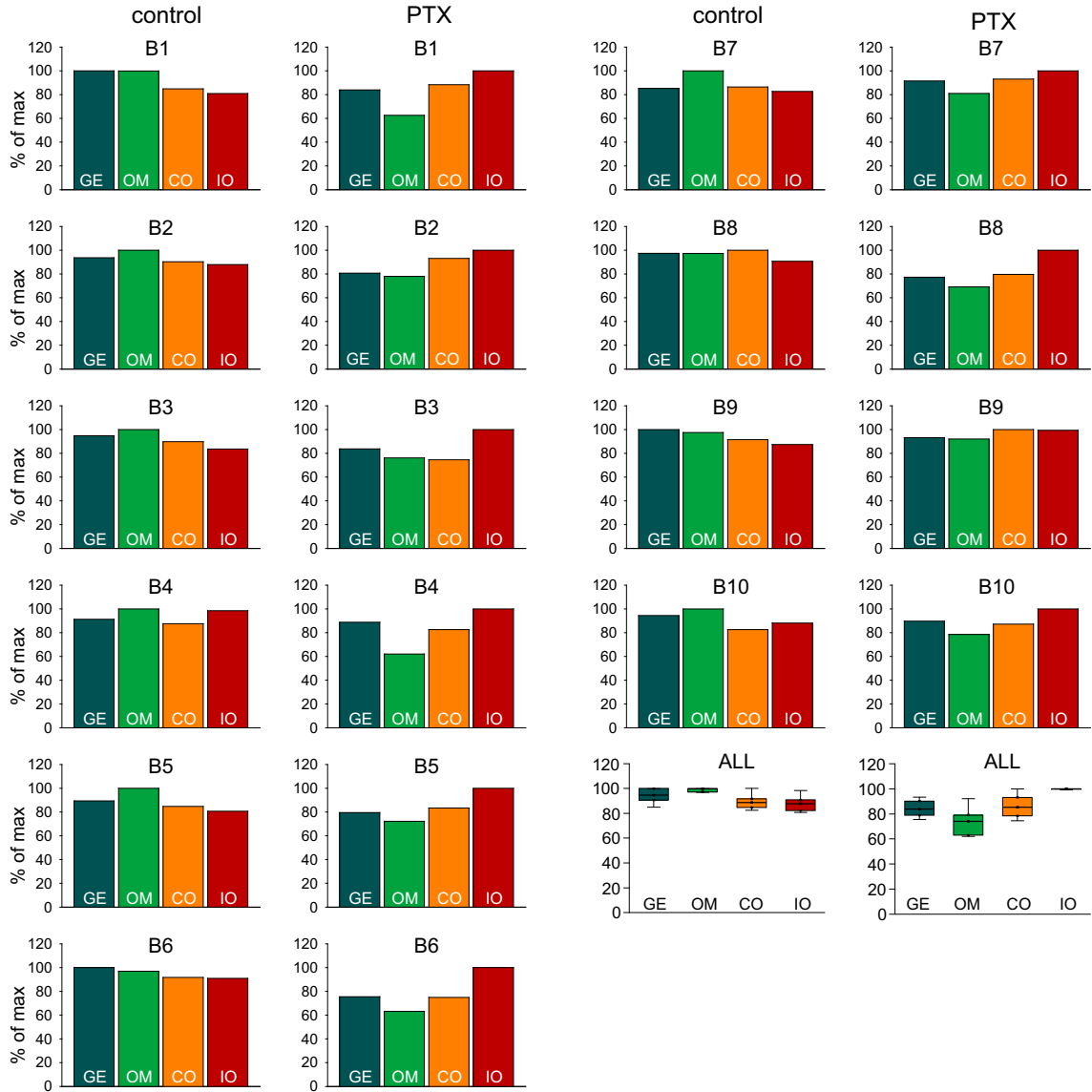
Figure 3.29: Tuning curves of PN3. *For each bouton the peak intensities were expressed as a percentage of the maximum response. To the left the tuning curves during control and to the right the tuning curves after PTX treatment were displayed. The box plot illustrates the difference within one odor. During control the tuning curves were not variable neither during control nor after PTX application. This was also illustrated by the similar boxes during control and after PTX application in the box plot. GE - geraniol; OM - odor mixture; CO - citronellal; IO - α-ionone.*

4 Discussion

The aim of this study was to identify the mechanisms that mediate the olfactory coding in the mushroom bodies of *P. americana*. Therefore, the intrinsic properties the Kenyon cells, elements within the MB circuitry were analyzed in the first part of this study. In the second part the spatial and temporal characteristics of the Kenyon cells' olfactory input were determined.

4.1 KC membrane properties

I used whole-cell patch-clamp recordings to provide a detailed analysis of ionic currents present in KCs in an intact, adult brain preparation of *P. americana*. Kenyon cells are principle components of the MBs, which are important centers for multi-modal processing, sensory processing and learning. Electrophysiological recordings during olfactory stimulation in *Drosophila* (Turner *et al.*, 2008), locusts (Perez-Orive *et al.*, 2002; Perez-Orive *et al.*, 2004) and optical recordings in honey bees (Szyszka *et al.*, 2005) revealed a sparse representation of olfactory signals in the MBs. On the single cell level this was reflected in very low spontaneous activity, high spiking threshold, stimulus selectivity and weak olfactory responses with very few APs or no APs per stimulus. One major aim of this study was to analyze the ionic mechanisms that mediate these typical firing properties of KCs.

4.1.1 Odor responses in KCs

One significant finding of this thesis was that KCs of *P. americana*, which were generally odor responsive responded to more than one odor. Only in 3 of 25 recordings APs were elicited, but the general odor responsiveness was visible in all of the three recordings.

This is contradictory to previous reports from in locusts, flies and honey bees. Several studies have shown that odor responses in KCs are sparse in terms of APs evoked and that every KC only responded to a subset of odors. With calcium imaging of GFP-based calcium sensors (G-CaMP) as used in *Drosophila* (Wang *et al.*, 2004) or calcium sensitive dyes as used in *Apis* (Szyszka *et al.*, 2005) few APs in number elicited in KCs of *P. americana* might be overlooked because the sensors are not sensitive enough to resolve single APs. Anyhow, the results the present thesis, where many odors elicited responses in the KCs, are in contrast to those reported from locusts (Perez-Orive *et al.*, 2002; Perez-Orive *et al.*, 2004) and *Drosophila* (Turner *et al.*, 2008; Murthy *et al.*, 2008). In both animals, intracellular recordings of KCs have shown that KCs only respond to one or few odors. The fact that *Periplaneta* KCs respond to many odors might be attributed to not perfectly matched internal solutions, resulting in depolarized membrane potentials and hyperexcitability. However, after breaking into the cell no significant depolarization of the membrane potential was observed. Additionally, the recordings were stable over up to 2 h of recording with no great changes in excitability and odor responsiveness. Another explanation for this increased responsiveness could be not perfectly adjusted odor concentrations. Maybe all odors used in this study induced non specific responses because of their general supersaturation. This would also imply that PNs uniformly respond to the odors presented. But, as shown in the second part of this study, the evoked responses to different odors differed substantially in PNs and not every PN responded to every odor presented (Husch *et al.*, 2009). Thus, it is unlikely that the responses of the KCs shown in this study are unspecific. For locusts, generalist KCs, which responded to all presented odors, have also been mentioned, whereas the authors did not further described these cells in detail (Perez-Orive *et al.*, 2002; Ito *et al.*, 2008). Whether *Periplaneta* KCs' characteristics differ or match the studies cited above can not be decided at present.

4.1.2 General features of KCs

All recordings in this study were performed in an intact brain preparation, in which the currents are not altered by the culturing procedure or development.

Given that the complex arborizations are still intact, perfect voltage control across the whole neuron cannot be assumed. After blocking all conductances that were not investigated, the current waveforms usually did not indicate voltage control problems (e.g. no delay of current onset, no jumps in the voltage dependence) suggesting that they originated mostly from well voltage-clamped regions. Given the long, thin primary neurite, I assumed that a major part of the currents originates from the cell bodies.

Morphological and immunohistochemical studies in various insect species showed that KCs consist of various subpopulations (Mizunami *et al.*, 1998; Strausfeld & Li, 1999b; Strausfeld *et al.*, 2003). In this study, KCs were identified by the size and position of the cell bodies in the calyces. Single cell labeling confirmed their identity in all cases performed. Given our level of analysis, all stained neurons had a similar axonal branching pattern in the MB's neuropil: The axon is situated along the pedunculus towards the lobes, where it bifurcates into the vertical and medial lobe. In the calyces, however, their dendritic branching patterns varied substantially (Fig. 3.1). Nevertheless, I did not find systematic differences in the electrophysiological properties that would justify a separation into distinct functional KC classes and accordingly, pooled the data for the analysis. However, it is important to emphasize that a further analysis of physiological and morphological properties of KCs might reveal more sub-types.

By characterizing the intrinsic firing properties and its underlying ionic currents I found specific functional properties, like the activation threshold and current densities of I_{Ca} and $I_{O(Ca)}$, that make them well suited to support sparse representation of sensory signals in the MBs, further supporting the hypotheses that sparseness is, at least in part, mediated by the KCs' intrinsic properties. Because neuronal properties are largely determined by the types of ion channels expressed and by the rate of channel expression for different channel types, I consider such a detailed analysis of the biophysical properties an important step towards a clear understanding how sensory signals are processed on the single cell and circuit level in these prominent multimodal processing centers of the insect brain.

	I_A	$I_{K,ST}$	$I_{K(V)}$	$I_{O(Ca)}$	I_{Na}	I_{Ca}
Activation threshold (mV)	-40	-25	-25	-20	-40	-60
G_{max} or I_{max}	8.2 ± 1.4 nS	5.9 ± 3.6 nS	4.8 ± 1.3 nS	2.4 ± 1 nA	420 ± 130 pA	350 ± 80 pA
V_{max} (mV)	30	40	50	25 ± 11	-6 ± 5	0.6 ± 4.6
$V_{0.5act}$ (mV)	-13 ± 4.3	-9.3 ± 7.8	0 ± 4.6	-	-	-17.4 ± 3.6
s_{act}	12.1 ± 1.7	10.4 ± 3	13.2 ± 1.5	-	-	12.7 ± 3
$G_{max} C_M^{-1}$ or $I_{max} C_M^{-1}$	2.6 ± 0.62 nS pF^{-1}	1.3 ± 0.3 nS pF^{-1}	1.6 ± 0.6 nS pF^{-1}	600 ± 340 pA pF^{-1}	140 ± 50 pA pF^{-1}	190 ± 60 pA pF^{-1}(tail)
Inactivation threshold (mV)	-80	-90	-	-	-70	-55
$V_{0.5inact}$ (mV)	-56 ± 5	-50 ± 5	-	-	-48 ± 4	-40 ± 5
s_{inact}	8.6 ± 0.9	13.2 ± 2.3	-	-	5.4 ± 0.5	10.8 ± 2.8

Table 4.1: Electrophysiological parameters of Kenyon cells. The resting potential was -55 $\pm$ 10 mV, the input resistance was 2.5 $\pm$ 1 GΩ and the whole-cell capacitance was 2.7 $\pm$ 0.8 pF. To calculate the current densities we used the values for the whole-cell capacitance from measurements with the specific extra-/intracellular salines.

4.1.3 Voltage activated currents

Although all recorded *P. americana* KCs could generate Na$^+$ driven APs when injected with depolarizing current, all cells had little or no spontaneous activity. During sustained depolarizing current injection all neurons displayed a strong spike frequency adaptation. Only 30% of the KCs produced graded subthreshold depolarizations, of which only 25% gave rise to APs. These data, showing a very low spike probability both spontaneously and during sensory stimulation are in full agreement with recent studies in *Drosophila* (Turner *et al.*, 2008) and locusts (Perez-Orive *et al.*, 2002; Perez-Orive *et al.*, 2004). Based on these previous data it has been proposed that for sparse coding, intrinsic and synaptic properties of the KC circuitry combine to generate relatively brief windows for synaptic integration in the KCs, thus causing them to operate as coincidence detectors that are only sensitive to their highly synchronized input (Perez-Orive *et al.*, 2002; Perez-Orive *et al.*, 2004; Assisi *et al.*, 2007). Current clamp recordings, for example, demonstrated the existence of subthreshold active properties that amplify and
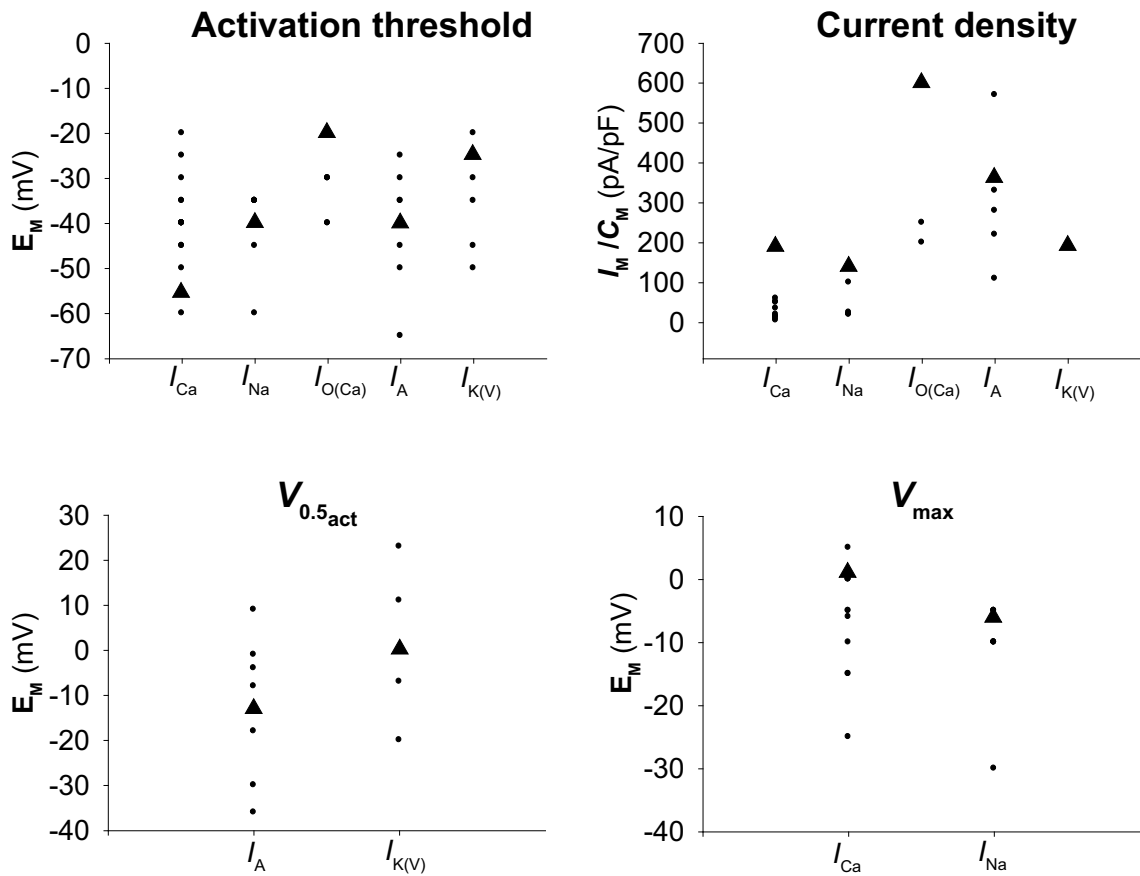
Figure 4.1: Summary figure. *Comparison of own results with those found in literature. Triangles represent own results while circles represent results from the literature.*

sharpen synaptic input (Perez-Orive *et al.*, 2002; Perez-Orive *et al.*, 2004).

I analyzed a set of voltage and/or Ca^{2+}-dependent inward (I_{Ca}, I_{Na}) and outward currents (I_A, $I_{K(V)}$, $I_{K,ST}$, $I_{O(Ca)}$) that significantly contribute to intrinsic firing properties (see table 4.1). In general, these currents were similar to currents found in other insect spiking neurons (Achenbach *et al.*, 1997; Benkenstein *et al.*, 1999; Bickmeyer *et al.*, 1994; Brône *et al.*, 2003; Byerly & Leung, 1988; Grolleau & Lapied, 2000; Grünewald, 2003; Grünewald *et al.*, 2004; Heidel & Pflüger, 2006; Hewes, 1999; Husch *et al.*, 2008; Kloppenburg & Hörner, 1998; Kloppenburg *et al.*, 1999b; Laurent *et al.*, 2002; Lucas & Shimahara, 2002; Pelz *et al.*, 1999; Schäfer *et al.*, 1994; Wicher & Penzlin, 1997; Wicher, 2001; Worrell & Levine, 2008; Wright & Zhong, 1995; Wüstenberg *et al.*, 2004, Fig. 4.1) . For example, the voltage operating range of the transient sodium current observed in *P. americana* KCs is similar (Fig. 4.1)to transient Na^+ currents observed in locusts DUM neurons (Brône *et al.*, 2003; Heidel & Pflüger, 2006), in honey bee Kenyon cells (Schäfer *et al.*, 1994), and in olfactory receptor neurons (Lucas & Shimahara, 2002), *Drosophila* embry-

onic neurons (Byerly & Leung, 1988), cricket giant interneurons (Kloppenburg & Hörner, 1998), and honey bee antennal motoneurons (Kloppenburg *et al.*, 1999b).

As in many other insect neurons, the voltage activated K^+ currents found in KCs included transient (I_A, $I_{K,ST}$) and more sustained components $I_{K(V)}$. I_A activates and inactivates rapidly and is 4-AP sensitive (Fig. 3.3), whereas $I_{K,ST}$ is 4-AP insensitive with slower activation and inactivation kinetics than I_A. $I_{K(V)}$ activates relatively slowly and does not inactivate significantly during a sustained voltage step. I_A is half-maximally activated at -13 mV (s = 12.1). This is 5 to 20 mV more depolarized than I_A in locusts DUM neurons (Heidel & Pflüger, 2006), locusts lamina neurons (Benkenstein *et al.*, 1999), cockroach DUM neurons (Grolleau & Lapied, 1995) but 9 to 21 mV more hyperpolarized than I_A in cricket giant interneurons (Kloppenburg & Hörner, 1998), honey bee antennal motoneurons (Kloppenburg *et al.*, 1999b) and honey bee KCs (Pelz *et al.*, 1999). The value for half-maximal inactivation of I_A in *P. americana* KCs (-56 mV; s = 8.6) is close to that described for KCs of the honey bee (Pelz *et al.*, 1999) and is 3 to 29 mV more positive than found for I_A in locusts DUM neurons (Heidel & Pflüger, 2006), locusts lamina neurons (Benkenstein *et al.*, 1999), cockroach DUM neurons (Grolleau & Lapied, 1995) and in honey bee antennal motoneurons (Kloppenburg *et al.*, 1999b).

In *P. americana* the voltage dependence for $I_{K,ST}$ was in the same range of I_A (I_A : $V_{0.5_{act}}$ = 13; $I_{K,ST}$: $V_{0.5_{act}}$ = -9.3). This current was previously recorded in honey bee KCs (Wüstenberg *et al.*, 2004). In the honey bee the voltage dependence was not investigated in detail, but it was assumed that the parameters are in the same range as I_A. In *Drosophila* larval mushroom body neurons 4-AP insensitive potassium currents seemed to have comparable time constants (Wright & Zhong, 1995).

$I_{K(V)}$ in KCs also resembles delayed-rectifier type K^+ currents of insect neurons described elsewhere (Benkenstein *et al.*, 1999; Kloppenburg & Hörner, 1998; Kloppenburg *et al.*, 1999b, Fig. 4.1). It is TEA sensitive, activates more slowly than I_A and $I_{K,ST}$, and shows little or no voltage inactivation. However, the activation threshold of -30 mV and the half-maximal voltage for activation (0 mV; s = 13.1) observed in this study is 11 to 23 mV more negative than values reported

for the delayed K^+ currents described cricket giant interneurons (Kloppenburg & Hörner, 1998) and honey bee antennal motoneurons (Kloppenburg *et al.*, 1999b) and 7 to 20 mV more positive than described in locusts lamina cells (Benkenstein *et al.*, 1999).

The values for the mean conductance densities of the K^+-currents (I_A : G_A = 2.6 nS pF^{-1}; $I_{K(V)}$: $G_{K(V)}$ = 1.6 nS pF^{-1}; $I_{K,ST}$: $G_{K,ST}$ = 1.3 nS pF^{-1}) are in the same range as reported for K^+ currents in locusts lamina cells (Benkenstein *et al.*, 1999) and locusts DUM neurons (Heidel & Pflüger, 2006). The values for I_A and $I_{K(V)}$ are slightly smaller than described for honey bee Kenyon cells and projection neurons (Grünewald, 2003), which might be due to the fact that in the present study two different conductances were isolated. The peak current density of I_{Na} was also in the same range as reported for olfactory receptor cells (Lucas & Shimahara, 2002) and slightly larger than in locusts DUM neurons (Heidel & Pflüger, 2006).

A detailed analysis, revealed that certain functional parameters of two currents, I_{Ca} and $I_{O(Ca)}$, are in the range that they might be predestined to significantly assist sparse coding.

I_{Ca} starts to activate at membrane potentials around -55 mV (Fig. 3.8), which is a very low activation threshold compared to I_{Ca} in many other insect spiking neurons (Benkenstein *et al.*, 1999; Grolleau & Lapied, 1996; Grünewald, 2003; Hewes, 1999; Husch *et al.*, 2008; Kloppenburg & Hörner, 1998; Schäfer *et al.*, 1994; Wicher & Penzlin, 1994; Worrell & Levine, 2008; Husch *et al.*, 2009; Byerly & Leung, 1988, Fig. 4.1). A second remarkable feature of I_{Ca} is its' very high current density, which is 2 to 4 fold higher than in antennal lobe neurons of *P. americana* (Husch *et al.*, 2008) and 2 fold larger than Ba^{2+} currents in DUM neurons (Heidel & Pflüger, 2006). With these properties - a low activation threshold and a high current density - I_{Ca} is likely to contribute to the highly nonlinear subthreshold properties that boost and sharpen the subthreshold EPSPs as reported in KCs (Perez-Orive *et al.*, 2002; Perez-Orive *et al.*, 2004).

$I_{O(Ca)}$ also has an unusually large amplitude. The mean current density of 600 pA pF^{-1} is about 3 fold higher than in locusts DUM neurons (Heidel & Pflüger, 2006) and 2 fold higher than in moth olfactory receptor neurons (Lucas &

Shimahara, 2002). $I_{O(Ca)}$ starts to activate at much more depolarized membrane potentials than I_{Ca}, indicating its strong voltage-dependence and suggesting that this outward current is not active at subthreshold membrane potentials. In combination, the large I_{Ca} and the large, high-threshold $I_{O(Ca)}$ are likely to support the typical intrinsic firing properties of the KCs, including the strong spike frequency adaptation during depolarizing current injection and the small number of APs during olfactory stimulation.

4.1.4 Tonic GABAergic inhibition

In addition to the intrinsic properties, I also analyzed the impact of GABAergic inhibition on the membrane potential. Immunohistochemical studies have shown that in many insect species the calyces receive massive GABAergic input by several neurons (Bicker, 1999; Homberg *et al.*, 1987; Yamazaki *et al.*, 1998). In *P.americana* three different classes of extrinsic GABAergic neurons arborize in the mushroom body neuropil (Yamazaki *et al.*, 1998). Two of these innervate the calyces. The first neuron class also arborizes in the surrounding neuropil of the vertical lobe and has its cell bodies located at the base of the optical lobes (giant calycal neurons). The second class originates from the circumesophageal connective and project to the calyces. Additionally the presence of both ionotropic GABA$_A$ and metabotropic GABA$_B$ receptors has been demonstrated in the calyces of *Drosophila* (Yasuyama *et al.*, 2002; Enell *et al.*, 2007) and *Periplaneta* (Sattelle *et al.*, 2000).

I found that application of picrotoxin, a blocker of the ionotropic GABA$_A$ receptor led to an increase in the input resistance and the resting potential, which suggests that the KCs receive tonic inhibition by which the sparseness might be strengthened. Blocking the metabotropic GABA$_B$ receptors also resulted in an increase of the input resistance and the resting potential. In this context it is interesting that the ionotropic GABA receptors of honey bee KCs are modulated by intracellular Ca^{2+} (Grünewald & Wersing, 2008). The influx of Ca^{2+} during an action potential, for example, might increase the inhibition mediated by ionotropic GABA receptor which could prevent the neuron from further firing. These results support not only the idea of feedforward inhibition (Perez-Orive *et al.*, 2002;

Perez-Orive *et al.*, 2004) but also that constant inhibition suppresses spontaneous activity and therefore sharpens odor responses in the mushroom body.

However, combined application of both GABA blockers resulted in drastic changes of the odor responses and in one case, spontaneous rhythms were evoked. These responses have never been observed before, neither during single application of both blockers nor during control conditions. For locusts, it has been reported that in addition to fast oscillatory input to the KCs, PN exhibited inhibitory patterns on a much slower time scale and these patterns were not sensitive to PTX (MacLeod & Laurent, 1996; MacLeod *et al.*, 1998). At this point of analysis I can not unequivocally determine the origin of the slow patterns observed in KCs when all inhibitory input is blocked. Recent studies in *Drosophila* showed that both ORNs and PNs are modulated through both $GABA_A$ and $GABA_B$ receptors (Olsen *et al.*, 2007; Olsen & Wilson, 2008). To test whether the observed responses are induced by local circuits in the calyces, or by rhythmic input from PNs, highly localized application of both blockers and/or simultaneous recordings of PNs and KCs have to be applied.

4.2 Imaging of PN output

In the second part of this thesis I analyzed the spatial and temporal aspects of odor evoked synaptic output patterns at the PN boutons. I was able to show that the output sites of olfactory projection neurons are modulated by GABA considering both spatial and temporal aspects. I used whole-cell current-clamp recordings combined with calcium imaging to analyze the actual output of single PN boutons on the KCs. A recent study in honey bees showed presynaptic olfactory information processing in the MBs and suggested that this in mediated by GABAergic microcircuits (Szyszka *et al.*, 2005). One major goal of this study was to show that output sites of the same PN are differentially modulated in spatial and temporal aspects by GABAergic inhibition.

4.2.1 Spatial intensity mosaic

PNs are the relay for transmission of the olfactory information from the antennal lobes to the mushroom bodies. In recent studies it has been shown that a spatial map of odor evoked activity in the antennal lobes exists and that this map occurs to be preserved among animals (Galizia *et al.*, 1999; Wang *et al.*, 2003). Genetically labeled PNs in *Drosophila* allowed the comparison of spike trains among different individuals (Wilson *et al.*, 2004). Additionally, morphological studies in *Drosophila* showed that the glomerular map is highly preserved in the lateral lobes and also in MB calyces (Marin *et al.*, 2002; Wong *et al.*, 2002). In the lateral lobes a stereotype map for axonal branching was found and also in the calyces, zones for different PN classes were clearly distinguishable (Tanaka *et al.*, 2004; Jefferis *et al.*, 2007). Imaging experiments suggested that this morphological stereotypy is not only present at the innervation patterns but also at the functional response patterns of KCs. Wang *et al.* (2004) were able to show that spatial distributed groups of KCs responded to different odor qualities. But the electrophysiological responses of genetically labeled KCs shows no significant stereotype (Murthy *et al.*, 2008). Based on this results a number of factors have been suggested that may account for the absence of KCs stereotypies (Cachero & Jefferis, 2008), among them the amount of GABAergic inhibitory input. It is known for several insect species that in addition to the map formed by the PNs the calyces receive massive input from other neurons among them GABAergic neurons (Yasuyama *et al.*, 2002; Ganeshina & Menzel, 2001; Strausfeld & Li, 1999a; Bicker, 1999; Homberg *et al.*, 1987; Yamazaki *et al.*, 1998). Together with the KCs these neurons form microglomeruli in the calyces of fly and honey bees (Yasuyama *et al.*, 2002; Ganeshina & Menzel, 2001). Immunohistochemical studies have shown that the GABAergic neurons in the calyces of *Drosophila* make synapses onto either PNs and KCs (Yasuyama *et al.*, 2002). The olfactory information which is already processed by the antennal lobe neurons is thus not mandatory transmitted unmodified to the KCs, but might also be modulated by the different neurons within the circuitry in the calyces. If PNs only transmit the information from the antennal lobes to the mushroom bodies all recorded responses in individual boutons should be similar. This was only true in case of

the third example. In this particular PN all boutons responded with similar patterns. These boutons showed equal tuning to the different odors, whereas the recorded electrophysiological response of the PN differed to the recordings from other PNs. Usually, PNs respond with longer, complex periods of excitation and inhibition. This response pattern was present in the first and second example of the PNs shown here. This complex response pattern is formed by local inhibitory and excitatory circuits within the antennal lobes (Shang *et al.*, 2007; Olsen & Wilson, 2008; Olsen & Wilson, 2008; Wilson & Laurent, 2005).

It has been reported that calcium concentrations correlate well with total spiking activity (Galizia & Kimmerle, 2004; Root *et al.*, 2007; Silbering *et al.*, 2008; Svoboda *et al.*, 1997), but this correlation is not perfect. When comparing the response to odor mixture and α-ionone in PN1 (Fig 3.13) or to odor mixture and 1-hexanol in PN2 (Fig 3.19) it is obvious that the spiking patterns were similar whereas the fluorescence increases at the output sites are considerably different. This points to the conclusion that high frequency spike trains not inevitable result in large transients at the output site. Accordingly, fluorescence increase is not sufficient to determine the spike rate. In contrast precisely timed action potentials elicited stronger responses at the output site. Comparing benzaldehyde before and after application of PTX (Fig. 3.19) in PN2 shows that the fluorescence level increased, even though the spike rate decreased. These results suggest that precise timing of single spikes is sufficient to produce exact output. Lower frequency spike train may produce better summation of presynaptic calcium than high frequency spike rates.

Recent studies in honey bee assumed already presynaptic inhibition of PN output (Szyszka *et al.*, 2005). In this study the authors show with calcium imaging of PN dendrites in the AL, the PN boutons and the KC soma that odor driven activity is sharpened during the processing steps. In the present study the transmitted information of the glomerulus to the output site of single neurons was investigated. With the combination of electrophysiological recordings and calcium imaging it was possible to investigate the direct output of particular neurons. This allows direct comparison of bouton signals. Application of PTX might alter the spiking pattern by modulating the whole circuit within the AL, whereas

the transmission to the boutons should not be affected. This means, any changes in the bouton specific tuning must arise from circuits within the calyces. I have shown two examples where tuning to different odors in distinct boutons was unambiguously different in the control and significantly more similar after PTX treatment (Figs. 3.17 and 3.23). Possible mechanisms are GABAergic feedback neurons, which have been suggested from neuroanatomical works on honey bees, flies and locusts (Ganeshina & Menzel, 2001; Yasuyama *et al.*, 2002; Leitch & Laurent, 1996). These neurons are supposed to form microcircuits with PNs and KCs and hence sharpen olfactory input to the KCs. For the locusts this GABAergic input is thought to mediate the sparse coding by inhibiting the KCs and not PNs but electronmicroscopic studies in Drosophila have shown that PN boutons also receive input from GABAergic synapses (Yasuyama *et al.*, 2002). In the cockroach the calyces also receive GABAergic input by several neurons but in contrast to the recurrent neuron reported in locusts and honeybee (Leitch & Laurent, 1996; Ganeshina & Menzel, 2001), these neurons provide no direct recurrent input from the lobes to the calyces (Yamazaki *et al.*, 1998; Strausfeld & Li, 1999b). Strausfeld and Li (1999) mentioned the overlap of dendrites beside the vertical lobes and terminals of medial lobes efferent. Together these neurons might form a recurrent feedback loop from the mushroom body lobes to the calyces. Whether the microcircuits, as reported for honey bee and *Drosophila*, are also apparent in cockroaches is still unknown, but conceivable. From this point of analysis it is not clear whether the observed modulation arises from the microcircuitry which forms reciprocal synapses between the PNs and GABAergic neurons, or whether the feedback loop is activated by means of KCs, medial lobe efferent and GABAergic recurrent neurons.

4.2.2 Temporal mosaic

In addition the spatial intensity map which has been discussed above, the temporal pattern of the odor evoked signals in the boutons has been analyzed. This temporal pattern is determined by the spiking pattern that was measured at the cell body and arises from circuitry dynamics in the AL. This pattern, defined as latency to the maximum response, appears to be modulated in the different

boutons, as shown in Fig. 3.15, where latencies differed several hundreds of milliseconds. Furthermore, I was able to show that an elaborate spike pattern also results in complex response patterns at the output site. Slight differences of ∼100 ms in the latencies to the peak fluorescence change may be explained by different distances to the recording site. For larger differences of hundreds of milliseconds (Fig. 3.15) delay between different boutons another mechanism has to be suggested. In locusts, it has been shown that highly synchronized input to KCs is essential to produce any response to an odor (Laurent, 2002; Stopfer *et al.*, 2003). In addition, each KC receives input from about 50 % of about 800 PNs and that this synapses are very weak (Jortner *et al.*, 2007). Assuming that KCs in cockroaches also receive information from many PN boutons, this would lead to the following conclusion: different PN boutons which all synapse on the same KC have to be synchronous, whereas different boutons of the same PN that synapse onto distinct KCs, should respond in different ways. This could be confirmed in PN1 (Fig. 3.15). Different boutons of the same PN had their individual maximum at different points of time. This variability was completely lost after application of PTX and all boutons responded approximately simultaneous to different odors. This is in coherence with previous results from locusts. Here, single KCs tend to produce more spikes to different odors after inhibition was blocked by PTX (Perez-Orive *et al.*, 2004), which means that more PN boutons must be active at the same time.

Currently, the lack of temporal modulation in PN2 and PN3 is not unequivocally assignable. The lack of temporal fine tuning in PN2 might be caused by a relative low sample frequency of 10 Hz. High frequencies as shown from the electrophysiological recordings thus might have been overlooked. Therefore, high sample frequencies are desirable, which can be achieved by laser scanning microscopy or two-photon laser scanning microscopy. This would help to analyze whether single action potentials produce the same amount of output at different boutons. In PN3 the lack of temporal tuning to different odors might be a cell specific issue. This particular PN only responded to 4 out of 11 odors, which is a considerably lower response probability than reported for other PNs (Perez-Orive *et al.*, 2002). Additionally, the electrophysiological response was less com-

plex as shown for the other two PNs and as expected from firing responses of typical PNs (Husch *et al.*, 2009).

4.2.3 Methodical aspects

To analyze the spatial and temporal properties of odor driven activity in the MB I measured calcium transients in the bouton of selectively stained PNs.

Throughout this study relatively high concentrations (800 μM) of high affinity Ca^{2+} indicator were loaded into the cells. The concentration at the recording site could not be determined and effects of the indicator on the signal were not analyzed. The changes in indicator concentrations might also have effects on the signal. Thus, the experiments were performed as fast as possible. Accordingly no evident changes in background fluorescence were observed throughout the experiments. It has been shown that changes in calcium fluorescence are mainly evoked by voltage- and/or transmitter activated Ca^{2+} channels. These are located both pre- and postsynaptic. Methodically it can not be distinguished where the signal is generated. In *Drosophila* it has been shown that few input sites to the boutons are opposed to many output sites to the KCs. Thus, in the present study it is more likely that the measured transients originate from presynaptic activity rather than from the postsynapse.

One disadvantage of the CCD camera set up is the low penetration into the tissue. Only the upper 100 μm are accessible for the CCD camera. Fortunately, all recorded PNs were of type 2 as described by Strausfeld & Li (1999b) and therefore all boutons were localized in the upper rim of the calyces. I assume that the recorded transients represent those in other parts of the MB. Only the medial calyx was accessible for imaging because the lateral calyx was slightly displaced due to the bent optical lobe. However, there is no study which reports any differences between the two calyces. All anatomical studies have shown that both medial and lateral calyx receive the identical input and the Kenyon cell organization is indistinguishable (Weiss, 1974; Strausfeld *et al.*, 1998).

4.3 Conclusions

In this study I was able to show that the synaptic circuit within the mushroom bodies of the cockroach *P. americana* and the intrinsic membrane properties of the KCs combine to generate the responses in KCs, which have been reported here and for other insects. Olfactory information which is transmitted by olfactory projection neurons to the higher order brain centers is further processed at the presynaptic site. This processing might be a form of olfactory learning, which is known to take place in the mushroom bodies. The tuning of different boutons towards distinct odors in terms of intensity and temporal precision would enhance the response probability of the following KC. Within the KCs tonic inhibition prevents KCs from spontaneous activity and might be released when the matching odor is presented. In combination with the large I_{Ca} this possible mechanism would boost EPSPs resulting in APs. Once APs are elicited and Ca^{2+} flows into the cell, the large conductance of $I_{O(Ca)}$ is activated. This conductance terminates activity. This silencing mechanism might be supported by an upmodulation of the GABAergic inhibition by intracellular Ca^{2+}.

4.4 Outlook

This study gives first insight into cellular mechanisms, which mediate olfactory coding within the mushroom bodies. However, this study gives rise to a number of questions, which will have to be addressed in more detail in future experiments.

- GABA antagonists need to be applied more precisely to confine the affected network. This should provide more information about the origin of slow temporal patterns, which were observed in the KCs during simultaneous application of both GABA antagonists.

- Odor evoked responses to different odor concentrations should be investigated in KCs. Different KCs may respond in different ways to different odor concentrations.

- Imaging experiments should be performed with high temporal and spatial resolution to further manifest the findings in this study. Additionally, the sample size should be increased in terms of odor presentation to ensure the reproducibility of spatio-temporal patterns.

- Electronmicroscopic analysis of single boutons in *Periplaneta* would be highly desirable to confirm the presence of microcircuits as shown in *Drosophila* and *Apis*.

References

ACHENBACH, H., WALTHER, C., & WICHER, D. 1997. Octopamine modulates ionic currents and spiking in dorsal unpaired median (DUM) neurons. *Neuroreport*, **8**(17), 3737–41.

AOKI, K., KOSAKAI, K., & YOSHINO, M. 2008. Monoaminergic modulation of the Na+-activated K+ channel in Kenyon cells isolated from the mushroom body of the cricket (Gryllus bimaculatus) brain. *J Neurophysiol*, **100**(3), 1211–1222.

ARMSTRONG, C. M., & BEZANILLA, F. 1974. Charge movement associated with the opening and closing of the activation gates of the Na channels. *J Gen Physiol*, **63**(5), 533–52.

ASSISI, C., STOPFER, M., LAURENT, G., & BAZHENOV, M. 2007. Adaptive regulation of sparseness by feedforward inhibition. *Nat Neurosci*, **10**(9), 1176–1184.

BAZENOV, M., STOPFER, M., RABINOVICH, M., ABARBANEL, H. D.I., SEJNOWISK, T. J., & LAURENT, G. 2001. Model of cellular and network mechanisms for odor-evoked temporal patterning in the locust antennal lobe. *Neuron*, **30**(2), 569–81.

BAZHENOV, M., STOPFER, M., SEJNOWSKI, T. J., & LAURENT, G. 2005. Fast odor learning improves reliability of odor responses in the locust antennal lobe. *Neuron*, **46**(3), 483–92.

BENKENSTEIN, C., SCHMIDT, M., & GEWECKE, M. 1999. Voltage-activated whole-cell K+ currents in lamina cells of the desert locust schistocerca gregaria. *J Exp Biol*, **202 (Pt 14)**, 1939–51.

BICKER, G. 1999. Histochemistry of classical neurotransmitters in antennal lobes and mushroom bodies of the honeybee. *Microsc Res Tech*, **45**(3), 174–83.

BICKMEYER, U., RÖSSLER, W., & WIEGAND, H. 1994. Calcium Channel Currents in Cultured Pars Intercerebralis Neurosecretory Cells of Adult Locusta Migratoria. *J Exp Biol*, **197**(1), 393–8.

BOECKH, J., & TOLBERT, L. P. 1993. Synaptic organization and development of the antennal lobe in insects. *Microsc Res Tech*, **24**(3), 260–80.

BOECKH, J., ERNST, K.D., SASS, H., & WALDOW, U. 1984. Anatomical and physiological characteristicsof individual neurones in the central antennal-pathways of insects. *J. Insect Physiol.*, **30**(1), 15–26.

BOECKH, J., ERNST, K. D., & SELSAM, P. 1987. Neurophysiology and neuroanatomy of the olfactory pathway in the cockroach. *Ann N Y Acad Sci*, **510**, 39–43.

BRÔNE, B., TYTGAT, J., WANG, D-C., & VAN KERKHOVE, E. 2003. Characterization of Na(+) currents in isolated dorsal unpaired median neurons of Locusta migratoria and effect of the alpha-like scorpion toxin BmK M1. *J Insect Physiol*, **49**(2), 171–182.

BYERLY, L., & LEUNG, H. T. 1988. Ionic currents of Drosophila neurons in embryonic cultures. *J Neurosci*, **8**(11), 4379–93.

CACHERO, S., & JEFFERIS, G.S.X.E. 2008. Drosophila olfaction: the end of stereotypy? *Neuron*, **59**(6), 843–845.

COUTO, A., ALENIUS, M., & DICKSON, B.J. 2005. Molecular, anatomical, and functional organization of the Drosophila olfactory system. *Curr Biol*, **15**(17), 1535–1547.

DAVIS, R. L. 2004. Olfactory learning. *Neuron*, **44**(1), 31–48.

DE BRUYNE, M., & BAKER, T. C. 2008. Odor detection in insects: volatile codes. *J Chem Ecol*, **34**(7), 882–897.

DODT, H. U., & ZIEGLGÄNSBERGER, W. 1994. Infrared videomicroscopy: a new look at neuronal structure and function. *Trends Neurosci*, **17**(11), 453–8.

DUBNAU, J., CHIANG, A. S., & TULLY, T. 2003. Neural substrates of memory: from synapse to system. *J Neurobiol*, **54**(1), 238–53.

DUJARDIN, F. 1850. Mémoire sur le systéme nerveux des insectes. *Ann Sci Nat Zool*, **14**, 195–206.

EISTHEN, H. L. 2002. Why are olfactory systems of different animals so similar? *Brain Behavior and Evolution*, **59**(5-6), 273–293.

ENELL, L., HAMASAKA, Y., KOLODZIEJCZYK, A., & NÄSSEL, D.R. 2007. gamma-Aminobutyric acid (GABA) signaling components in *Drosophila*: immunocytochemical localization of GABA(B) receptors in relation to the GABA(A) receptor subunit RDL and a vesicular GABA transporter. *J Comp Neurol*, **505**(1), 18–31.

EVERS, J. F., SCHMITT, S., SIBILA, M., & DUCH, C. 2004. Progress in functional neuroanatomy: precise automatic geometric reconstruction of neuronal morphology from confocal image stacks. *J Neurophysiol*, **93**, 2331–2342.

FAHRBACH, S. E. 2006. Structure of the mushroom bodies of the insect brain. *Annu Rev Entomol*, **51**, 209–32.

FISHILEVICH, E., & VOSSHALL, L.E. 2005. Genetic and functional subdivision of the Drosophila antennal lobe. *Curr Biol*, **15**(17), 1548–1553.

FLANAGAN, D., & MERCER, A. R. 1989. An Atlas and 3-D Reconstruction of the Antennal Lobes in the Worker Honey Bee, Apis-Mellifera 6 (Hymenoptera, Apidae). *International Journal of Insect Morphology & Embryology*, **18**(2-3), 145–159.

GALIZIA, C. G., & KIMMERLE, B. 2004. Physiological and morphological characterization of honeybee olfactory neurons combining electrophysiology, calcium imaging and confocal microscopy. *J Comp Physiol A Neuroethol Sens Neural Behav Physiol*, **190**(1), 21–38.

GALIZIA, C. G., & SZYSZKA, P. 2008. Olfactory coding in the insect brain: molecular receptive ranges, spatial and temporal coding. *Entomologia Experimentalis Et Applicata*, **128**(1), 81–92.

GALIZIA, C. G., SACHSE, S., RAPPERT, A., & MENZEL, R. 1999. The glomerular code for odor representation is species specific in the honeybee *Apis mellifera*. *Nature Neuroscience*, **2**(5), 473–478.

GANESHINA, O., & MENZEL, R. 2001. GABA-immunoreactive neurons in the mushroom bodies of the honeybee: an electron microscopic study. *J Comp Neurol*, **437**(3), 335–349.

GROLLEAU, F., & LAPIED, B. 1995. Separation and identification of multiple potassium currents regulating the pacemaker activity of insect neurosecretory cells (DUM neurons). *J Neurophysiol*, **73**(1), 160–71.

GROLLEAU, F., & LAPIED, B. 1996. Two distinct low-voltage-activated Ca^{2+} currents contribute to the pacemaker mechanism in cockroach dorsal unpaired median neurons. *J Neurophysiol*, **76**(2), 963–76.

GROLLEAU, F., & LAPIED, B. 2000. Dorsal unpaired median neurones in the insect central nervous system: towards a better understanding of the ionic mechanisms underlying spontaneous electrical activity. *J Exp Biol*, **203 Pt 11**, 1633–48.

GRÜNEWALD, B. 2003. Differential expression of voltage-sensitive K^+ and Ca^{2+} currents in neurons of the honeybee olfactory pathway. *J Exp Biol*, **206**(Pt 1), 117–29.

GRÜNEWALD, B., & WERSING, A. 2008. An ionotropic GABA receptor in cultured mushroom body Kenyon cells of the honeybee and its modulation by intracellular calcium. *J Comp Physiol A Neuroethol Sens Neural Behav Physiol*, **194**(4), 329–340.

GRÜNEWALD, B., WERSING, A., & WÜSTENBERG, D. G. 2004. Learning channels. Cellular physiology of odor processing neurons within the honeybee brain. *Acta Biol Hung*, **55**(1-4), 53–63.

HAMILL, O. P., MARTY, A., NEHER, E., SAKMANN, B., & SIGWORTH, F. J. 1981. Improved Patch-Clamp Techniques for High-Resolution Current Recording from Cells and Cell-Free Membrane Patches. *Pflugers Archiv-European Journal of Physiology*, **391**(2), 85–100.

HANSSON, B. S. 2002. A bug's smell–research into insect olfaction. *Trends Neurosci*, **25**(5), 270–4.

HEIDEL, E., & PFLÜGER, H. J. 2006. Ion currents and spiking properties of identified subtypes of locust octopaminergic dorsal unpaired median neurons. *Eur J Neurosci*, **23**(5), 1189–206.

HEISENBERG, M. 1998. What do the mushroom bodies do for the insect brain? an introduction. *Learn Mem*, **5**(1-2), 1–10.

HEISENBERG, M. 2003. Mushroom body memoir: from maps to models. *Nat Rev Neurosci*, **4**(4), 266–75.

HEWES, R. S. 1999. Voltage-dependent ionic currents in the ventromedial eclosion hormone neurons of *Manduca sexta*. *J Exp Biol*, **202**(Pt 17), 2371–83.

HILDEBRAND, J. G., & SHEPHERD, G. M. 1997. Mechanisms of olfactory discrimination: Converging evidence for common principles across phyla. *Annual Review of Neuroscience*, **20**, 595–631.

HOMBERG, U., KINGAN, T. G., & HILDEBRAND, J. G. 1987. Immunocytochemistry of GABA in the brain and suboesophageal ganglion of *Manduca sexta*. *Cell Tissue Res*, **248**(1), 1–24.

HUSCH, A., HESS, S., & KLOPPENBURG, P. 2008. Functional parameters of voltage-activated Ca^{2+} currents from olfactory interneurons in the antennal lobe of *Periplaneta americana*. *J Neurophysiol*, **99**(1), 320–32.

HUSCH, A., PAEHLER, M., FUSCA, D., PAEGER, L., & KLOPPENBURG, P. 2009. Calcium current diversity in physiologically different local interneuron types of the antennal lobe. *J Neurosci*, **29**(3), 716–726.

ITO, I., ONG, R. C. Y., RAMAN, B., & STOPFER, M. 2008. Sparse odor representation and olfactory learning. *Nature Neuroscience*, **11**(10), 1177–1184.

JEFFERIS, G.S.X.E., POTTER, C.J., CHAN, A.M.AND MARIN, E.C., ROHLFING, T., MAURER, C.R., & LUO, L. 2007. Comprehensive maps of Drosophila higher olfactory centers: spatially segregated fruit and pheromone representation. *Cell*, **128**(6), 1187–1203.

JORTNER, R.A., FARIVAR, S.S., & LAURENT, G. 2007. A simple connectivity scheme for sparse coding in an olfactory system. *J Neurosci*, **27**(7), 1659–1669.

KAY, L.M., & STOPFER, M. 2006. Information processing in the olfactory systems of insects and vertebrates. *Semin Cell Dev Biol*, **17**(4), 433–442.

KLOPPENBURG, P., & HÖRNER, M. 1998. Voltage-activated currents in identified giant interneurons isolated from adult crickets *Gryllus bimaculatus*. *J Exp Biol*, **201**(17), 2529–2541.

KLOPPENBURG, P., FERNS, D., & MERCER, A. R. 1999a. Serotonin enhances central olfactory neuron responses to female sex pheromone in the male sphinx moth *Manduca sexta*. *J Neurosci*, **19**(19), 8172–8181.

KLOPPENBURG, P., KIRCHHOF, B. S., & MERCER, A. R. 1999b. Voltage-activated currents from adult honeybee (*Apis mellifera*) antennal motor neurons recorded in vitro and in situ. *J Neurophysiol*, **81**(1), 39–48.

KOSAKAI, K., SATOH, K., & YOSHINO, M. 2008. Octopaminergic modulation of the single Ca2+ channel currents in Kenyon cells isolated from the mushroom body of the cricket brain. *J Insect Physiol*, **54**(12), 1479–1486.

LAISSUE, P. P., REITER, C., HIESINGER, P. R., HALTER, S., FISCHBACH, K. F., & STOCKER, R. F. 1999. Three-dimensional reconstruction of the antennal lobe in *Drosophila melanogaster*. *J Comp Neurol*, **405**(4), 543–52.

LAURENT, G. 2002. Olfactory network dynamics and the coding of multidimensional signals. *Nature Reviews Neuroscience*, **3**(11), 884–895.

LAURENT, G., & DAVIDOWITZ, H. 1994. Encoding of Olfactory Information with Oscillating Neural Assemblies. *Science*, **265**(5180), 1872–1875.

LAURENT, G., WEHR, M., & DAVIDOWITZ, H. 1996. Temporal representations of odors in an olfactory network. *J Neurosci*, **16**(12), 3837–47.

LAURENT, S., MASSON, C., & JAKOB, I. 2002. Whole-cell recording from honeybee olfactory receptor neurons: ionic currents, membrane excitability and odourant response in developing workerbee and drone. *Eur J Neurosci*, **15**(7), 1139–52.

LEITCH, B., & LAURENT, G. 1996. GABAergic synapses in the antennal lobe and mushroom body of the locust olfactory system. *J Comput Neurosci.*, **372**(4), 487–514.

LUCAS, P., & SHIMAHARA, T. 2002. Voltage- and calcium-activated currents in cultured olfactory receptor neurons of male *Mamestra brassicae* (Lepidoptera). *Chem Senses*, **27**(7), 599–610.

MACLEOD, K., & LAURENT, G. 1996. Distinct mechanisms for synchronization and temporal patterning of odor-encoding neural assemblies. *Science*, **274**(5289), 976–979.

MACLEOD, K., BCKER, A., & LAURENT, G. 1998. Who reads temporal information contained across synchronized and oscillatory spike trains? *Nature*, **395**(6703), 693–698.

MARIN, E. C., JEFFERIS, G. S., KOMIYAMA, T., ZHU, H., & LUO, L. 2002. Representation of the glomerular olfactory map in the *Drosophila* brain. *Cell*, **109**(2), 243–55.

MERCER, A. R., HAYASHI, J. H., & HILDEBRAND, J. G. 1995. Modulatory effects of 5-hydroxytryptamine on voltage-activated currents in cultured antennal lobe neurones of the sphinx moth *Manduca sexta*. *J Exp Biol*, **198 (Pt 3)**, 613–27.

MERCER, A. R., KLOPPENBURG, P., & HILDEBRAND, J. G. 1996. Serotonin-induced changes in the excitability of cultured antennal-lobe neurons of the sphinx moth *Manduca sexta*. *J Comp Physiol [A]*, **178**(1), 21–31.

MIZUNAMI, M., IWASAKI, M., OKADA, R., & NISHIKAWA, M. 1998. Topography of four classes of Kenyon cells in the mushroom bodies of the cockroach. *J Comp Neurol*, **399**(2), 162–75.

MURTHY, M., FIETE, I., & LAURENT, G. 2008. Testing odor response stereotypy in the *Drosophila* mushroom body. *Neuron*, **59**(6), 1009–1023.

OLSEN, S. R., & WILSON, R. I. 2008. Lateral presynaptic inhibition mediates gain control in an olfactory circuit. *Nature.*

OLSEN, S. R., BHANDAWAT, V., & WILSON, R. I. 2007. Excitatory interactions between olfactory processing channels in the *Drosophila* antennal lobe. *Neuron*, **54**(1), 89–103.

OLSHAUSEN, B.A., & FIELD, D.J. 2004. Sparse coding of sensory inputs. *Curr Opin Neurobiol*, **14**(4), 481–487.

PELZ, C., JANDER, J., ROSENBOOM, H., HAMMER, M., & MENZEL, R. 1999. I_A in Kenyon cells of the mushroom body of honeybees resembles shaker currents: kinetics, modulation by K^+, and simulation. *J Neurophysiol*, **81**(4), 1749–59.

PEREZ-ORIVE, J., MAZOR, O., TURNER, G. C., CASSENAER, S., WILSON, R. I., & LAURENT, G. 2002. Oscillations and sparsening of odor representations in the mushroom body. *Science*, **297**(5580), 359–365.

PEREZ-ORIVE, J., BAZHENOV, M., & LAURENT, G. 2004. Intrinsic and circuit properties favor coincidence detection for decoding oscillatory input. *J Neurosci*, **24**(26), 6037–47.

PIPPOW, A. 2008. Differences of Ca^{2+} handling properties and differential processing of olfactory information in identified central olfactory neurons. *Phd thesis*. **University of Cologne**.

ROOT, C. M., SEMMELHACK, J. L., WONG, A. M., FLORES, J., & WANG, J. W. 2007. Propagation of olfactory information in Drosophila. *Proc Natl Acad Sci U S A*, **104**(28), 11826–31.

ROSPARS, J. P., & HILDEBRAND, J. G. 1992. Anatomical identification of glomeruli in the antennal lobes of the male sphinx moth Manduca sexta. *Cell Tissue Res*, **270**(2), 205–27.

SACHSE, S., & GALIZIA, C. G. 2002. Role of inhibition for temporal and spatial odor representation in olfactory output neurons: a calcium imaging study. *J Neurophysiol*, **87**(2), 1106–17.

SATTELLE, D. B., HARRISON, J. B., CHEN, H. H., BAI, D., & TAKEDA, M. 2000. Immunocytochemical localization of putative gamma-aminobutyric acid receptor subunits in the head ganglia of Periplaneta americana using an anti-RDL C-terminal antibody. *Neurosci Lett*, **289**(3), 197–200.

SCHÄFER, S., ROSENBOOM, H., & MENZEL, R. 1994. Ionic currents of Kenyon cells from the mushroom body of the honeybee. *J Neurosci*, **14**(8), 4600–12.

SHANG, Y., CLARIDGE-CHANG, A., SJULSON, L., PYPAERT, M., & MIESENBOCK, G. 2007. Excitatory Local Circuits and Their Implications for Olfactory Processing in the Fly Antennal Lobe. *Cell*, **128**(3), 601–612.

SILBERING, A. F., OKADA, R., ITO, K., & GALIZIA, C. G. 2008. Olfactory information processing in the *Drosophila* antennal lobe: Anything Goes? *J Neurosci*, **28**(49), 13075–13087.

STOPFER, M., JAYARAMAN, V., & LAURENT, G. 2003. Intensity versus identity coding in an olfactory system. *Neuron*, **39**(6), 991–1004.

STRAUSFELD, N. J., & LI, Y. S. 1999a. Organization of olfactory and multimodal afferent neurons supplying the calyx and pedunculus of the cockroach mushroom bodies. *Journal of Comparative Neurology*, **409**(4), 603–625.

STRAUSFELD, N. J., & LI, Y. S. 1999b. Representation of the calyces in the medial and vertical lobes of cockroach mushroom bodies. *Journal of Comparative Neurology*, **409**(4), 626–646.

STRAUSFELD, N. J., HANSEN, L., LI, Y. S., GOMEZ, R. S., & ITO, K. 1998. Evolution, discovery, and interpretations of arthropod mushroom bodies. *Learning & Memory*, **5**(1-2), 11–37.

STRAUSFELD, N. J., SINAKEVITCH, I., & VILINSKY, I. 2003. The mushroom bodies of *Drosophila melanogaster*: an immunocytological and golgi study of Kenyon cell organization in the calyces and lobes. *Microsc Res Tech*, **62**(2), 151–69.

SVOBODA, K., DENK, W., KLEINFELD, D., & TANK, D. W. 1997. In vivo dendritic calcium dynamics in neocortical pyramidal neurons. *Nature*, **385**(6612), 161–165.

SZYSZKA, P., DITZEN, M., GALKIN, A., GALIZIA, C. G., & MENZEL, R. 2005. Sparsening and temporal sharpening of olfactory representations in the honeybee mushroom bodies. *J Neurophysiol*, **94**(5), 3303–13.

TANAKA, N.K., AWASAKI, T., SHIMADA, T., & ITO, K. 2004. Integration of chemosensory pathways in the Drosophila second-order olfactory centers. *Curr Biol*, **14**(6), 449–457.

TURNER, G. C., BAZHENOV, M., & LAURENT, G. 2008. Olfactory representations by *Drosophila* mushroom body neurons. *J Neurophysiol*, **99**(2), 734–46.

WANG, J. W., WONG, A. M., FLORES, J., VOSSHALL, L. B., & AXEL, R. 2003. Two-photon calcium imaging reveals an odor-evoked map of activity in the fly brain. *Cell*, **112**(2), 271–82.

WANG, Y., GUO, H. F., POLOGRUTO, T. A., HANNAN, F., HAKKER, I., SVOBODA, K., & ZHONG, Y. 2004. Stereotyped odor-evoked activity in the mushroom body of *Drosophila* revealed by green fluorescent protein-based Ca^{2+} imaging. *J Neurosci*, **24**(29), 6507–14.

WEHR, M., & LAURENT, G. 1996. Odour encoding by temporal sequences of firing in oscillating neural assemblies. *Nature*, **384**(6605), 162–166.

WEISS, M. J. 1974. Neuronal connections and function of Corpora-Pedunculata in brain of american cockroach, *Periplaneta americana* (L). *Journal of Morphology*, **142**(1), 21–69.

WICHER, D. 2001. Peptidergic modulation of insect voltage-gated Ca(2+) currents: role of resting Ca(2+) current and protein kinases A and C. *J Neurophysiol*, **86**(5), 2353–62.

WICHER, D., & PENZLIN, H. 1994. Ca^{2+} currents in cockroach neurones: properties and modulation by neurohormone D. *Neuroreport*, **5**(9), 1023–6.

WICHER, D., & PENZLIN, H. 1997. Ca^{2+} currents in central insect neurons: Electrophysiological and pharmacological properties. *J Neurophysiol*, **77**(1), 186–199.

WILSON, R. I., & LAURENT, G. 2005. Role of GABAergic inhibition in shaping odor-evoked spatiotemporal patterns in the *Drosophila* antennal lobe. *J Neurosci*, **25**(40), 9069–79.

WILSON, R. I., & MAINEN, Z. F. 2006. Early events in olfactory processing. *Annu Rev Neurosci*, **29**, 163–201.

WILSON, R. I., TURNER, G. C., & LAURENT, G. 2004. Transformation of olfactory representations in the *Drosophila* antennal lobe. *Science*, **303**(5656), 366–70.

WONG, A. M., WANG, J. W., & AXEL, R. 2002. Spatial representation of the glomerular map in the Drosophila protocerebrum. *Cell*, **109**(2), 229–41.

WORRELL, J.W., & LEVINE, R.B. 2008. Characterization of voltage-dependent Ca^{2+} currents in identified Drosophila motoneurons in situ. *J Neurophysiol*, **100**(2), 868–878.

WRIGHT, N. J., & ZHONG, Y. 1995. Characterization of K$^+$ currents and the cAMP-dependent modulation in cultured *Drosophila* mushroom body neurons identified by lacZ expression. *J Neurosci*, **15**(2), 1025–1034.

WÜSTENBERG, D. G., BOYTCHEVA, M., GRÜNEWALD, B., BYRNE, J. H., MENZEL, R., & BAXTER, D. A. 2004. Current- and voltage-clamp recordings and

computer simulations of Kenyon cells in the honeybee. *J Neurophysiol*, **92**(4), 2589–603.

YAMAZAKI, Y., NISHIKAWA, M., & MIZUNAMI, M. 1998. Three classes of GABA-like immunoreactive neurons in the mushroom body of the cockroach. *Brain Res*, **788**(1-2), 80–6.

YASUYAMA, K., MEINERTZHAGEN, I. A., & SCHURMANN, F. W. 2002. Synaptic organization of the mushroom body calyx in *Drosophila melanogaster*. *J Comp Neurol*, **445**(3), 211–26.

List of Figures

Danksagung

Ohne Hilfe wäre diese Arbeit nicht zu Stande gekommen. Ich danke insbesondere:

Prof. Dr. Peter Kloppenburg für die die besondere Unterstützung und Ermöglichung dieser Arbeit. Ohne die unzähligen fruchtbaren Diskussionen wäre diese Arbeit mit Sicherheit nicht zu Stande gekommen.

Prof. Dr. Ansgar Büschges für die Erstellung des Zweit-Gutachtens und die Unterstützung während der ganzen Arbeit.

Helmut Wratil für seine exzellente technische und persöhnliche Hilfe bei allen schweren und leichteren Problemen. Du bist der beste Assistent, den man sich wünschen kann.

Ron Harris-Warrick für die wertvollen Kommentare zu diesem Manuskript.

Meinen Kollegen, die mich immer wieder aufzumuntern wussten. Andreas Husch für seine Einführung in die patch-clamp Technik und die Musik-Geschichte. Andreas Pippow für die ständige Hilfe, bei jedweden statistischen und Kalzium Problemen, ganz besonderen Dank für die Hilfe bei der Auswertung der Imaging Daten. Moritz Paehler danke ich für die Hilfe bei TILL, Hard- und Software Problemchen, auch wenn die Klickgeschwindigkeit manchmal einfach zu hoch für mich war. Sabine Schleicher danke ich ganz besonders für die schöne Rekonstruktion des Schabengehirns. Debora Fusca, Simon Hess und Lars Paeger danke ich für die zahlreichen Korrekturen an meinem Manuskript. Ich danke euch allen von ganzem Herzen, ohne euch wäre diese Arbeit nicht möglich gewesen.

Vera, Thorsten Lisa und Ronja Krauland für die wunderschönenen Eifeltage- und abende und die schönen D & D Abenteur in den Reichen von Faerûn. Ausserdem danke ich Thorsten und Volker für die essenzielle Hilfe mit Latex und der Formatierung.

Meinen Eltern möchte ich danken für die enorme Unterstützung und den Glauben an mich und meinen Weg. Ohne euch wäre diese Arbeit um einiges schwerer gewesen.

Ich möchte Alex, Cora und Sandra danken für die Anmeldung und Erinnerungen bei gefühlten 90 % der Praktika. Ohne eure Hilfe wäre ich niemals über das Vor-Diplom hinaus gekommen. Mein Dank gilt ausserdem Maike und Dani für die seelische Unterstützung in Freiburg und den vielen, vielen einzigartigen Erlebnissen mit euch.

Meinen Freunden Alex, Andi, Pia, Nic, Miri, Diana und Claudia dafür dass ihr immer für mich da wart und immer an mich geglaubt habt und mich bei Zeiten ablenken konntet.

Zuletzt danke ich meinem Andi. Dinge aus anderen Blickwinkeln zu sehen und gelassen zu bleiben hat geholfen diesen Weg zu Ende zu gehen. Ich danke Dir für alles was du für mich getan hast. Ich freue mich auf die gemeinsame Zukunft!

Vielen Dank!

Erklärung

Ich versichere, dass ich die von mir vorgelegte Dissertation selbständig angefertigt, die benutzten Quellen und Hilfsmittel vollständig angegeben und die Stellen der Arbeit - einschließlich Tabellen, Karten und Abbildungen -, die andere Werke im Wortlaut oder dem Sinn nach entnommen sind, in jedem Einzelfall als Entlehnung kenntlich gemacht habe; dass diese Dissertation noch keiner anderen Fakultät oder Universität zur Prüfung vorgelegen hat; dass sie - abgesehen von den unten angegebenen Teilpublikationen - noch nicht veröffentlicht worden ist sowie, dass ich eine solche Veröffentlichung vor Abschluss des Promotionsverfahrens nicht vornehmen werde. Die Bestimmungen diese Promotionsordnung sind mir bekannt. Die von mir vorgelegte Dissertation ist von Prof. Dr. Peter Kloppenburg betreut worden.

Köln, den 12.05.2009

Teilpublikationen

Article

Der erste Teil dieser Dissertation ist zur Publikation eingereicht worden:

DEMMER, H. AND KLOPPENBURG, P. 2009. Intrinsic membrane properties and synaptic input of Kenyon cells as mechanisms for sparse coding? *submitted in J Neurophysiol.*

Posters and Abstracts

DEMMER,H. AND KLOPPENBURG, P. 2009. Synaptic Input and intrinsic membrane properties as potential mechanisms for sparse coding in cokroach Kenyon cells. *Proceedings of the 32th Göttingen Neurobiology Conference and the 8th Meeting of the German Neuroscience Society.*

PIPPOW, A., DEMMER, H., FUSCA, D., HESS, S., HUCH, A., PAEHLER, M., WRATIL,H., POUZAT,C. AND KLOPPENBURG, P. 2008. Distinct calcium handling properties of identified insect olfactory interneurons. *Annual Meeting of the Society for Neuroscience(SfN). Program No. 363.5 Abstract, Washington, DC.*

DEMMER, H., HESS, S., HUSCH, A., PAEHLER, M. AND KLOPPENBURG, P. 2007. Physiological and morphological characterisation of interneurons in the insect olfactory pathway. *Annual Meeting of the Society for Neuroscience(SfN). Program No. 277.8 Abstract, Washington, DC.*

DEMMER,H. FUSCA, D. AND KLOPPENBURG, P. 2007. Physiological properties of Kenyon cells recorded in an intact brain preparation. *Proceedings of the 31th Göttingen Neurobiology Conference and the 7th Meeting of the German Neuroscience Society.*

DEMMER, H. AND KLOPPENBURG, P. 2006. In situ characterization of Kenyon Cells of *Periplaneta americana. Neuro-Visonen 4 , Perspektiven in Nordrhein-Westfalen, Düsseldorf, Germany*

DEMMER, H., WRATIL, P. AND KLOPPENBURG, P. 2006 Neurophysiological characterization of insect Kenyon cells in situ. *5th Forum of European Neuroscience (Fens). A074.5*

Curriculum vitae

Dipl. Biol. Heike Demmer

CAMPUSS ADDRESS
University of Cologne; Instute for Zoology/Physiology
Molecular and Cellular Neruophysiology
Weyertal 119, 50931 Köln
E-mail: hdemmer@uni-koeln.de;
Tel: +(49)-221-470-5828

Date of Birth: 11.03.1979
Place of Birth: Cologne

Education

2005 – 2009	**University of Cologne; Intitute for Zoology/Physiology** PhD thesis in Zoology in the laboratory of Prof. Dr. Peter Kloppenburg: Cellular Mechanisms for Olfactory Information Processing in Mushroom Bodies
2004 – 2005	**University of Cologne; Intitute for Zoology/Physiology** Diploma thesis with mayor in zoology and minors: genetics and biochemistry: Characterization of the A-Type Potassium Current and the Modulatory Effects of 5-HT on Voltage-Activated Calcium Currents in Olfactory Interneurons of *Periplaneta americana*
2001 – 2004	**University of Cologne** Study of Biology
April 2001	**Albert-Ludwigs-Universität Freiburg** Pre-diploma
1998 - 2001	**Albert-Ludwigs-Universität Freiburg** Study of Biology

Professional Experiences

2005 – 2009	University of Cologne; Laboratory of Prof. Dr. Peter Kloppenburg
2001	Three month internship at Bayer CropScience

Lebenslauf

Dipl. Biol. Heike Demmer

CAMPUSS ADDRESSE
Universität zu Köln, Zoologisches Institut
Molekulare and Zelluläre Neurophysiologie
Weyertal 119, 50931 Köln
E-mail: hdemmer@uni-koeln.de;
Tel: +(49)-221-470-5828

Geburtstag: 11.03.1979
Geburtsort: Köln

Ausbildung

2005 – 2009	**Universität zu Köln, Zoologisches Institut/Tierphysiologie** Dr. Arbeit im Fach Zoologie im Labor von Prof. Dr. Peter Kloppenburg zum Thema: Cellular Mechanisms for Olfactory Information Processing in Mushroom Bodies
2004 – 2005	**Universität zu Köln, Zoologisches Institut/Tierphysiologie** Diplom Arbeit mit dem Hauptfach Zoologie und den Nebenfächern Genetik und Biochemie zum Thema: Characterization of the A-Type Potassium Current and the Modulatory Effects of 5-HT on Voltage-Activated Calcium Currents in Olfactory Interneurons of *Periplaneta americana*
2001 – 2004	**Universität zu Köln** Biologie Studium
April 2001	**Albert-Ludwigs-Universität Freiburg** Vordiplom
1998 - 2001	**Albert-Ludwigs-Universität Freiburg** Biologie Studium

Berufliche Tätigkeiten

2005 – 2009	wissenschaftliche Mitarbeiterin im Labor von Prof. Dr. Peter Kloppenburg
2005	wissenschaftliche Hilfskraft im Labor von Prof. Dr. Peter Kloppenburg
2001	Dreimontaige Tätigkeit als Werkstudentin bei Bayer CropScience

Köln, den 12.05.2009 _____